

Dissertation
submitted to the
Combined Faculties for the Natural Sciences and for Mathematics
of the Ruperto-Carola University of Heidelberg, Germany
for the degree of
Doctor of Natural Science

presented by

Diplom-Phys. Michael Bertschik
born in Braunschweig

Oral examination: 26. Mai 2004

The Kinematical Parameters of Minor Mergers and their Observational Traces

Referees:

Prof. Dr. Andreas Burkert

Prof. Dr. Hans-Walter Rix

Abstract

Die kinematischen Eigenschaften von Minor Merger und ihre beobachtbaren Spuren

In dieser Arbeit wurden sog. Minor Merger untersucht, Verschmelzungen zweier galaktischer Objekte im Massebereich von 1:20 bis 1:5, motiviert von der Idee und verschiedenen Beobachtungen, dass unsere Milchstrasse in ihrer Vergangenheit einen Minor Merger erfuhr. Im Rahmen einer Reihe von numerischen Simulationen, die die kosmologische Strukturbildung von dunkler Materie nachbildeten, wurden verschiedene Eigenschaften von Minor Merger untersucht. Es erwies sich, dass der Pericenterabstand in Einheiten des Virialradius des grösseren Halos mit der Zeit variiert: Er ist kleiner zu höheren Rotverschiebungen. Ebenso finden sich zu höheren Rotverschiebungen mehr parabolische Orbits. Der Vergleich mit den Simulationen und Beobachtungen von Major Merger ergab, dass der Verschmelzungsparameter in etwa übereinstimmt mit den Erwartungen von Major Merger, während die Verschmelzungsrate abweicht. Der Spinparameter des grösseren Halos ist nach dem Merger grösser. Eine Winkelabhängigkeit zwischen den Spinachsen konnte nicht gefunden werden. Es fand sich, dass eine Galaxie wie die Milchstrasse durchschnittlich einen Minor Merger durchmacht pro Hubblezeit, wobei der wahrscheinlichste Zeitpunkt dafür etwa 7Gyr zurückliegt. Die auf diese Weise gewonnenen Informationen über die Kinematik von Minor Merger wurden für weitere Simulationen von Kollisionen einer galaktischen Scheibe mit einem Satelliten benutzt. Es ergab sich, dass es schwierig ist, Reste des Satelliten vor dem Hintergrund des Halos auszumachen. Die Satellitenpartikel befinden sich auf Orbits, die sich kaum von denen der Halopartikel unterscheiden. Die Geschwindigkeitsverteilung der Partikel in Blickrichtung zeigt nur schwache Spuren des Satelliten selbst, während andere Effekte wie die Aufheizung der stellaren Scheibe zu einer dicken Scheibe recht gut sichtbar sind.

The Kinematical Parameters of Minor Mergers and their Observational Traces

This work was motivated by observations that galaxies like our Milky Way are undergoing merger with galactic satellites and leaving behind observational traces. The thick disk of our Milky Way may be due to a collision with a satellite of substantial mass of the galaxy, i.e. 1:20 to 1:5, what we call a "minor merger". First, we derived in cosmological simulations the kinematical properties of dark matter halos that are minor merging and their abundance in space and time. We found that minor merger were most likely at a time 7Gyrs ago and happened typically once for a Milky Way sized halo. Their pericenter distances and their eccentricities varied with time, we found smaller pericenter distances and more parabolic orbits in the past. The merging rate differed significantly from the simulated and observed merging rate of major merger while the merging parameter roughly matched expectations from major merger. There was no dependency of the angles between orbit and spin axes of the objects found and no dependency of the mass ratios on redshift. We put these informations into more detailed simulations of a stellar galactic disk that merges with a satellite to see whether an observer in the disk is able to observe traces from this minor merger. We found that the satellite particles are hard to distinguish from halo objects, while the LOSVD shows only few traces of satellite remnants. Effects like heating of the galactic disk were clearly visible.

Contents

1	Introduction	1
2	Background	3
2.1	Cosmology and cosmological structure formation	3
2.1.1	Cosmology in short	3
2.1.2	Structure formation: Development of density fluctuations	5
2.1.3	Dark Matter	9
2.1.4	Inflation, Quintessence and the Cosmological Constant	12
2.2	Minor Merging Milky Way?	14
2.2.1	Satellites and Tidal Streams	15
2.2.2	Hints on Minor Merger of the Milky Way	17
2.3	Conclusion and Discussion	22
3	Numerics	23
3.1	The Code WINE	23
3.1.1	The Gravity Part: the Tree	23
3.1.2	The Gravity Part: Force Computation	24
3.1.3	Parallel Computing	24
3.1.4	Other Features	24
3.2	The GRAPE System	24
3.3	GRAPE and WINE	27
4	Methods	29
4.1	Cosmological Initial Conditions with GRAFIC	29
4.2	FOF: friends-of-friends Algorithm	31
4.3	Initial Conditions for a Minor Merging Galaxy	32
4.3.1	The Disk	33
4.3.2	The Halo	34
4.3.3	The Satellite (Hernquist Profile)	36
4.4	An Algebraic Approach to the Kepler Problem	37
4.5	The Simulation Parameter	39
4.5.1	The Cosmology Part	39
4.5.2	The Galaxy Part	40
4.5.3	The Criteria for Minor Merger	41
4.6	Conclusion and Discussion	41

5	Results from cosmological simulations	43
5.1	Comparison of WINE to other codes and methods	43
5.2	The abundance and frequency of Minor Merger	44
5.3	The orbital parameter of Minor Merger	46
5.4	The angles in minor merging events	53
5.5	Minor merger and the spin parameter of the halo	58
5.6	Discussion and Conclusion	62
6	Results from galaxy simulations	63
6.1	The Analysis	63
6.2	Results	85
6.3	Discussion	86
7	Discussion and Conclusions	89
8	Outlook	91
A	Figures	93

Chapter 1

Introduction

The true delight is in the finding out, rather than in the knowing.
Isaac Asimov

Research in cosmology has made significant progress in the last ten years: COBE mapped the cosmic background radiation (Smoot et al., 1990) and found quadrupole fluctuations (Smoot et al., 1992). These fluctuations were the seeds for the cosmological structure and the base for every galaxy and galaxy cluster. Some years later observations of distant supernovae of type Ia (Riess et al., 1998; Perlmutter et al., 1997) suggested that there is some sort of “dark energy” which accelerates the expansion of the universe and additionally suggested that our universe has flat geometry $\Omega = 1$ (as predicted, or better: demanded by the hypothesis of inflation (Guth, 1981)). The rebirth of Einstein’s cosmological constant Λ had of course influence on theoretical and numerical considerations regarding the development of cosmological structure. This cosmic structure was mapped in observations like the 2dF-Survey (Hawkins et al., 2003). Together with the rapid gain of computing power in numerical simulations it was possible to follow the growth of structure of especially dark matter in the universe in more and more detail. Still, there are of course problems, e.g. the “over abundance” of small satellites in galaxies in numerical simulations compared to observations (Moore et al., 1999; Klypin et al., 1999) or the “cusp-core” controversy regarding the center of dark matter halos (Navarro et al., 1997; Ghigna et al., 2000; Burkert, 1995).

Despite of these problems there are commonly believed models and theories in the field. The “cosmological community” believes that our universe started in a hot, dense phase called “big bang”. Soon after the big bang ($\sim 10^{-35}$ s), there was a phase called “inflation” where the distances between two points were increased by a factor of 10^{43} (!) and the geometry of the universe was flattened to $k = 0$ (Euclidean geometry). Several hundred thousand years later matter decoupled from radiation, the universe became “transparent” for light (light we can still see as “cosmic microwave background radiation”). Gravitation leads to clumping of cooled matter and in the end gravitational collapse results in the formation of stars and planets. Matter in the universe consists mainly of so-called “dark matter”, some collisionless, weakly interacting particles dominating the clumping process and galaxy dynamics. This extremely short story of the universe is today’s standard picture which of course has some caveats. Especially the nature of dark matter and its nemesis “dark energy” is unknown and of research interest in the moment. Nevertheless it is impressive that mankind was able to get a glimpse of the genesis and evolution of

the universe while standing on a lonely planet around an ordinary sun in the outer parts of a standard galaxy.

This is the point where this work comes in: What can we know about this standard galaxy called “Milky Way”? What are we able to derive and to reveal about our galaxy by observation and theoretical considerations?

This work focuses on the possibility that our galaxy underwent collisions with smaller satellites motivated by different observations mentioned in chapter 2. The likelihood and the parameters of such a collision are derived within the cosmological context of structure formation in chapter 5. The application of the results from cosmology to galactic dynamics is shown in chapter 6. The methods necessary for this derivation and numerical techniques are described in chapter 4 resp. chapter 3. Results and concluding remarks as well as an outlook are presented in chapter 7 and chapter 8.

Chapter 2

Background

Space is big. Really big. You just won't believe how vastly, hugely, mind-boggling big it is.
The Hitchhiker's Guide to the Galaxy

In this chapter the physical background underlying this work is explained. The first part summarizes cosmological physics, the development of fluctuations in an expanding universe and the implications of the presence of dark matter and dark energy. The second part describes observations of minor mergers of galaxies in general and for the special case of our Milky Way.

2.1 Cosmology and cosmological structure formation

2.1.1 Cosmology in short

The simplest metric one can find for a homogenous, isotropic universe (which is covering the observations quite well and gives substance to the cosmological principle¹) is the *Robertson-Walker metric*. Its line element is:

$$ds^2 = dt^2 - R^2(t) \left(\frac{dr^2}{1 - kr^2} + r^2(d\theta^2 + \sin^2\theta d\phi^2) \right) \quad (2.1)$$

Here r , θ and ϕ are the three comoving spatial coordinates, $R(t)$ is the scale factor and k characterizes the curvature (fig.2.1²).

All the dynamics of the universe is hidden in the time dependent scale factor $R(t)$ which is described by the Einstein field equations (Einstein, 1916):

$$R_{\mu\nu} - \frac{1}{2}Rg_{\mu\nu} - \Lambda g_{\mu\nu} = 8\pi GT_{\mu\nu} \quad (2.2)$$

Here $R_{\mu\nu}$ is the Ricci tensor, $T_{\mu\nu}$ the energy-momentum tensor, $g_{\mu\nu}$ the metric tensor and Λ the cosmological constant ($\Lambda \equiv 8\pi G\rho_V/c^2$). If we assume a perfect fluid and neglect

¹The cosmological principle states that all positions and directions are equal. We do not have a special position within the universe of any kind.

²There is a caveat in these visualizations: the surfaces are curved in a higher spatial dimension what is actually not true within general relativity where curvature is an "inner curvature" without additional spatial dimensions

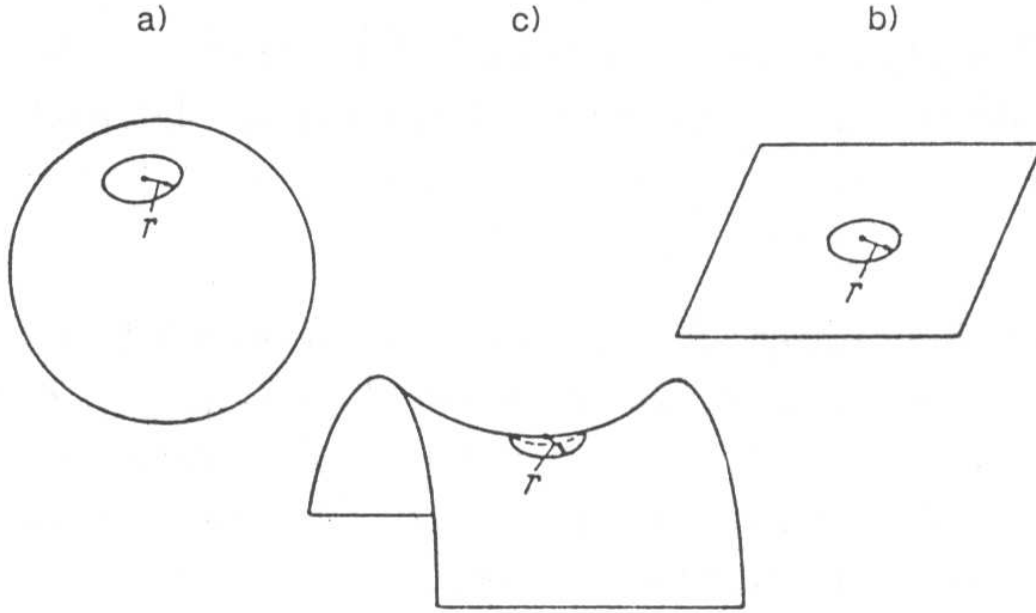


Figure 2.1: Three visualizations of the curvature dependent on k : a) denotes a closed universe with $k = 1$, b) a hyperbolic universe with $k = -1$ and c) a flat universe with $k = 0$ (Klapdor-Kleingrothaus & Zuber, 1997)

“smaller” inhomogeneities like galaxies and galaxy clusters the energy-momentum tensor is:

$$T_{\mu\nu} = \text{diag}(\rho + \rho_V, -p, -p, -p) \quad (2.3)$$

From the time component one yields

$$\frac{\dot{R}^2}{R^2} + \frac{k}{R^2} = \frac{8\pi G}{3}(\rho + \rho_V) \quad (2.4)$$

and from the spatial components

$$2\frac{\ddot{R}}{R} + \frac{\dot{R}^2}{R^2} + \frac{k}{R^2} = -8\pi G p \quad (2.5)$$

we get the *Einstein-Friedmann-Lemaître* equations. From this one gets

$$\frac{\ddot{R}}{R} = -\frac{4\pi G}{3}(\rho - 2\rho_V + 3p). \quad (2.6)$$

Since we observe redshift of distant galaxies we need non-static solutions of these equations. A positive Λ means acceleration of the expansion and is suggested by different observations (Riess et al., 1998; Perlmutter et al., 1997; Bennett et al., 2003). If additionally $k = 0, -1$ we have only positive solutions and we get an ever-expanding universe. For $k = 1$ we get a critical value:

$$\Lambda_c = 4 \left(\frac{8\pi G}{c^2} M \right)^{-2} \quad (2.7)$$

Recent observations suggest a positive value of Λ with $\Omega_\Lambda \sim 0.7$ and $\Omega_{matter} \sim 0.3$ and therefore a flat universe with $\Omega_{tot} = 1$ ($k = 0$) as proposed by inflationary models ³.

Light waves are stretched by the expanding universe. This leads to redshifted light from distant sources. The redshift z is defined as:

$$z = \frac{\lambda_0}{\lambda_1} - 1 = \frac{R(t_0)}{R(t_1)} - 1 \quad (2.8)$$

where the index 0 denotes the time of receipt (usually *now*) and the index 1 the time of emission. Additionally one defines the Hubble parameter H as

$$H = \frac{\dot{R}(t)}{R(t)} \quad (2.9)$$

and the Hubble constant H_0 as a local value measured today

$$H_0 = \frac{\dot{R}(t_0)}{R(t_0)} \quad (2.10)$$

For convenience one introduces the dimensionless parameter h_0 with

$$h_0 = \frac{H_0}{100 \text{km s}^{-1} \text{Mpc}^{-1}} \quad (2.11)$$

with $h_0 = 0.71$ as a commonly used value today.

2.1.2 Structure formation: Development of density fluctuations

How can structure evolve in an expanding universe? Let's start with the definition of a density contrast (Peebles, 1980, Klapdor-Kleingrothaus & Zuber, 1997)

$$\delta(\vec{x}) = \frac{\delta\rho(\vec{x})}{\langle\rho\rangle} = \frac{\rho(\vec{x}) - \langle\rho\rangle}{\langle\rho\rangle} \quad (2.12)$$

with $\langle\rho\rangle$ the mean density of the background. So regions with a density $\delta > 1$ lead to gravitational collapse. The subsequent question now is: how does one get a $\delta=1$ from initial conditions which are quite isotropic and homogenous? As soon as $\delta = 1$ the growth is non-linear and the development to bound structures goes quickly.

The problem of the gravitational growth of structures was studied first by Jeans in 1902. Here, a Newtonian approximation is used to describe the growth of small perturbations and take a static model ($\dot{R} = 0$) of an ideal fluid with density ρ . This gives following basic equations:

$$\frac{\partial\rho}{\partial t} + \nabla(\rho\vec{v}) = 0 \quad \text{continuity equation} \quad (2.13)$$

$$\frac{\partial\vec{v}}{\partial t} + (\vec{v} \cdot \nabla)\vec{v} + \frac{1}{\rho}\nabla\rho + \nabla\Phi = 0 \quad \text{Euler equation} \quad (2.14)$$

³ Ω is defined as $\Omega = \rho/\rho_{crit}$ where ρ is the average matter density and $\rho_{crit} = \frac{3H_0^2}{8\pi G}$

2.1 Cosmology and cosmological structure formation

with the gravitational potential Φ given by the Poisson equation

$$\nabla^2\Phi = 4\pi G\rho \quad (2.15)$$

If one assumes small perturbations of these quantities (e.g. $\rho = \rho_0 + \rho_1$ with $\rho_1 \ll \rho_0$) it is allowed to use linearized equations, and we get

$$\frac{\partial^2\rho_1}{\partial t^2} - v_s^2\nabla^2\rho_1 = 4\pi G\rho_0\rho_1 \quad (2.16)$$

Here adiabatic perturbations are assumed, i.e. the sound speed v_s is

$$v_s = \sqrt{\frac{\partial p}{\partial \rho}} \quad (2.17)$$

In a static case we have as solutions plane waves $\exp(i(\vec{k} \cdot \vec{r}) - \omega t)$ with the dispersion relation

$$\omega^2 = v_s^2 k^2 - 4\pi G\rho_0. \quad (2.18)$$

In the non-static case equation (2.16) can be rewritten, and we find for the density contrast

$$\frac{d^2\delta}{dt^2} + 2\left(\frac{\dot{R}}{R}\right)\frac{d\delta}{dt} = \delta(4\pi G\rho_0 - v_s^2 k^2). \quad (2.19)$$

We can derive from this dispersion relation a critical value ($\omega = 0$) called *Jeans wavelength* k_j

$$k_j = \sqrt{\frac{4\pi G\rho_0}{v_s^2}} \quad (2.20)$$

Solutions with $k > k_j$ describe sound waves where the inner pressure gradient is big enough to withstand gravitation. For $k < k_j$ (complex ω) the solutions describe exponentially increasing or decreasing modes. One can define the so-called *Jeans mass* M_j as the mass which is within a sphere with radius $\lambda_j/2 = \pi/k_j$

$$M_j = \frac{4\pi}{3} \left(\frac{\pi}{k_j}\right)^3 \rho_0 = \frac{\pi^{5/2}}{6} \frac{v_s^3}{G^{2/3}\rho_0^{1/2}} \quad (2.21)$$

Masses bigger than the Jeans mass are unstable against gravitational collapse. The instability caused by the gravitation of over-dense regions is stronger than the internal pressure gradient. In contrast to the general solution (2.19) we now look at the special case of large wavelengths ($k < k_j$) and therefore negligible pressure $v_s^2 k^2$) for a universe with $\Omega_0 = 1$.

For $\Omega_0 = 1$ we have

$$4\pi G\rho = \frac{2}{3t^2} \quad \text{and} \quad \frac{\dot{R}}{R} = \frac{2}{3t} \quad (2.22)$$

Therefore equation (2.19) can be rewritten as

$$\frac{d^2\delta}{dt^2} + \left(\frac{4}{3t}\right)\frac{d\delta}{dt} - \frac{2}{3t^2}\delta = 0 \quad (2.23)$$

We solve this differential equation with a power law ansatz

$$\delta = At^{2/3} + Bt^{-1} \quad (2.24)$$

The second expression represents damped modes and can be neglected nowadays. The first expression describes growing modes with the following dependencies

$$\delta \sim t^{2/3} \sim R = (1+z)^{-1} \quad (2.25)$$

This means that expansion slows down the growth of perturbations from exponential to a power law.

We now follow the evolution of a Jeans mass as a function of time (details in Kolb & Turner, 1990). For simplicity we assume a universe with photons and baryons only, i.e. $\rho = \rho_B + \rho_Y$. In the radiation-dominated phase the pressure is caused by photons, and we have $v_s^2 = 1/3c^2$. We write the Jeans mass as:

$$M_J = 2.8 \cdot 10^{30} z^{-3} \Omega_B h^2 M_\odot \quad (2.26)$$

The Jeans mass increases proportional to R^3 . A Jeans mass of one solar mass corresponds roughly to redshift $z = 10^{10}$ and grows to typical galaxy mass at $z = 3 \cdot 10^6$. A dramatic change occurs at the time of recombination at redshift $z = 1200$. This is caused by the sudden decrease of the sound speed after decoupling because the pressure is now only build up by non-relativistic hydrogen atoms:

$$v_s^2 = \frac{5}{3} \frac{kT}{m_H} \quad (2.27)$$

This results in a sudden drop of the Jeans mass at this time from $\sim 10^{16} M_\odot$ to $10^6 M_\odot$ (see fig.2.2). Interestingly, this is the typical mass for a globular cluster which belongs to the oldest objects in the universe.

This simple model needs at least two extensions to be of sufficiently usefulness:

1. Weakly interacting particles like neutrinos can leave regions of higher density without affecting the matter in these regions. This leads to a “smearing-out” of inhomogeneities and is called *free streaming*. The typical scale for the smearing-out is:

$$\lambda_{fs} \simeq 30(\Omega_X h^2)^{-1} \left(\frac{T_X}{T}\right)^4 \text{ Mpc} \quad (2.28)$$

Here X denotes the weak interacting particle. For neutrinos we have $T_\nu/T \approx 0.71$ and

$$\lambda_{fs} \simeq 20 \left(\frac{m_\nu}{30\text{eV}}\right)^{-1} \text{ Mpc} \quad (2.29)$$

corresponding to mass scale of

$$M_{fs} \simeq 4 \cdot 10^{14} \left(\frac{m_\nu}{30\text{eV}}\right)^{-2} M_\odot \quad (2.30)$$

Smaller mass scales are washed out and there is no structure formation.

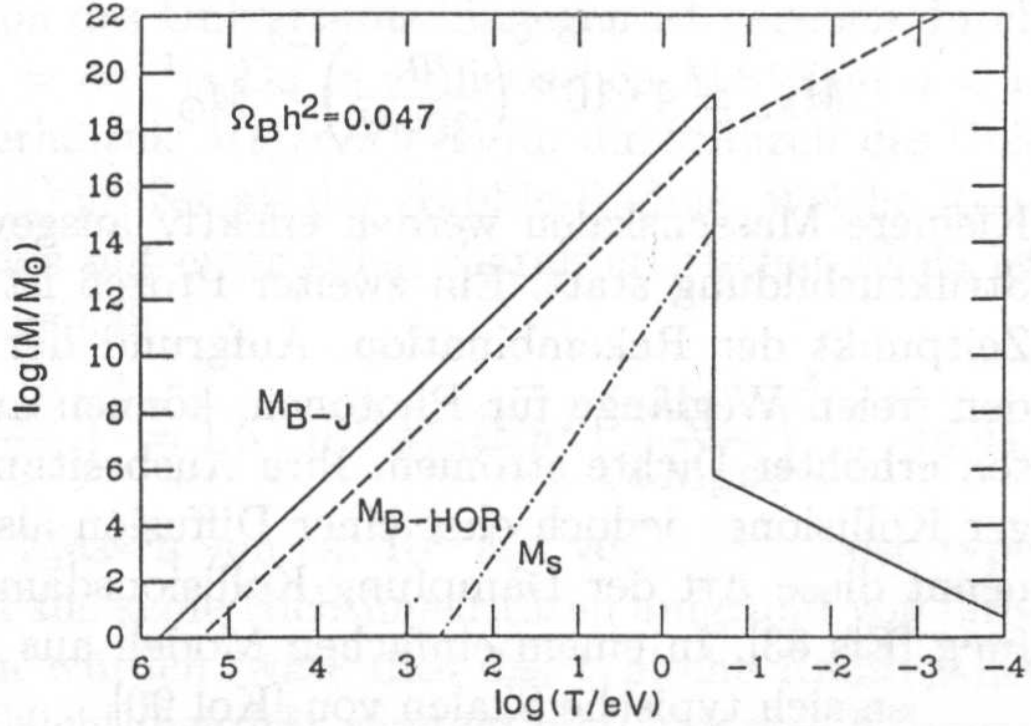


Figure 2.2: The development of the Jeans mass in an expanding universe. The straight line denotes the Jeans mass in baryons M_{B-J} , the dashed line the Jeans mass within the horizon M_{B-HOR} and the dashed-dotted line the Silk mass M_S . The strong decline occurs at the time of decoupling because of the strong decline of the sound speed. Assumed here is a baryonic mass of $\Omega_B h^2 = 0.047$. (Kolb & Turner, 1990)

2. The second process comes into play at the time of recombination: photons are able to diffuse out of the denser regions. This is called *Silk dampening*. In a simple model with photons and baryons the typical scales are:

$$\lambda_S \simeq 3.5 \left(\frac{\Omega_0}{\Omega_B} \right)^{1/2} (\Omega_0) \quad (2.31)$$

resp. the *Silk mass*

$$M_S \simeq 6.2 \cdot 10^{12} \left(\frac{\Omega_0}{\Omega_B} \right)^{3/2} (\Omega_0 h^2)^{3/4} M_\odot \quad (2.32)$$

This also washes out small scales because of the frequent interaction between photons and baryons in the photon-baryon plasma.

2.1.3 Dark Matter

From a cosmological point of view⁴ the above picture of an universe with photons and baryons only is not sufficient: as we have today a density contrast of order $\delta \sim 1$ on cosmological scales according to eq.2.25 these perturbations were of order $\delta \sim 10^{-3}$ at the time of recombination ($z \sim 1500$). This is in conflict with results from measurements of the cosmic microwave background radiation (i.e. COBE, BOOMERANG, MAXIMA, WMAP) which states maximum fluctuations of order $\delta \sim 10^{-5}$. There must be some sort of gravitating matter which is able to enhance the density contrast before or after the phase of recombination: it is called *dark matter*. Astrophysicists discuss essentially two different kinds of dark matter⁵:

1. *Hot dark matter (HDM)* consists of relativistic particles (e.g. neutrinos with masses of $10eV$). Their mobility is responsible for washing out any small perturbations and supports the development of massive structures (see eq.2.30). From these huge structures smaller structures evolve by fragmentation (Zel'dovich, 1993): the so-called *top-bottom* scenario. Unfortunately galaxies form quite late in *HDM* models which is inconsistent with observations of quasars and galaxies at $z > 4$ (Ma & Bertschinger, 1994; Hut & White, 1984).
2. *Cold dark matter (CDM)* consists of “heavy” particles (at least at GeV scale, most prominent is the lightest super-symmetric particle, the *Neutralino*) and produces potential wells before recombination where the baryons afterwards can fall in. Here the Jeans mass is of order of a globular cluster (see eq.2.32). Therefore these objects are the first ones to evolve in a young universe. Bigger objects are then build up by smaller ones: the so-called *bottom-top* or *hierarchical clustering* models. CDM models predict a large number of substructure even in small groups like our local group (Moore et al., 1999). This is not covered by observation yet but it is still possible that we have “dark satellites” around (Stoehr et al., 2002) and that additional effects (i.e. *re-ionization* after recombination) were able to pull gas out of these structures which therefore remain invisible.

There exist assumptions of an intermediate phase of dark matter, the so-called *warm dark matter (WDM)* which would correspond to neutrinos of keV. Still, the favorite model at this time is the CDM model together with a non-vanishing cosmological constant in a universe which underwent an inflation phase at the beginning (see section 2.1.4), say:

$$\Omega_{DM} + \Omega_b + \Omega_\gamma + \Omega_\Lambda \equiv 1 \quad (2.33)$$

where

- Ω_{DM} is the amount of dark matter in the universe. We used the recently found value $\Omega_{DM} = 0.2268$ (Bennett et al., 2003).
- Ω_b is the amount of baryonic matter in the universe. We used the value $\Omega_b = 0.0432$.

⁴Of course there are more arguments for dark matter: flat rotation curves, nucleosynthesis restricts baryonic matter, the virial velocity within galaxy clusters etc.

⁵We refer her to the commonly used picture. Of course there are alternatives to dark matter proposed, e.g. MOND, where a certain additional acceleration is assumed on galactic scales (Milgrom, 1983).

2.1 Cosmology and cosmological structure formation

- Ω_γ is the amount of photons in the universe. We used $\Omega_\gamma = 5.118 \times 10^{-5}$.
- Ω_Λ is the amount of dark energy in the universe (2.1.4). We used the value $\Omega_\Lambda = 0.73$.

An additional cosmological constant Λ within a CDM model essentially “stretches” the time till $z = 0$ so that structure has more time to evolve.

How does a universe made of dark matter evolve? We remember the density field (2.12):

$$\delta(\vec{x}) = \frac{\delta\rho(\vec{x})}{\langle\rho\rangle} = \frac{\rho(\vec{x}) - \langle\rho\rangle}{\langle\rho\rangle} \quad (2.34)$$

If we apply a Fourier analysis of the density field within a finite volume L^3 :

$$\delta(\vec{x}) = \sum_{\vec{k}} \delta_{\vec{k}} e^{i\vec{k}\vec{x}} \quad (2.35)$$

where the wavenumber k is dependent on the boundary conditions:

$$\vec{k} = \vec{n} \frac{2\pi}{L} \quad (2.36)$$

where \vec{n} is an integer vector. The Fourier components $\delta_{\vec{k}}$ are:

$$\delta_{\vec{k}} = \frac{1}{L^3} \int_V \delta(\vec{x}) e^{-i\vec{k}\vec{x}} d^3x \quad (2.37)$$

If we assume a Gaussian random field (as proposed by inflation, see section 2.1.4) we get for the mean and for the variance of the Fourier components:

$$\langle\delta_{\vec{k}}\rangle = 0 \quad (2.38)$$

$$\langle\delta_{\vec{k}}^2\rangle = \sigma^2 = \sum_{\vec{k}} \langle|\delta_{\vec{k}}|^2\rangle = \frac{1}{L^3} \sum_{\vec{k}} \delta_{\vec{k}}^2 \quad (2.39)$$

Since the volume L^3 is finite we have only a finite number of wave numbers \vec{k} . This seems to be unphysical because the universe is assumed to infinite if it is flat. Recently, there were claims that within the cosmic microwave background a “cut-off” frequency exists and therefore a hint on a finite universe with a distinct geometry (Luminet et al., 2003) have been found⁶, but this is not confirmed yet.

For the transformation to (quasi)-continuous values we assume $L \rightarrow \infty$. Therefore we can write:

$$\sigma^2 = \frac{1}{L^3} \sum_{\vec{k}} \delta_{\vec{k}}^2 \quad \rightarrow \quad \frac{1}{2\pi} \int_0^\infty P(k) k^2 dk \quad (2.40)$$

This equation defines the so called *power spectrum* $P(k)$. The statistics of the power spectrum is defined completely by the Gaussian random field. Coming from observations with an universe with a broad spectrum without designated scales one could apply a more general ansatz which is scale-invariant:

$$P(k) = Ak^n \quad (2.41)$$

⁶Luminet et al., 2003 claimed that the weak wide-angle temperature in the CMBR points to a finite universe with dodecahedral shape.

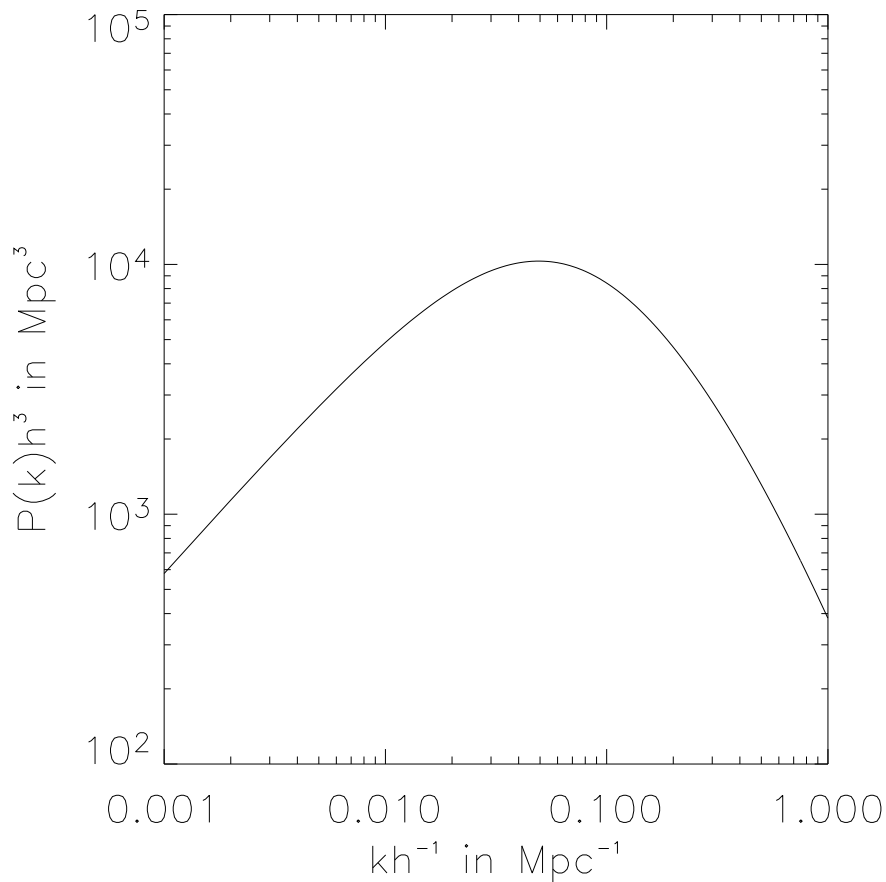


Figure 2.3: The power spectrum of a cold dark matter model according to eq.2.44. See text for more information about the maximum

Harrison-Zel'dovich (Zel'dovich, 1993) proposed a special spectrum with the spectral index $n = 1$. This spectral index is also proposed by the inflation hypothesis (the cause for fluctuations are of quantum mechanical nature and therefore not correlated) and was found quite exact by WMAP (Bennett et al., 2003).

Of course this spectrum was changed due to influences (*free streaming, Silk dampening*) as mentioned above. Without these influences the power spectrum would have kept its power law form. Within a *HDM* model free streaming would force all scales below a certain wavelength λ_{max} to be washed out. Within a *CDM* model it is becoming more interesting: as seen in fig.2.3 the power spectrum has a maximum at $\lambda_{peak} \sim 13/(\Omega h^2)$. In fact, this is the extent of the horizon at the recombination era. It means that during the radiation dominated era perturbations are crossing the horizon into the observable universe and are the seeds for further structure formation. For small scales $\lambda \ll \lambda_{peak}$ the power spectrum $P(k)$ behaves asymptotically like $k^{n-4} \log k$ (fig.2.3) with $n = 1$. This

form of the power spectrum is caused by (re-)entry of perturbations into the horizon. Fluctuations smaller than the horizon at time t_{peak} are caught by the expanding horizon during the radiation dominated epoch and do not grow because of the *Meszaros effect*⁷. Fluctuations bigger than the horizon ($> \lambda_{peak}$) are not affected since physical effects are bound to the size of the horizon. All these kinds of effects on the power spectrum are described by a so-called *transfer function* $T(k)$:

$$T(k) = \{1 + [ak + (bk)^{3/2} + (ck)^2]^\nu\}^{-1/\nu} \quad (2.42)$$

with arbitrary values for a , b and c . This function modifies an initial power spectrum at time t_0 and enables us to get a power spectrum at later time t_1 after the effects faded away:

$$P(k, t_1) = T^2(k, t_1) \left(\frac{D_+(t_1)}{D_+(t_0)} \right) P(k, t_0) \quad (2.43)$$

Here function D_+ denotes the linear, scale invariant growth of structures. To get a more general power spectrum one uses

$$P(k) = A' k T(k)^2 \quad (2.44)$$

with A' an arbitrary factor dependent on the time one looks at (fig.2.3). We will encounter these formulas again in a later chapter (4.1).

2.1.4 Inflation, Quintessence and the Cosmological Constant

Up to now the term *inflation* was mentioned several times. What does it actually mean? Within classical cosmology (as seen in section 2.1.1) there is no answer to following questions⁸:

1. *Why is the universe so flat?* From the field equations one yields

$$\Omega - 1 = \frac{\rho(t)}{\rho_c(t)} = \frac{k}{R^2(t)H^2(t)} \quad (2.45)$$

with $k = -1, 0, 1$. We now assume a conservative estimate in concordance with observations for the density of our universe today:

$$0.1\rho_c \leq \rho_0 \leq 10\rho_c. \quad (2.46)$$

Every deviation from $\rho_c(t)$ is growing with time towards the big bang: in a radiation dominated universe $\rho \sim R^{-4}$ and in a matter dominated universe $\rho \sim R^{-3}$. Therefore, to produce a universe with curvature near to flatness the deviation from flatness $10^{-36}s$ after the big bang must have been

$$\frac{|\rho(t) - \rho_c(t)|}{\rho_c(t)} \leq 10^{-50} \quad (2.47)$$

Even 1s after the big bang the deviation must have been smaller than 10^{-14} and therefore incredible flat. There is no reason for this flatness beyond special (better: strange) initial conditions.

⁷The *Meszaros effect* describes non-relativistic, collisionless particles in a radiation background, i.e. cold dark matter particles before the phase of decoupling of radiation and baryonic matter. (Meszaros, 1974)

⁸We left out here the question for monopoles and redirect to the literature for this (e.g. Klapdor-Kleingrothaus & Zuber, 1997)

2. *Why is the CMBR so isotropic?* The radius of the *event horizon* in an expanding universe is given by:

$$d_{eh}(t) = R(t) \int_0^t \frac{dt'}{R(t')} \quad (2.48)$$

Two points separated by $2d_{eh}$ from each other are not physically connected and cannot influence each other (e.g. exchange energy, heat, momentum). For the case of GUT⁹ symmetry breaking at temperatures of $\sim 10^{15}$ GeV, today's temperature of the cosmic microwave background and the relation $T \propto R^{-1}$ we get that R increased by a factor of $\sim 10^{26}$. The time for the GUT symmetry breaking was 10^{-35} s and therefore the horizon diameter was $2d_{ev} \simeq 10^{-27}$ m. This corresponds to a today's horizon diameter of $\simeq 1$ m. But the CMBR is isotropic on scales of 10^{26} m, i.e. we observe the same temperature in different directions and in regions which are not causally connected.

We have seen the influence of a cosmological constant resp. vacuum energy on the dynamics of the universe in eq.2.4 and eq.2.5. If the vacuum energy is the dominant factor we get exponential increasing solutions for the time-dependent behavior of the scale factor $R(t)$:

$$R(t) \simeq R(0)e^{Ht} \quad (2.49)$$

where $H = \sqrt{8\pi G\rho_V/3}$. Universes where the vacuum energy is responsible for exponential growth are called *inflationary universes*. Standard inflation is restricted to the GUT symmetry breaking phase. A scalar, weak interacting Higgs¹⁰ field Φ_H is requirement for a dominating vacuum energy. Via spontaneous symmetry breaking, i.e. the ground state does not have the full symmetry, the energy expectation value of the vacuum is not zero but below the value of the "normal" vacuum. This state is called *false vacuum* and within this state an exponential expansion is possible (Guth, 1981). The transition to "normal" expansion is done by tunneling to the "normal" vacuum state. There were different forms of potentials discussed which are able to let inflation happen, e.g. the *Coleman-Weinberg potential* $V_{CW}(\Phi) = 1/2B\sigma^4 + B\Phi^4(\ln(\Phi^2/\sigma^2) - 1/2)$ (see fig.2.4) or the *Linde potential* $V_L(\Phi) = \lambda\Phi^4$ (Klapdor-Kleingrothaus & Zuber, 1997).

In any case of an exponential expansion phase in the early universe the problems mentioned above can be solved quite naturally: flatness occurs by stretching out any fluctuations to trans-horizon scales, the isotropy in small regions was transferred to all scales.

More recently (Wetterich, 1995) proposed a new connection between inflation and the cosmological constant. He claims that the dark energy resp. cosmological constant could be caused by a scalar field left over from inflation. This field is called *quintessence field* and has the energy density and pressure

$$\rho_Q = \frac{1}{2}\dot{\Phi}^2 + V(\Phi) \quad p_Q = \frac{1}{2}\dot{\Phi}^2 - V(\Phi) \quad (2.50)$$

⁹GUT=Grand Unified Theory: theory which unifies three of the four known forces, electromagnetism, the weak force and the strong force. Such a theory is not found yet. Earlier versions, so-called SU5 theories, have been rejected by experiments finding the lifetime of the proton longer than predicted by the theories.

¹⁰The Higgs field is part of the *standard model* of particle physics. The *Higgs mechanism* assigns the masses to special elementary particles. The field quantum of the Higgs field, the *Higgs particle* is the last one to be found within the standard model

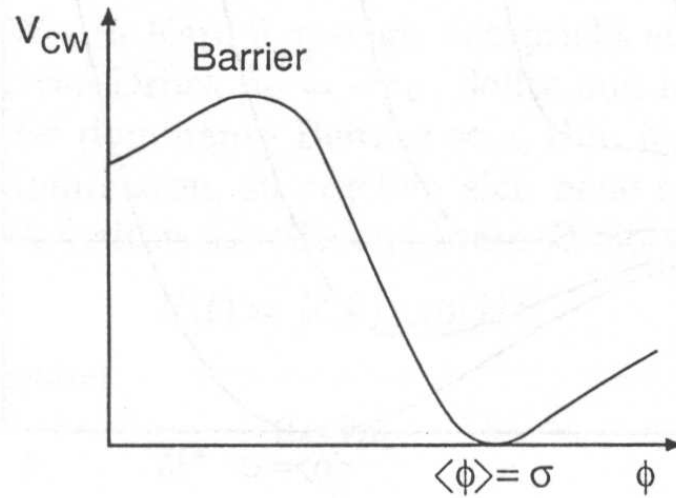


Figure 2.4: The Coleman-Weinberg potential as an example for a potential field (here: temperature dependent Higgs field) that can induce an inflationary expansion phase of an universe. σ is the vacuum state to where the field tunnels through the barrier. (Klapdor-Kleingrothaus & Zuber, 1997)

where $V(\Phi)$ is similar to the potentials used in inflation theories (see above). It is practical to define a constant equation of state with

$$\omega = \frac{p_Q}{\rho_Q} \quad (2.51)$$

A cosmological constant would have $\omega = 1$ while in quintessential models it differs from the value 1. Observations constraining the value to $1 \leq \omega \leq -1/3$ (Wang & Steinhardt, 1998) are quite difficult. A time-dependent value $\omega(t)$ is more general and even more difficult to verify. The advantage of quintessence is that it gives an explanation for the value of the dark energy with only little fine-tuning (Doran et al., 2001). Fig.2.5 shows the time-dependence of density parameter and clarifies that there is no clear difference between these models.

Wetterich, 2002 extended the quintessence models and tried to derive a “dark matter term” out of quintessence. Here he took into account that the scalar field responsible for the dark energy could have fluctuations on galactic scales which “mimics” dark matter. This interesting alternative has still to be proven.

2.2 Minor Merging Milky Way?

We are insignificantly creatures on a small rock orbiting a very average star in the outer suburbs of one of a hundred thousand million galaxies.

Stephen W. Hawking

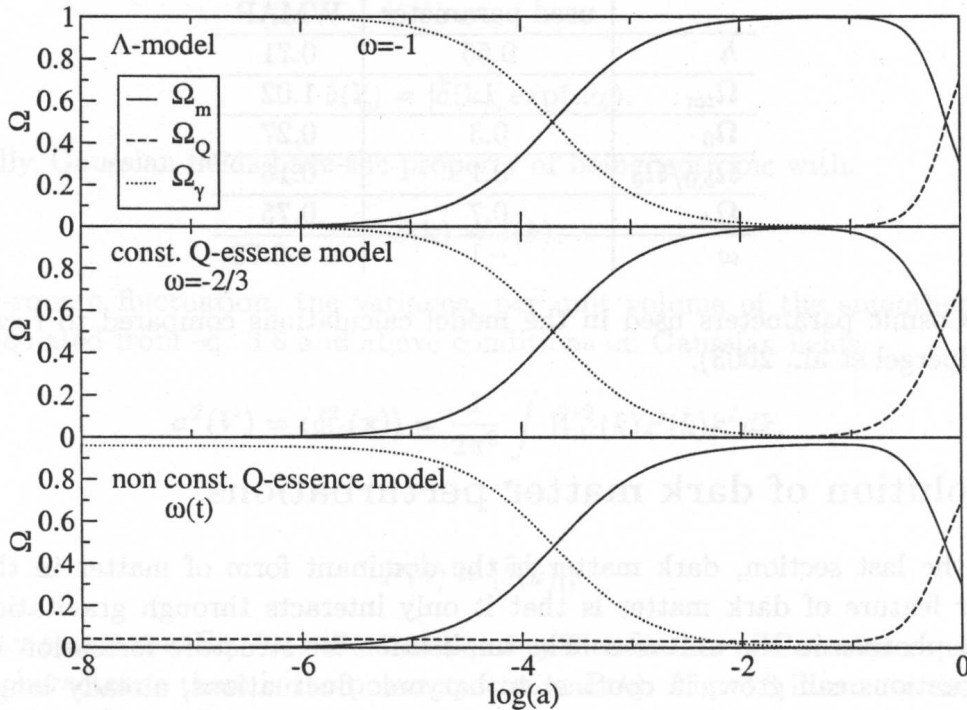


Figure 2.5: A comparison in the evolution of density parameters Ω dependent on cosmological constant resp. dark energy models. There are only slight differences which are not distinguishable in observations yet. (Khochofar, 2003)

2.2.1 Satellites and Tidal Streams

CDM models predict a large number of substructure around galactic halos. This leads to the quite famous “satellite problem” of CDM which has been stressed by Klypin and Moore in 1999 (Klypin et al., 1999, Moore et al., 1999). The problem is stated as “the lack of small satellites in observations of the local group compared to numerical simulations of local group objects” (see fig.2.6).

One would expect from simulations that there are about ten to hundred times more satellites than what we see in observations. There is an ongoing debate about the satellite problem, since it is not clear what causes the discrepancy: is it the missing feedback in CDM simulations which is able to push out gas out of the satellites so that they are present but dark (a hint to this could be given by the detection of nearly dark objects with high velocity dispersion of the stars in these objects)? Or is structure formation suppressed on small scales (as proposed by people who favor some kind of warm dark matter, see section 2.1.3)? The future has to show us a definite solution to this. We now focus on existing satellites around galactic halos, especially satellites disrupted while on their orbits around giant galaxies.

A nice example of a “tidal stream” and a disrupted satellite is the Sagittarius dwarf galaxy.

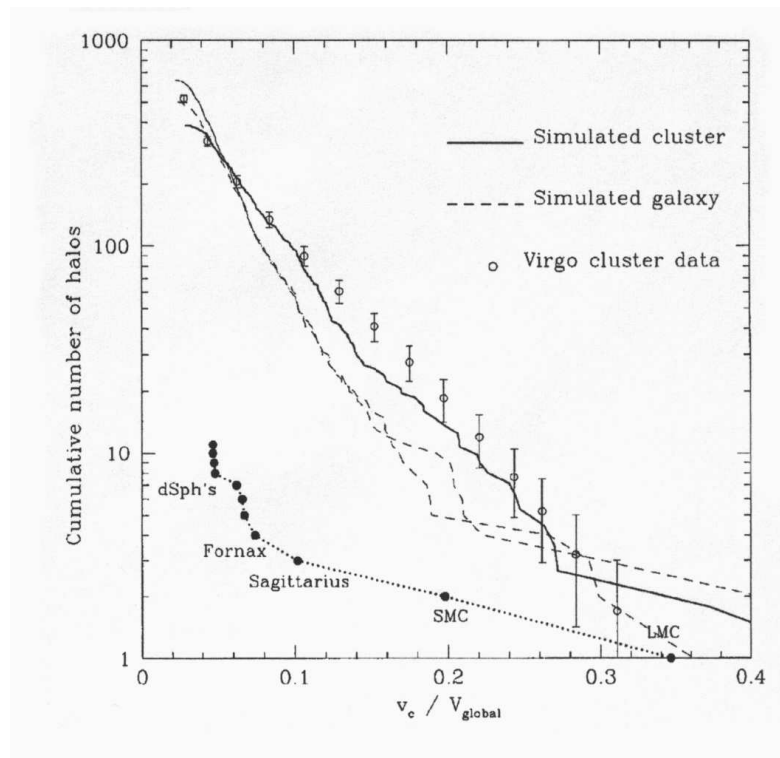


Figure 2.6: Cumulative number of cosmic substructure over the circular velocities within the Milky Way, the Virgo Cluster, and models of comparable masses (Moore et al., 1999) showing the “satellite problem”. Note that simulations can fit the abundance of halos in the Virgo cluster but fail miserably for the local group.

Detected in 1994 (Ibata et al., 1994), this galaxy with estimated mass of $10^7 M_{\odot}$ is on an orbit with the orbital plane nearly perpendicular to the galactic plane and is disrupted by the tidal field of our galaxy. This disruption leads to a so-called tidal stream of stars which is tracing the orbit of the dwarf galaxy.

Another nice example is Pal5, a globular cluster with estimated mass of $5 \times 10^4 M_{\odot}$ and nice leading and trailing streams. This tidal stream can also be modeled in numerical simulations to derive the depth and the shape of the Milky Way potential (Dehnen et al., 2004).

These are examples for small satellites being tidally disturbed/disrupted by the Milky Way. We also have examples for bigger satellites in the vicinity: the Large and the Small Magellanic Cloud. The Magellanic Clouds are a close binary of Irregular dwarf galaxies and are the nearest galactic neighbors to the Milky Way. The Large Magellanic Cloud (LMC) is at a distance of ≈ 52 kpc from us, the Small Magellanic Cloud (SMC) is at a distance of ≈ 63 kpc. The LMC has a mass of 6 to $20 \times 10^9 M_{\odot}$, the SMC 1 to $6 \times 10^9 M_{\odot}$. Together with our Milky Way the Magellanic Clouds form a loose triplet sharing a common barycenter located about 5 kpc from the center of our galaxy in the direction of the LMC (van der Marel et al., 2002, Weinberg, 1995). The LMC and SMC are on an orbit around this barycenter. This orbit is traced by the well known Magellanic Stream which consists mainly of neutral

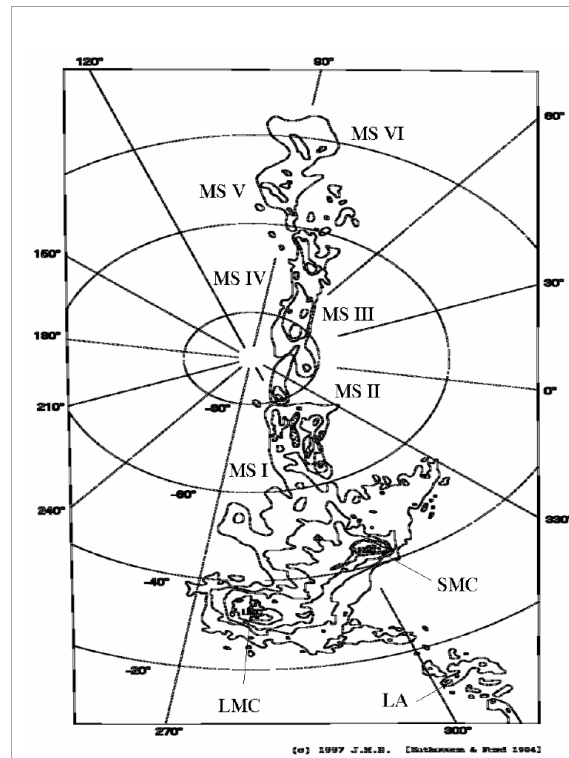


Figure 2.7: The Magellanic stream as it is seen on the sky. Shown here is the distribution of HI gas (Mathewson, 1985).

hydrogen (HI) stretching from horizon-to-horizon through the south galactic pole (see fig.2.7).

The stream is induced by the interaction of the MC's with the tidal field of our Milky Way (Mathewson, 1985). It can be reproduced well in numerical simulations (Maddison et al., 2002, Connors et al., 2004). Recent observational and theoretical analyses state that the clouds are close to peri-Galacticon (van der Marel et al., 2002, Gardiner et al., 1994, based on Murai & Fujimoto, 1980): closest approach of the clouds to the galaxy occurred ≈ 200 Myr ago with time for a complete orbit of ≈ 1.5 Gyr. Rough estimates yield that the LMC will merge with our Milky Way within the next ≈ 8 Gyrs (Lin et al., 1995) which makes it a perfect candidate for a so-called “minor merger” (i.e. mass ratio between merging galactic objects of 1:5 to 1:20).

2.2.2 Hints on Minor Merger of the Milky Way

Since there will be some time left until the Milky Way undergoes a minor merger with the LMC (and before that it will suffer from a major merger with the equally sized M31, the Andromeda galaxy) we now focus on following question: Did the Milky Way experience a minor merger in the past?¹¹ Depending on the time that has elapsed since this

¹¹It is clear that the Milky Way did not experience a major merger since it has an intact, flat disk which would have been destroyed in a major merger (Naab, 1998)

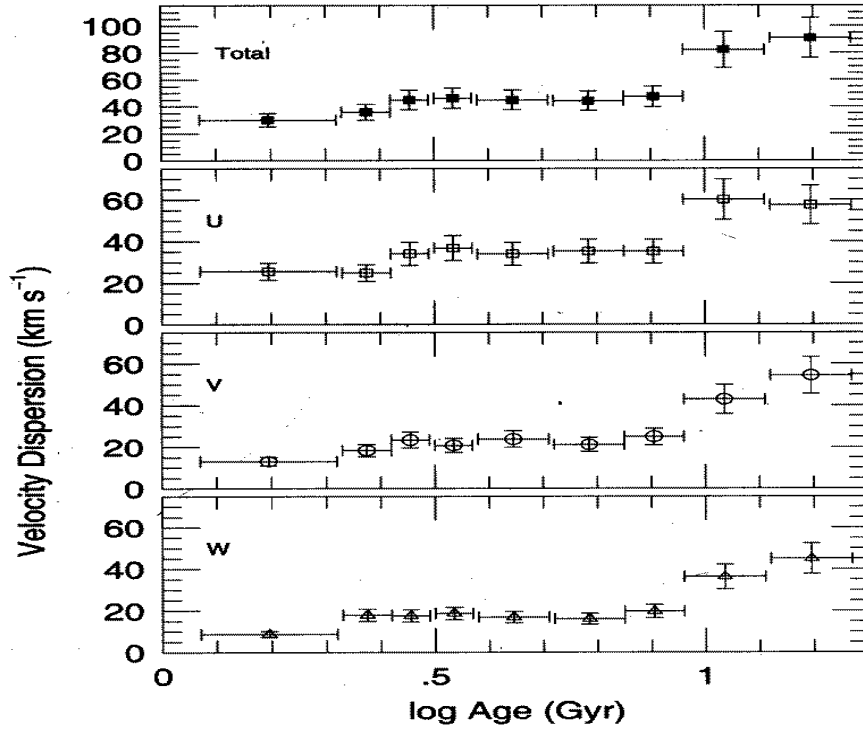


Figure 2.8: The “jump” in the velocity dispersion of old stars designating the “thick disk” - caused by a minor merger? (Quillen & Garnett, 2000)

minor merger one could observe streams of stars and gas left behind by the smaller companion and the impact of the merging event on the stellar disk (e.g. warping, heating, bar-inducing). We now give a short overview of possible hints on past minor merger events in the Milky Way.

A heated Milky Way?

It is a well known fact that the infall of a satellite with a substantial mass fraction of the stellar disk heats the disk, i.e. increases the vertical scale length and velocity dispersion of the disk stars (Toth & Ostriker, 1992, Velazquez & White, 1999, Bertschik, 2001). This can be demonstrated in the following way. The vertical kinetic energy K of a thin disk, depends on its velocity dispersion σ_z :

$$K_{disk,z} \propto M_{disk} \sigma_z^2 \quad (2.52)$$

where M_{Disk} is the mass of the disk. The kinetic energy of a satellite with mass M_{Sat} on a circular orbit with circular velocity v_c is:

$$K_{sat,z} \propto M_{sat} v_c^2 \quad (2.53)$$

Equating eq.2.52 with eq.2.53 yields the part f that leads to a certain vertical velocity

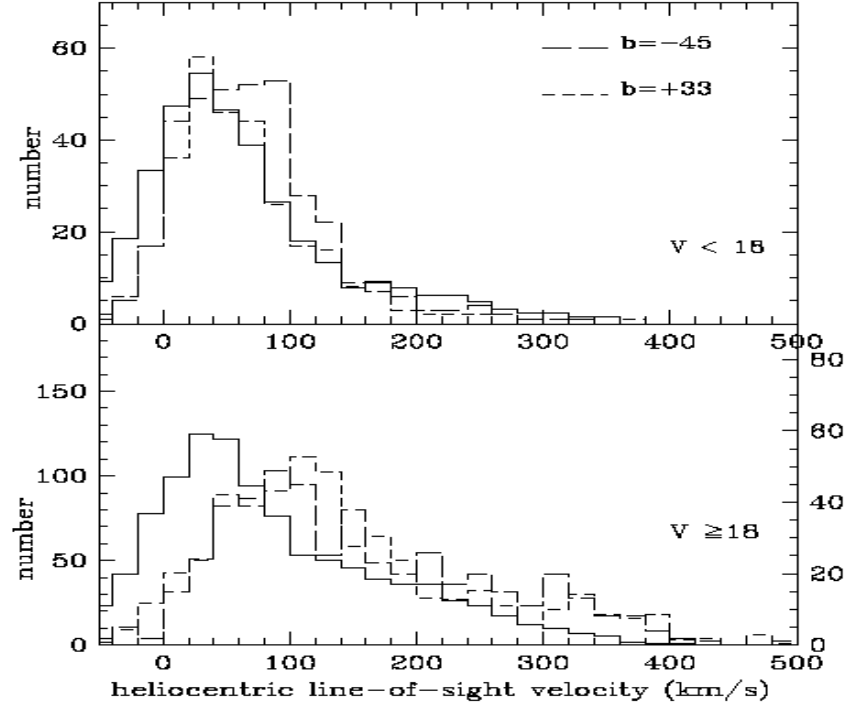


Figure 2.9: Line-of-sight velocity distributions of stars with $b=+33$ and $b=-45$. Upper graph: stars with V-band magnitude smaller than 18. Lower graph: stars with V-band magnitude higher than 18. Note that these stars have different velocity distributions than expected from the thin disk stars (solid line) - they are rotating slower than the thin disk stars (~ 100 km/s). Note also the bump in the distribution in the bottom graph at LOSV of ~ 300 km/s which corresponds to a counter-rotating population - remnants of a merged satellite? (Gilmore et al., 2002)

dispersion caused by the conversion of the kinetic energy of the satellite:

$$f \equiv \frac{M_{sat}}{M_{disk}} \sim \left(\frac{\sigma_z}{v_c} \right)^2 \quad (2.54)$$

For $\sigma_z \sim 40$ km/s and $v_c \sim 200$ km/s we get $f \sim 0.04$. This means that the disk has to accrete 4% of its mass to gain a velocity dispersion of 40 km/s. Of course this estimate is rough: it ignores that stars escape from the system and do not contribute to the heating anymore (e.g. in tidal tails). Additionally, the interaction with a dark matter halo is left out, making the heating more efficient in this estimate. But we have a general result that we can use for observations: *a hint for a minor merger in a stellar disk is a stellar component with an on average bigger scale height (meaning higher velocity dispersion)*. Gas in the disk is able to cool and dissipate its kinetic energy after the merger. Star formation from this gas again would be able to form a thin disk.

In fact, our Milky Way comprised such a kind of stellar population: the **thick disk**. As the name said, this component has a higher scale height than the much more massive thin disk and consists of predominantly old stars in contrast to the thin disk with younger stars

2.2 Minor Merging Milky Way?

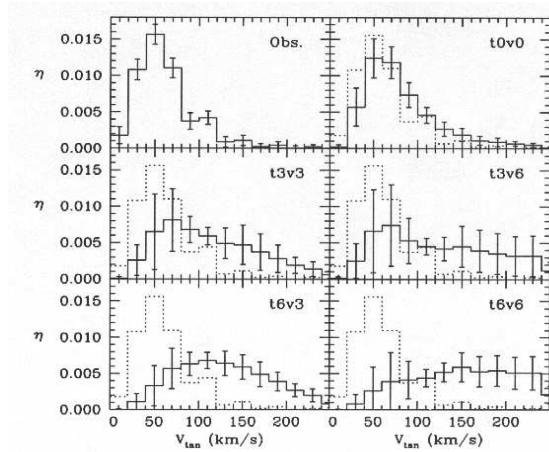


Figure 2.10: Results from Monte-Carlo simulations done by Torres et al., 2001. They modeled the tangential velocity distributions of white dwarfs of the galactic disk after the input of kinetic energy by, for example, a minor merger. The top left picture shows the observed distribution, the other pictures show results from simulations with increasing time (t in Gyrs) and/or increasing kinematical kick (factor v). In concordance with observations is an infalling satellite with $\sim 4\%$ of the disk mass (Torres et al., 2001). Note that the “smearing-out” of the distribution is dependent on time and magnitude of the kinematical kick.

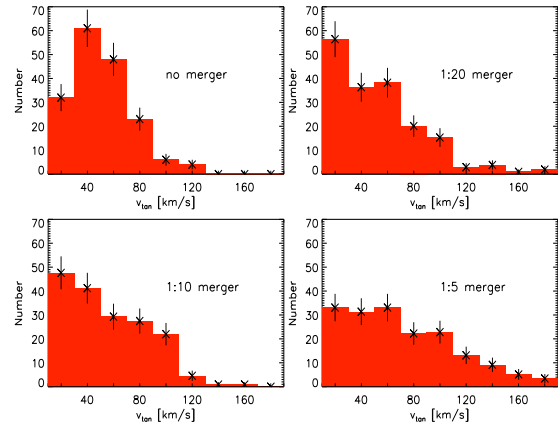


Figure 2.11: Results from numerical simulations (Bertschik & Burkert, 2003) showing the impact of an infalling satellite with decreasing mass ratio, i.e. increasing size of the satellite. In concordance with observations is an infalling satellite with $\sim 5\%$ of the disk mass. Note that the velocities are redistributed to higher velocities after the merger event. The magnitude of this redistribution is dependent on the mass ratio.

(like our sun). As Quillen & Garnett, 2000 found (fig.2.8), the increase of scale height of these population occurred quite suddenly, making a dynamically fast and efficient event like an infall of a satellite very likely. On the other hand, the thin disk suggests that there was no substantial minor merging event in the near past (i.e. lifetime of the thin disk). Different estimates yield a maximum accreted mass of $\sim 4\%$ within the last 5-6 billion years (Toth & Ostriker, 1992, Torres et al., 2001, Bertschik & Burkert, 2003). As seen in fig.2.10 and fig.2.11, a concordance value for the mass accreted by the Milky Way within the last 6 Gyrs is $\sim 5\%$ of the disk mass. Nevertheless, this does not exclude a more massive minor merger event earlier in the past.

Streams of past Minor Mergers?

A satellite in an accretion event or in a minor merger is generally disrupted by the bigger object and distributes its stars and gas along its orbit. The bigger object works on the satellite with tidal forces before it enters denser regions of the bigger object and work on the satellite with gravitational friction when it is within the denser regions. The satellite is deformed and losing material which leads to its disruption. This disruption was modeled in numerical simulations as well as in analytical considerations (Dehnen et al., 2004, Mihos, 2004). We have now another general result that we can use for observations: a

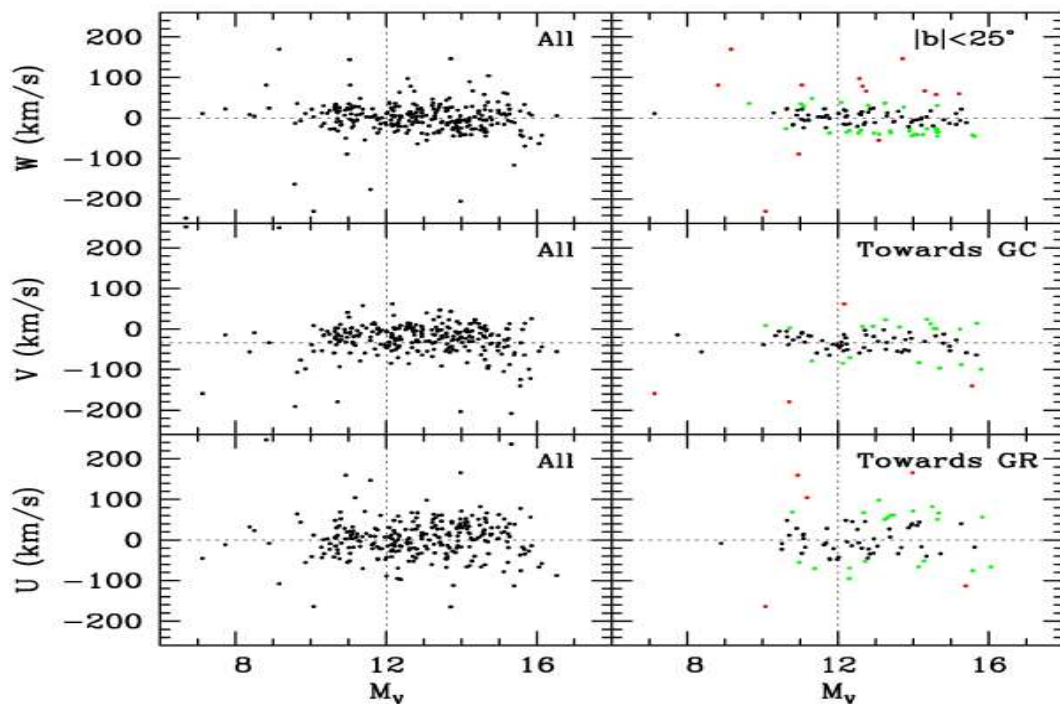


Figure 2.12: Velocities of old (~ 6 Gyrs) white dwarfs in galactic velocities U , V and W with respect to the V -band magnitude. Upper graph: white dwarfs within $b=25$, middle graph: white dwarfs towards galactic center, lower graph: white dwarfs towards galactic rotation. The difference between the left and the right panel is the additional color coding on the right: black color designates velocities within 1σ of the mean, green means velocities within 2σ and red designates velocities within 3σ . Note that there is a significant population of white dwarfs in W velocity exceeding the 3σ -expectation - remnants of a minor merger? (Torres et al., 2002)

hint for a minor merger in a stellar disk is material that moves on significantly different orbits than the disk material.

In fact, there are observations of certain stellar populations indicating a special origin like a merging or accreting event. As Gilmore et al., 2002 pointed out they found such a kind of population that is counter-rotating with respect to the stars of the thin disk. Additionally, they found that the thick disk rotates more slowly than the thin disk, supporting the idea of an merger origin (fig.2.9, Gilmore et al., 2002).

Another observation was done by Yanny et al., 2003. They stated that they found a ring-like structure in the galactic disk plane around our Milky Way. This ring may well be the remnant of an disrupted satellite (fig.2.13, Martin et al., 2004).

Additionally, there are observations of some old white dwarfs (fig.2.12, Torres et al., 2002) with velocities quite different from the thin disk stars: There are significantly more white dwarfs in the high-velocity regime than expected from statistics. Their origin is unknown yet but they may be disk stars which have been brought out of their original orbit by a merger as well as the remnants of an disrupted satellite.

2.3 Conclusion and Discussion

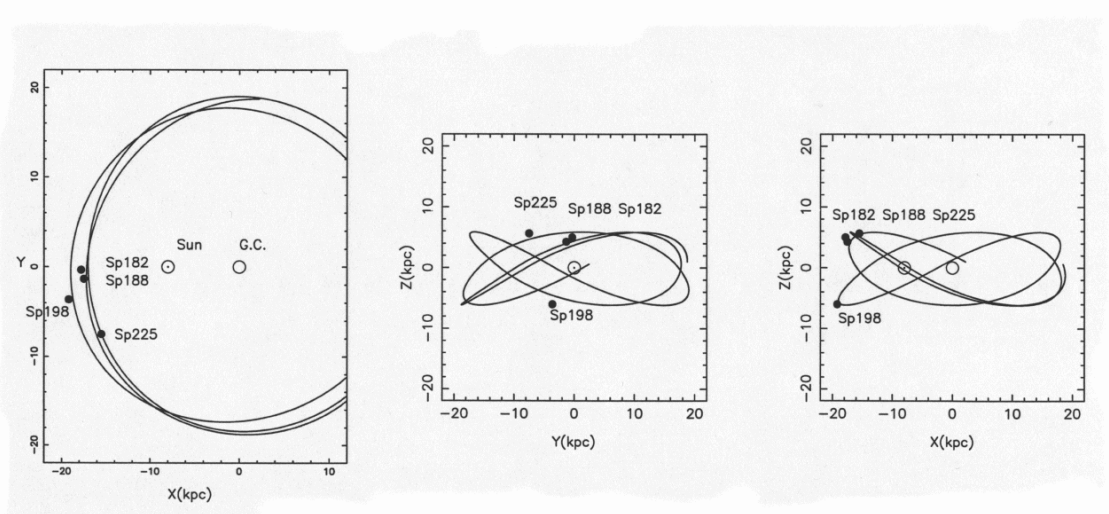


Figure 2.13: Galactic projections of the possible orbits of the stars in the ringlike stream detected by Yanny et al., 2003

2.3 Conclusion and Discussion

We saw that from a cosmological point of view there are many reasons to expect lots of substructure around halos of the size of our Milky Way. The concordance model Λ CDM with cosmological parameters found by WMAP supports hierarchical structure formation where bigger structures are build up by the merging of smaller structures. This merging history is not finished yet, we can still see even smaller objects in merging processes with bigger galaxies (e.g. Schwarzkopf & Dettmar, 2000a, Schwarzkopf & Dettmar, 2000b Bertschik, 2001). But how often do these “minor merger” occur? What distributions of mass ratios within a certain mass range can we expect? What are the kinematical parameters of such a merging event? What are the effects of such minor merger on a stellar disk? Can they be detected by looking at velocity distributions?

These questions will be addressed in this work.

Chapter 3

Numerics

A philosopher once said, 'It is necessary for the very existence of science that the same conditions always produce the same results'. Well, they don't!

Richard P. Feynman

This chapter presents some information necessary for carrying out numerical simulations. With increase of computer speed, computational physics has become more and more important for testing (more or less) simple models in physics. The first part focuses on the code WINE and its features. The second part of this chapter describes the special hardware GRAPE used with the code.

3.1 The Code WINE

The theory group at the Max-Planck-Institut für Astronomie developed an own evolution code for simulations for a wide range of astrophysical problems. Since it is somewhat hard to find a good acronym for a new project (which is quite common within the astronomical society) we called this code WINE: What an Interesting name for a New Evolution code¹. WINE simulates collisionless N-body problems as well as gas dynamics using the SPH formalism and is optimized for different computer architectures (ordinary PCs, special purpose hardware, parallel computers).

3.1.1 The Gravity Part: the Tree

Wine uses a binary, mutual nearest neighbour tree structure (Press tree) for particle book-keeping. Thus the tree structure closely follows the geometrical structure of the modeled system. This tree structure can be used for several subsequent time steps before the tree has to be rebuilt. The tree has been modified from the original form (Press, 1986):

- The tree is traversed for groups of particles to increase computational efficiency (Barnes, 1990). This also improves the speed of the special purpose hardware GRAPE (see chapter 3.2).

¹Probably with a final version of the code the name will change to *VINE*: Very Interesting Name for an Evolution code

3.2 The GRAPE System

- The tree traversal is performed with the “depth first” method of Dubinski (Dubinski, 1996). That results in an additional speedup.
- Distant tree nodes must pass a refined opening criterion given by Warren&Salmon (Warren & Salmon, 1995). The criterion allows to control the maximum absolute force error due to each node.

3.1.2 The Gravity Part: Force Computation

The gravitational forces can either be calculated on parallel computers (shared memory systems), general purpose CPUs (e.g. Intel or AMD based) or on the special purpose hardware GRAPE (see chapter 3.2). The tree traversal as well as the actual computation of the gravitational force is fully parallelized, which makes it very efficient on multiprocessor systems with attached GRAPE boards. The user is free to choose between two different integrators: Leap-Frog and Runge-Kutta.

3.1.3 Parallel Computing

WINE is written as a parallel code using the OpenMP directives. All tree operations, the gravity calculations and the SPH calculations are parallelized. Experience with a 2D version has shown a nearly linear speedup to at least 8 processors on systems with 10^5 particles.

3.1.4 Other Features

The speed of WINE is increased further by using individual time steps for the particles. This allows the computation of highly active regions without wasting time on computing less active regions to same accuracy. We use the individual time step scheme of Hernquist&Katz (Hernquist & Katz, 1989).

In addition to the usual artificial viscosity, the SPH method uses a Balsara viscosity (Balsara, 1990) and time-dependent viscosity coefficients (Morris & Monaghan, 1997) in order to reduce unwanted dissipative effects.

For the N-body particles, an adaptive softening method has been implemented in addition to the usual Plummer softening. This new method improves the resolution in high density regions.

Furthermore, periodic boundary conditions and cosmological expansion have been added to the code in order to calculate cosmological problems.

Due to its modular structure, additional features (e.g. SPH ionization, star formation, feedback, MHD) can be added easily to the code.

3.2 The GRAPE System

The theory group at the MPA uses several different boards of the so called GRAPE system. The GRAPE system follows the simplest approach to the N-body problem: it sums up the forces exerted by each particle to every particle. This offers a large dynamic range in spatial resolution and is not limited by the choice of a special geometry of the problem. On the other side it suffers from calculation time that scales with $\mathcal{O}(N^2)$ while other

calculations (e.g. time integration) scale with $\mathcal{O}(N)$. There are two common solutions to this problem:

1. One uses the fact that near particles influences the trajectory of a particle more than far away particles. Tree codes collect together the particles far away and build up groups which are handled like a single particle (with a quadrupole moment). This reduces the calculation time to one growing with $\mathcal{O}(N \log N)$.
2. One hard-wires the calculation algorithm on a chip and parallelizes it to gain calculation time by brute force calculation power.

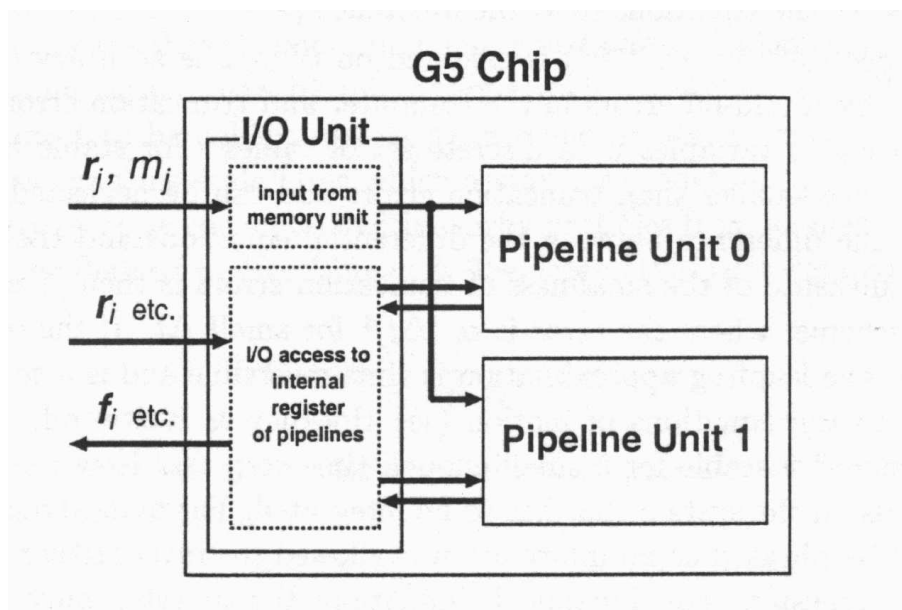


Figure 3.1: The structure of the GRAPE5 chip

The second point is the way the GRAPE project followed by Kawai et al., 2000 in the last decades and they gave it the name: GRAVity PipelinE. In this sense the GRAPE chip is a RISC (Reduced Instruction Set Chip, compare to CISC: Complex Instruction Set Chip) chip “to the max”: there is only one instruction followed by the chip. Kawai et al., 2000 specially designed, pipelined and highly parallelized the gravitational force between two particles:

$$\vec{F}_i = - \sum_{j \neq i} \frac{Gm_i(\vec{x}_i - \vec{x}_j)}{(|\vec{x}_i - \vec{x}_j|^2 + \epsilon^2)^{3/2}} \quad (3.1)$$

Fig.3.3 shows the basic structure of a GRAPE-5-system. The GRAPE board is connected to a host workstation where an appropriate code is running and handling the I/O. The host computer sends positions and masses of all particles of a simulation to the GRAPE system. The GRAPE board (fig.3.2) calculates the gravitational force between the particles (this calculation is done by the GRAPE chip, see fig.3.1) and sends it back to the host computer. As an additional feature, GRAPE delivers a list of neighbours inside a given radius

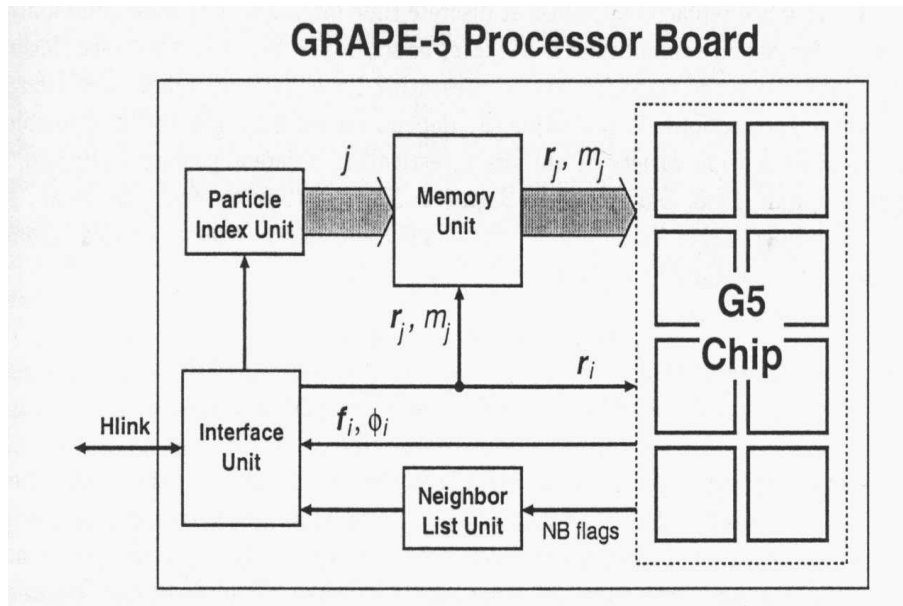


Figure 3.2: The structure of the GRAPE5 board

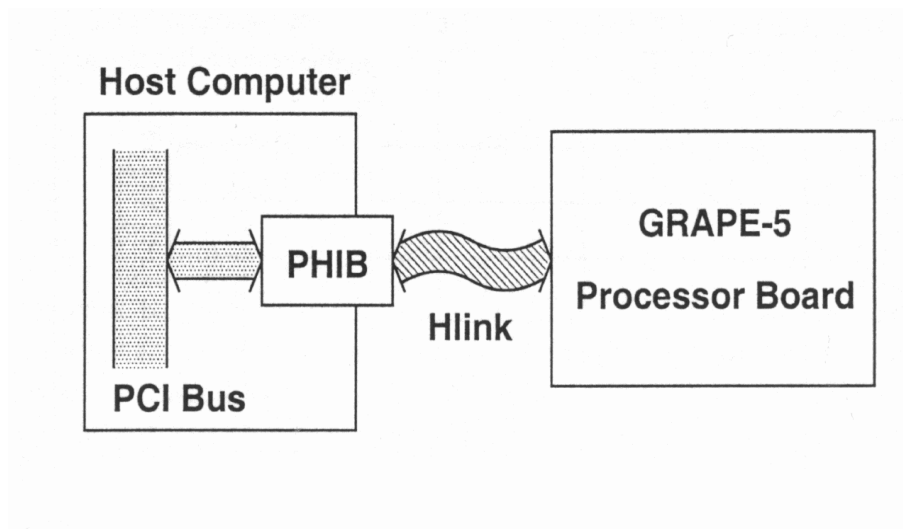


Figure 3.3: Scheme of the connection and communication of the GRAPE board with a host PC

around a particle. This neighbour list can be used within the SPH² formalism. All other calculations are done on the host computer.

The simulations for this work were done on GRAPE-5 boards with a peak performance of two pairwise force calculations per clock cycle. If assuming 30 operations for one force

²The *Smoothed Particle Hydrodynamics* (SPH) formalism was invented to describe systems including gas and/or fluids. SPH handles these phenomena by introducing an artificial viscosity and internal energy. This assures the dissipative nature of gas and fluids in contrast to dissipationless N-body systems

calculation, and 8 chips, each running with 80MHz, this results in a peak performance of 38.4Gflops. Fast as it is, a bottleneck is not the calculation power anymore but the transfer of the data forth and back through the interface. A collaboration between the MPIA and the University of Mannheim resulted in a new PCI-standard interface fast enough to handle the amount of data.

3.3 GRAPE and WINE

The simulations for this work were done with WINE using the special purpose hardware GRAPE. The cosmological simulations used the “cosmo module” of WINE meaning the expansion of space (modified acceleration and velocities of particles) and the periodic boundary conditions (modified acceleration and positions of particles). WINE is able to use the “best of both worlds” for optimal speed: the problem is formulated within the tree algorithm and the forces within the tree are calculated directly on the fast GRAPE hardware.

Chapter 4

Methods

I have the result, only I do not yet know how to get to it!
C.F. Gauss

This chapter presents the methods used for the setup of simulations and for their analysis. The first part focuses on the program GRAFIC used for the setup of cosmological initial conditions. The second part of this chapter describes the friends-of-friends algorithm and its parameter. The third part explains the setup of a simulation of a galactic disk undergoing a minor merger. The fourth part presents an algebraic approach to the Kepler problem. Last but not least we mention the parameters used in the simulations.

4.1 Cosmological Initial Conditions with GRAFIC

The program GRAFIC by Ed Bertschinger (Bertschinger, 2001) calculates a density and a velocity field for cosmological initial conditions via a Gaussian random field (as the name GRAFIC says: Gaussian Random Field Initial Conditions). To be more exact, GRAFIC normalizes the power spectrum of matter density fluctuations and generates the initial conditions for non-linear cosmic structure formation simulations. It produces the density fluctuation field $\delta(\vec{x})$ (that is $\delta\rho/\rho$) in comoving coordinates as a Gaussian random field. The power spectrum is calculated via a transfer function where the cosmological parameters are put in to derive quantities like the critical density. GRAFIC outputs both the density field and the initial positions and velocities of particles displaced from the lattice to produce that density field. The former object is useful for initializing cosmological gas dynamics solvers, while the latter quantities are needed for cosmological N-body simulations. They are related to each other using the Zel'dovich approximation:

$$\vec{x}(\vec{q}, \tau) = \vec{q} + D_+(\tau)\vec{d}(\vec{q}), \quad \vec{v}(\vec{q}, \tau) = \dot{D}_+(\tau)\vec{d}(\vec{q}); \quad \vec{\nabla} \cdot \vec{d} = -D_+^{-1}\delta(\vec{q}, \tau). \quad (4.1)$$

Here \vec{q} is a Lagrangian coordinate corresponding to the unperturbed comoving position of a mass element. GRAFIC takes these positions to be on a regular Cartesian grid with periodic boundary conditions. \vec{x} are the perturbed comoving positions. The perturbations grow in proportion with the cosmic growth factor $D_+(\tau)$ which depends on the cosmological model. The displacement field $\vec{d}(\vec{q})$ is obtained by calculating the inverse Laplacian of the linear density field using a fast Fourier transform. The approximation comes in

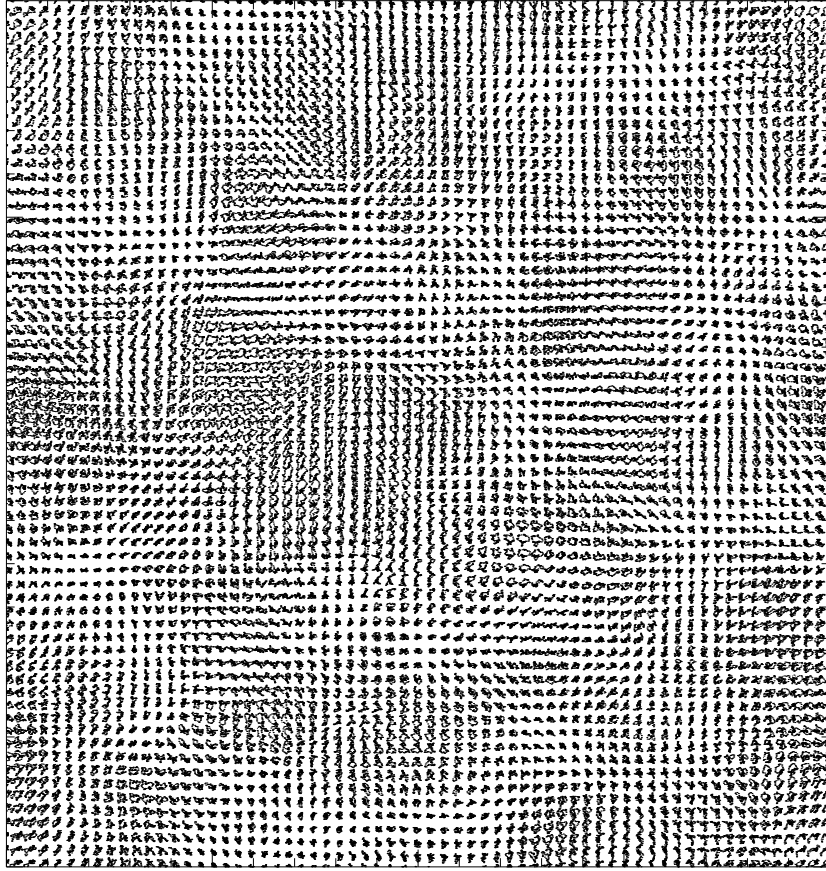


Figure 4.1: Initial conditions set up with GRAFIC. Shown is the density field at $z=42.9$ for a box with 20Mpc length in projection on one side of the box

the third equation of eq.4.1 which neglects terms of the order $O(\delta^2)$. GRAFIC automatically selects the output redshift high enough so that the maximum density fluctuation has amplitude 1. The proper peculiar velocity \vec{v} follows straightforwardly. GRAFIC includes subroutines that compute $D_+(\tau)$, $\dot{D}_+(\tau)$, $R(\tau)$ etc. for general Friedmann-Robertson-Walker-Lemaître models with matter, vacuum energy and curvature. Here we used GRAFIC to generate initial conditions for cosmological simulations with following cosmological parameters:

cosmological parameter	used value	value found by WMAP
h	0.71	0.71
Ω_{tot}	1.0	1.02
Ω_{matter}	0.27	0.27
Ω_{Λ}	0.73	0.75
$\Omega_{baryon}/\Omega_{matter}$	0.16	0.16
n	1.0	0.99
σ_8	0.9	0.9

4.2 FOF: friends-of-friends Algorithm

The algorithm FOF (Friends-Of-Friends) searches for gravitationally bound groups of particles within a simulation box (N-body shop, 2001, Davis et al., 1985). It uses only one parameter, the so-called *linking length* l which is defined as:

$$l = b \frac{d}{n^{1/3}} \quad (4.2)$$

where b is an empiric, dimensionless value (see below) and $n^{1/3}$ the particle density per unit length d . A particle belongs to a friends-of-friends group if it is within this linking length of any other particle in the group (see fig.4.2). After all such groups are found, those with less than a specified minimum number of group members are rejected. FOF then writes a file with the particle indices and the group number the particle belongs to. Our version of FOF was modified to read ASCII-files of our dumps. One has to choose

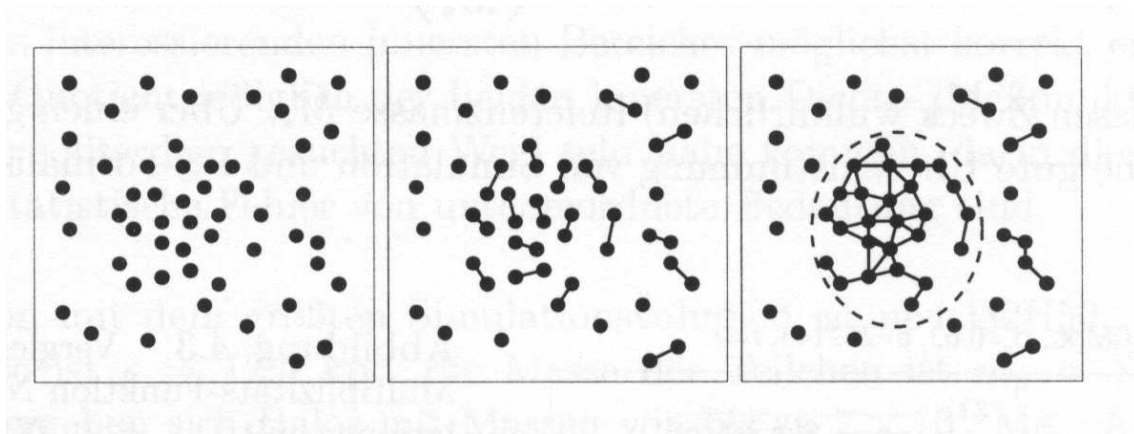


Figure 4.2: An example how the linking-length links a group together. The lines denote the connection of neighbor particles within the linking length, the dashed line shows the group found by FOF. (Graphic kindly provided by Helmut Hetzner)

carefully the linking length to get a reasonable clump with proper mass and radius. This has to be found empirically: the parameter b . For this one assumes a density which corresponds to a virial radius r_{200} , virial mass M_{200} and virial velocity v_{200} . The virial radius is that radius for which the mean density

$$\langle \rho \rangle = 200\rho_{crit} \quad (4.3)$$

4.3 Initial Conditions for a Minor Merging Galaxy

where $\rho_{crit} = \frac{3H^2}{8\pi G}$ is the critical density of the Einstein-de Sitter universe (this density changes slightly in Λ -dominated universes, see below). Therefore, the virial mass is

$$M_{200} = \frac{4\pi}{3} \langle \rho \rangle r_{200}^3 \quad (4.4)$$

and the virial velocity is

$$v_{200} = \sqrt{\frac{GM_{200}}{r_{200}}} = r_{200} \sqrt{\frac{4}{3} \pi \langle \rho \rangle G}. \quad (4.5)$$

For cosmologies with $\Lambda \neq 0$ the density contrast Δ_c develops different:

$$\Delta_c = 178 \begin{cases} \Omega^{0.30}, & \text{if } \Lambda = 0 \\ \Omega^{0.45}, & \text{if } \Omega + \Lambda = 1 \end{cases} \quad (4.6)$$

Therefore, the value for b changes to 0.164 for Λ CDM cosmologies (see e.g. Goetz et al., 1998) and is used in this work.

Of course the minimum number of particles in a FOF halo has to be chosen carefully. We chose 30 particles per halo as a minimum number which takes into account limited resolution, time and memory of our systems and still allows to calculate in a reasonable way values of virial masses, center of masses etc.

4.3 Initial Conditions for a Minor Merging Galaxy

The galactic disk model used in this work was worked out by Hernquist (Hernquist, 1993a) using observations of the stellar dynamics in our Milky Way. It describes a compound model of a galactic disk in a state of quasi-equilibrium. Hernquist used the fact that the lowest order moments of the Boltzmann equation are determined by the density distribution of the components. One calculates these moments and approximates the distribution function in velocity space by well known distribution functions (Gauss distribution). This procedure is an approximation, so the system will not be in equilibrium in the first place. But it should reach it in quite a short time.

The choice of components is related to the simulations mentioned later on. The model of a disk galaxy consists a disk (see section 4.3.1) and an alive (i.e. self-gravitating) dark matter halo (see section 4.3.2). The minor merging satellite is realized by a system with a Hernquist-density profile which is in agreement with observations of spherical dwarf galaxies and therefore a reasonable choice for a small companion merging with a galactic disk.

The units of length, mass and time are introduced as follows: the gravitational constant is $G = 1$, the exponential horizontal scale length $h = 1$ and the disk mass is $M_d = 1$. Scaled to the sizes of the Milky Way this leads to $M_d = 5.6 \times 10^{10} M_\odot$ as unit mass, $h = 3.5 \text{ kpc}$ as unit length, unit time $t_u = 1.31 \times 10^7 \text{ yr}$ and unit velocity $v_u = 262 \text{ km/s}$.

4.3.1 The Disk

In agreement with observations in our Milky Way and of other galaxies it is assumed that the density distribution declines exponentially with the cylindrical radius and that the system is isothermal (constant velocity dispersion) perpendicular to the galactic plane (Bahcall & Soneira, 1980):

$$\rho_d(R, z) = \frac{M_d}{4\pi h^2 z_0} \exp(-R/h) \operatorname{sech}^2\left(\frac{z}{z_0}\right). \quad (4.7)$$

Here M_d is the disk mass, h the radial scale length and $z_0/2$ the vertical scale height which according to observations is independent from the galactic radius (van der Kruit & Searle, 1981 van ver Kruit & Searle, 1982, fig.4.3)

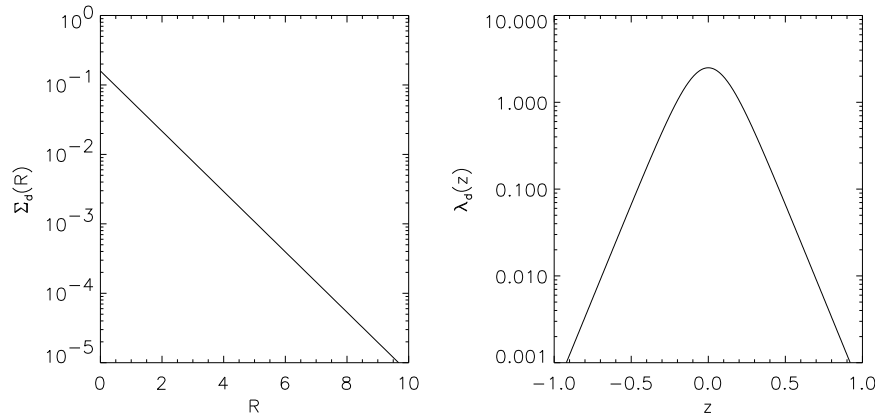


Figure 4.3: The surface density $\Sigma(R)$ of the disk versus the cylindrical radius (left) and the linear density $\lambda(z)$ perpendicular to the disk plane with $z_0 = 0.2$ (right).

The base for the setup of the velocities are the moments of the *collisionless Boltzmann equation* (also called *Vlasov equation*)

$$\frac{\partial f}{\partial t} + \vec{v} \frac{\partial f}{\partial \vec{r}} - \nabla \Phi \frac{\partial f}{\partial \vec{v}} = 0 \quad (4.8)$$

where f is a phase space distribution or distribution function of masses within the 6D phase space $d\vec{r} d\vec{v}$.

With the first and second moments specified, disk velocities are initialized as follows

1. draw v_z from a Gaussian distribution with dispersion $\sqrt{\overline{v_z^2}}$ where

$$\overline{v_z^2} = \pi G \Sigma(R) z_0 \quad (4.9)$$

with $\Sigma(R)$ the surface density of the disk.

2. calculate v_R by drawing from a Gaussian with dispersion $\sqrt{\overline{v_R^2}}$ where

$$\overline{v_R^2} \propto e^{(-\sqrt{R^2 + 2a_z^2}/h)} \quad (4.10)$$

4.3 Initial Conditions for a Minor Merging Galaxy

with a_s a arbitrary softening parameter (usually $a_s \sim h/4$) to avoid imaginary numbers.

3. compute the random component of the azimuthal velocity v_ϕ by drawing a Gaussian with dispersion $\sqrt{\sigma_\phi^2}$ where

$$\sigma_\phi^2 = \frac{v_R^2 \kappa^2}{4\Omega^2} \quad (4.11)$$

with κ the epicyclic frequency defined by $\kappa^2 = \frac{3}{R} \frac{\partial \phi}{\partial R} \frac{\partial^2 \phi}{\partial R^2}$ and Ω the angular frequency computed by the potential.

4. calculate the Cartesian velocities in the plane (i.e. v_x and v_y) by adding together v_R , the random azimuthal velocities and $\overline{v_\phi}$

4.3.2 The Halo

For the halo component it is necessary that it can reproduce the observed flat rotation curves of galaxies. Because the distribution of dark matter (if there is any) and its extent is not known, one has to choose a phenomenological ansatz for a potential-density pair that reads:

$$\rho_h(r) = \frac{M_h \alpha}{2\pi^{3/2} r_c} \frac{\exp(-r^2/r_c^2)}{r^2 + y^2}, \quad (4.12)$$

$$\Phi_h(r) = -\frac{GM_h(r)}{r} + \frac{GM_h \alpha}{\sqrt{\pi} r_c} Ei \left[-\left(\frac{r}{r_c}\right)^2 - q^2 \right] \quad (4.13)$$

with

$$M_h(r) = \frac{2M_h \alpha}{\sqrt{\pi}} \int_0^{\frac{r}{r_c}} \frac{x^2 \exp(-x^2)}{x^2 + q^2} dx. \quad (4.14)$$

Ei is a exponential integral:

$$Ei(z) = \int_{-z}^{\infty} \frac{\exp(-t)}{t} dt, \quad (4.15)$$

The normalization constant is α :

$$\alpha = \{1 - \sqrt{\pi} q \exp(q^2) [1 - \text{erf}(q)]\}^{-1}, \quad q = \frac{y}{r_c}. \quad (4.16)$$

In order to produce a flat rotation curve the density depends on r as:

$$\rho_h \propto r^{-2}. \quad (4.17)$$

A core radius y is introduced to avoid the singularity at the center. In addition, a cut-off radius reduces the effective extent of the halo which is justified: the outmost parts don't account significantly to the potential and their leaving-out reduces calculation time. Fig. (4.4) shows the halo density in comparison to the density of a modified isothermal sphere

$$\rho(r) = \frac{\rho_0}{1 + (r^2/y^2)}, \quad (4.18)$$

which is frequently used for an external potential of a halo. (Quinn et al., 1993; Quinn & Goodman, 1986). One recognizes the deviation for the cut-off radius at larger radii. The model with a cut off halo potential was widely used in numerical simulations. (u.a. Hernquist, 1993b; Hernquist et al., 1993; Walker et al., 1996; Heyl et al., 1996).

To calculate the velocity distribution of the halo particles one focuses on the case of a

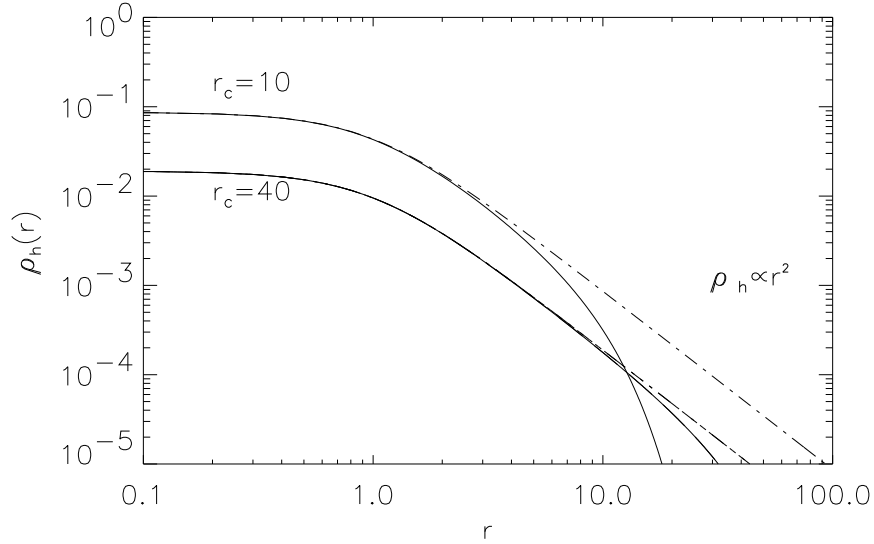


Figure 4.4: The solid line shows the density of the halo $\rho_h(r)$ versus r for two different cutoff radii. For comparison the dashed line denotes the density of a quasi isothermal sphere (4.18).

spherical, non-rotating system:

$$\overline{v_\theta^2} = \overline{v_\phi^2}. \quad (4.19)$$

For the case of isotropy one gets

$$\overline{v_r^2} = \overline{v_\theta^2} = \overline{v_\phi^2} \quad (4.20)$$

The velocity dispersion is given by the Jeans equation in spherical coordinates:

$$\overline{v_r^2} = \frac{1}{\rho_h(r)} \int_r^\infty \rho_h(r) \frac{d\Phi}{dr} dr = \frac{1}{\rho_h(r)} \int_r^\infty \rho_h(r) GM(r) dr. \quad (4.21)$$

where Φ owns all the gravitational input of all components and $M(r)$ is the cumulative mass function. If we perform numerical integration we get for the velocity distribution:

$$F(v, r) = 4\pi \left(\frac{1}{2\pi\sigma^2} \right)^{3/2} v^2 \exp(-v^2/2\overline{v_r^2}) \quad (4.22)$$

with the normalization

$$\int_0^\infty F(v, r) dv = 1, \quad (4.23)$$

Empirical tests yield that this configuration is quite stable even with addition of a stellar disk.

4.3.3 The Satellite (Hernquist Profile)

For the satellite we need a reasonable model of an extended particle distribution. The satellite is disrupted when merging with the galaxy and the particles are distributed elsewhere.

Spherical galaxies have an observed isophotal shape which can be described by the empirical brightness distribution (*de-Vaucouleurs law*)

$$\log_{10} \left[\frac{I(R)}{I(R_e)} \right] = -3.331 \left[\left(\frac{R}{R_e} \right)^{1/4} - 1 \right]. \quad (4.24)$$

Here R is the projected radius, R_e the effective radius of the isophote that is keeping the half of the total brightness, and I is the surface brightness.

Hernquist now describes a density distribution whose projected surface density reproduces the de-Vaucouleurs quite well (Hernquist, 1990; Burkert, 1993). The potential-density pair is:

$$\rho_h(r) = \frac{M}{2\pi} \frac{a}{r} \frac{1}{(r+a)^3} \quad (4.25)$$

and

$$\Phi(r) = \frac{-GM}{r+a} \quad (4.26)$$

with the cumulative mass distribution

$$M(r) = M \frac{r^2}{(r+a)^2}. \quad (4.27)$$

where M is the total mass and a the scale length of the system (see fig. 4.5).

For a non-rotating, spherical system (see section 4.3.2) which is in addition isotropic (i.e. $\beta(r) = 0$) we have $\overline{v_r^2} = \overline{v_\theta^2}$ and we get with eq. 4.26 and eq. 4.25:

$$\overline{v_r^2} = \frac{GM}{12a} \left\{ \frac{12r(r+a)^3}{a^4} \ln \left(\frac{r+a}{r} \right) - \frac{r}{r+a} \left[25 + 52 \frac{r}{a} + 42 \left(\frac{r}{a} \right)^2 + 12 \left(\frac{r}{a} \right)^3 \right] \right\}, \quad (4.28)$$

We have now an analytical solution for the radial velocity dispersion. For a spherical system the kinetic energy is:

$$T(r) = 6\pi \int_0^r \rho \overline{v_r^2} r^2 dr. \quad (4.29)$$

The total kinetic energy for $r \rightarrow \infty$ is:

$$T_{tot} = \frac{GM^2}{12a}. \quad (4.30)$$

The total potential energy is:

$$\Omega_{tot} = 2\pi \int_0^\infty \rho(r) \Phi(r) r^2 dr. \quad (4.31)$$

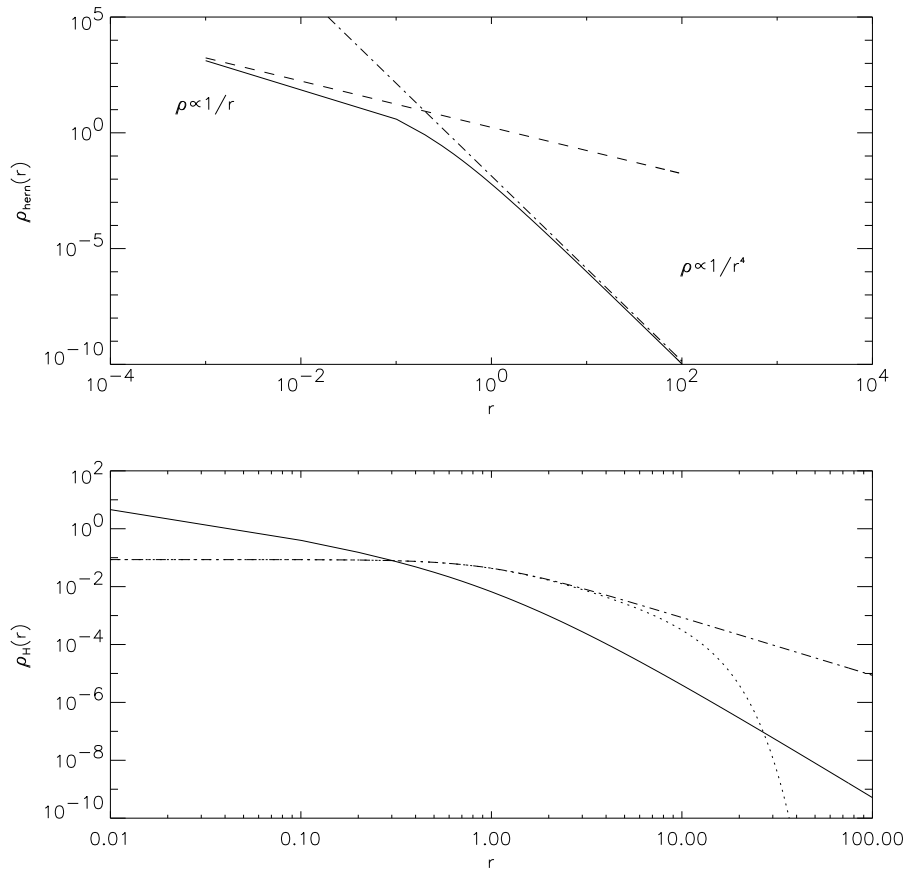


Figure 4.5: The upper picture shows the Hernquist density profile with scale length $a = 0.2$. In the picture below we have for comparison the Hernquist profile with scale length $a = 1.0$ (straight line), the cut profile (4.12) with $\gamma = 1.0$ (dotted line) and a modified isothermal sphere (4.18) with $\gamma = 1.0$ (dashed line).

That means for this model:

$$\Omega_{tot} = -\frac{GM^2}{6a} \quad (4.32)$$

In concordance with the virial theorem we get for this model in equilibrium $2T_{tot} + \Omega_{tot} = 0$. For a spherical, isotropic model $f(\mathbf{r}, \mathbf{v})$ is a function of the total specific energy $f(E)$. The distribution function can be calculated analytically via Abelian transformation. The coordinates and velocities are chosen such that their energies are covered by this distribution function.

4.4 An Algebraic Approach to the Kepler Problem

There are some cases in classical mechanics where mechanical systems show special symmetries which allow a different, an *algebraic* approach. An interesting example for these

4.4 An Algebraic Approach to the Kepler Problem

cases is the well-known *Kepler problem*: two bodies are falling freely in their gravitational potential. Within computational physics we use “unusual” coordinates (i.e. Cartesian coordinates instead of more useful spherical or cylindrical coordinates) therefore it would be useful to describe the problem *coordinate-free*. We present here an ansatz to handle the problem independently of the choice of coordinates. Let’s assume that we have already reduced the motion to that of a reduced mass $\mu = \frac{m_1 m_2}{m_1 + m_2}$ rotating in the corresponding fixed potential. The Hamiltonian of this restricted problem in Cartesian coordinates is:

$$H(\vec{x}, \vec{p}) = \frac{\vec{p}^2}{2\mu} - \frac{K}{\|\vec{x}\|}, \text{ with } K = Gm_1 m_2 \quad (4.33)$$

One immediately sees the rotation symmetry which results of course from the rotation symmetry of the gravitational potential and is typical for every central force problem. We know that the Noetherian conservation quantities to this central force problems are the three components of the angular momentum vector:

$$\vec{l} = \vec{x} \times \vec{p} = \mu \vec{x} \times \vec{v} \quad (4.34)$$

With a little differentiating work one proves that in addition to the angular momentum and the Hamiltonian the so-called *Runge-Lenz vector* is conserved, i.e. the Poisson brackets of its components with the Hamiltonian vanish. The Runge-Lenz vector is:

$$\vec{A} = \frac{1}{K\mu} \left(\vec{p} \times \vec{l} - \mu \vec{x} \frac{K}{\|\vec{x}\|} \right) = \frac{\vec{p} \times \vec{l}}{K\mu} - \frac{\vec{x}}{\|\vec{x}\|} \quad (4.35)$$

From this it is easy to derive the trajectory. We multiply the Runge-Lenz vector with \vec{x} :

$$\vec{x} \vec{A} = r \|\vec{A}\| \cos \phi = \frac{\vec{l}^2}{K\mu} - r \Rightarrow r = \frac{\vec{l}^2}{K\mu} \frac{1}{1 + \|\vec{A}\| \cos \phi} \quad (4.36)$$

Here ϕ is the angle between the time-constant Runge-Lenz vector \vec{A} and the spatial vector \vec{x} while $r = \|\vec{x}\|$. We can now define

$$r_{peri} = \frac{\vec{l}^2}{(1 + \epsilon)K\mu}, \quad \epsilon = \|\vec{A}\| \quad (4.37)$$

where r_{peri} is the pericenter distance and ϵ the eccentricity of trajectory.

It is clear that \vec{A}^2 is a conserved quantity as \vec{A} is. But it is not independent from other conserved quantities because \vec{l} and \vec{A} correspond already to six conservation quantities. We get through direct calculation

$$\vec{A}^2 = 1 + \frac{2E\vec{l}^2}{K^2\mu} \quad (4.38)$$

Here E is the total energy of the system which is of course conserved. The “classical” calculation shows exactly the same result while it requires extensive and complicated integration.

In (4.36) it is proven that \vec{A} points from the center of the trajectory to the peri-helium of the trajectory. And we see that for $\vec{l} \neq 0$ the form of the trajectory is determined by the sign of the total energy:

1. $E < 0$: following (3.2) the eccentricity is $0 \leq \epsilon < 1$ and the trajectory is *elliptical* with the special case of a circle for $\epsilon = 0$.
2. $E = 0$: following (3.2) the eccentricity is $\epsilon = 1$ and the trajectory is *parabolic*.
3. $E > 0$: following (3.2) the eccentricity is $\epsilon > 1$ and the trajectory is *hyperbolic*.

So we got the classical result with a much easier calculation and with usage of the special symmetry of the problem.

4.5 The Simulation Parameter

We now present the parameters used in the simulations done for this work. Since we conducted two different kinds of simulations we separate this section into the *cosmology part* and the *galaxy part*.

4.5.1 The Cosmology Part

We used GRAFIC (chap.4.1) to set up 30 cosmological boxes with cube-length of 20Mpc. Each box contains $80^3=512000$ particles which means a mass resolution of $5 \times 10^8 M_\odot$ and force resolution of $\epsilon = 5\text{kpc}$. From this simulations we derived kinematical parameters of minor merger events used later on in more detailed simulations including a stellar disk. This enables us to be as self-consistent as technical possible. The method - replacing one big cosmological simulations with lots of small ones - has one stumble stone: It neglects long-wave fluctuations which are present in the big box and of course suppressed in the small boxes (because GRAFIC calculates the random field with periodic boundaries within the box-length). But these large-scale fluctuations are responsible for structures on large scales, and we are interested in structures on small scales. So there is no back-draft for us in using this method.

Angle $\text{plane}_{orbit} - \text{plane}_{disk}$	r_{peri}	Angle $\vec{A} - \text{plane}_{disk}$
0°	10kpc	0°
30°	10kpc	0°
60°	10kpc	0°
90°	10kpc	0°
120°	10kpc	0°
150°	10kpc	0°
180°	10kpc	0°
90°	10kpc	45°
90°	10kpc	90°

Table 4.1: In this table the parameters of the simulation of a minor merging galaxy are listed. The first column lists the angles between the orbital plane of the satellite and the disk plane, the second shows the peri-center distance of the orbit, and the third column shows the angle between the Runge-Lenz vector \vec{A} and the disk plane

4.5.2 The Galaxy Part

We used the methods mentioned in section 4.3 to set up a galactic disk within a alive halo together with a satellite of 1/5 of the disk mass on a parabolic orbit around the galaxy. We put in 9 different orbital parameter (derived from the cosmological simulations) summed up in tab.4.1 to cover a wide range of possibilities and differences. The galactic disk consists of 100000 particles, the halo of 200000 particles and the satellite of 20000 particles, leading to a mass resolution of $5.6 \times 10^5 M_{\odot}$ for the disk and satellite and $8.4 \times 10^5 M_{\odot}$ for the halo particle and a force resolution of $\epsilon = 280 \text{pc}$. The mass ratios between the components was $M_{halo}:M_{disk}:M_{sat}=1:0.333:0.066$.

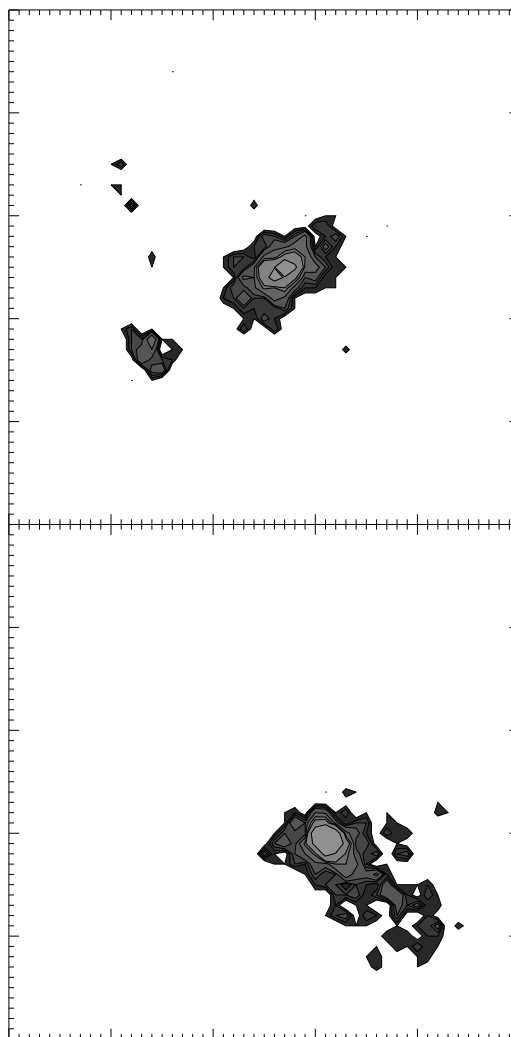


Figure 4.6: Two density plots of clusters which merged and were identified as a minor merger. Top: the two clumps before the collision. Bottom: the resulting clump of the merger. Note the feature at the right side, presumably some sort of tidal stream or remnant of the satellite. Time between the two pictures is 500 million years, length of the box is 100kpc

4.5.3 The Criteria for Minor Merger

We listed all halos found by FOF and at $z = 0$ we looked for every halo of the size of the Milky Way (which we define as $0.5-2 \times 10^{12} M_{\odot}$, corresponding to the estimated Milky Way mass as $\sim 10^{12} M_{\odot}$) (Binney & Tremaine, 1987). For these halos we climbed up the merger tree towards increasing z and checked for every dump if a merger with smaller halos occurred. That means that FOF detects one halo in a certain dump which consists of at least two progenitor halos detected in a dump before. From these mergers we picked out every merger that fulfill our minor merger definition, i.e. a mass ratio $\frac{M_{small\ halo}}{M_{big\ halo}}$ of 1:20=0.05 to 1:5=0.2. Additionally, each progenitor has to add at least 90% of its particles to the new halo - this prevents that a halo is disrupted by the interaction and contributes with only a few particles to the new halo (see fig.4.6 for an example). To extract only the statistics of minor merger that are comparable to big disk galaxies like our Milky Way we sorted out every halo which suffers from a major merger (i.e. mass ratio of 1:1 to 1:5).

4.6 Conclusion and Discussion

In this chapter we presented the methods and tools applied in this work. We have been as self-consistent as technically possible by using cosmological simulations to derive kinematical parameters of minor merger and putting these parameters into simulations of a disk galaxy merging with a small companion. Of course we were limited by computer power (i.e. time) and disk space so that the parameter range of the orbits simulated in the galaxy case may be not sufficient. But this work gives a good overview over the effects one can expect from a minor merger event consistent with cosmology and leaves enough for studies of this topic in the future.

Chapter 5

Results from cosmological simulations

The universe is full of peculiar coincidences.
Martin Rees

In this chapter the results from cosmological simulations are presented, meaning the orbital parameter, the abundance and time-dependence of Minor Merger and the spin parameter λ^1 on the mass ratio of the merger.

5.1 Comparison of WINE to other codes and methods

Since our code WINE is completely new, first of all we compared the output of WINE with another code: the TPM (Tree Particle Mesh) code by (Bode & Ostriker, 2003). Indirectly, this is also a comparison to the more famous code GADGET by Springel et al., 2001. We put in standard cosmology structure formation initial conditions (see chap.4) with box length of 20Mpc and 262144 particles and compared the number of halos of certain mass in a cumulative mass plot (see fig.5.2). Actually, the differences are insignificant, both codes essentially produce the same number of halos. To smaller masses the TPM code produced some more halos than WINE did. According to (Bode & Ostriker, 2003), this might be a problem of TPM itself since this discrepancy also is found in a comparison of TPM to GADGET (Bode & Ostriker, 2003). GADGET (Springel et al., 2001) and WINE are consistent in this feature. WINE apparently produces a reasonable number of halos in cosmological simulations.

In fig.5.1 we show an example of a cosmological simulation that ranges from $z = 2$ to $z = 0$ in steps of 1.2Gyr. Starting from initial conditions similar to the one seen in fig.4.1, we see here the increasing density contrast and the hierarchical build-up of structures. An analogon to this structure formation we see in fig.5.3, the summed up cumulative mass function for different redshifts. At $z = 0$ the mass function can be fitted with a function $\propto M^{-a}$ with $a = 0.819$.

In this figure the hierarchical structure formation is nicely seen:

- there are overall more smaller halos than bigger ones
- at higher redshift there is a lack of halos with higher masses (compared to lower redshifts) while smaller halos are already present

¹Do not mix up this λ with the cosmological constant Λ

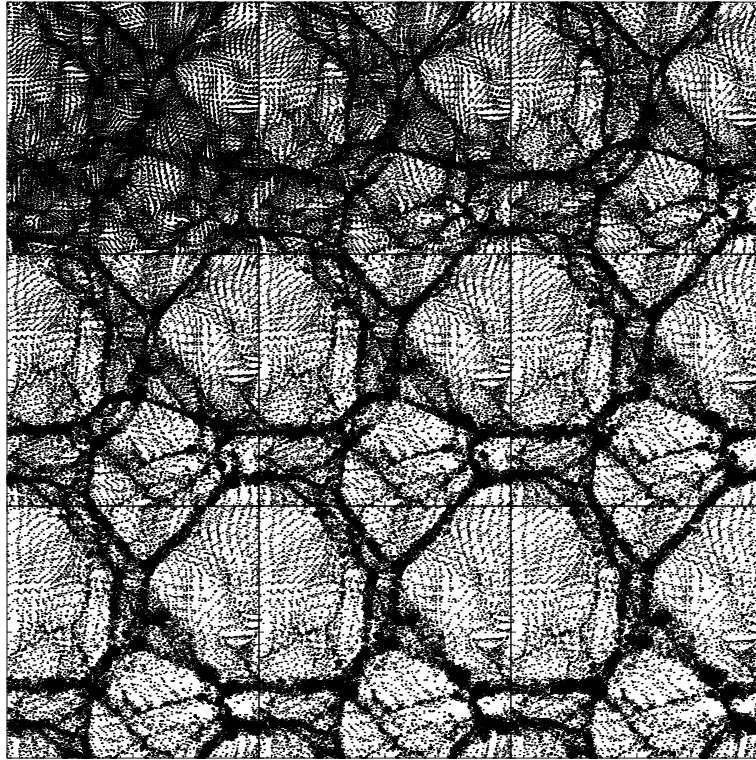


Figure 5.1: Example of structure formation in a simulation run: box length is 20Mpc, the time between two pictures is 1.2Gyr, time goes from left to right, from top to bottom. We are looking at a projection of one side of the box.

- a closer look reveals that at lower redshifts the number of smaller halos declines. This can be interpreted as a depletion of these halos via merging to bigger halos - as said in hierarchical clustering models. This is also found in other simulations (e.g. Jenkins et al., 2001) and in semi-analytical approaches (e.g. Press & Schechter, 1974, see fig.A.1). The limited resolution in the simulations may contribute little to this depletion.

All these tests prove the functionality of WINE for cosmological purposes.

5.2 The abundance and frequency of Minor Merger

The first interesting point about minor mergers is their abundance in space and time. Unfortunately, there does not exist any observational clue for the merger rate in time and space for minor merger. This is due to the difficulty in observing minor mergers out to medium or high redshift. Observations of ongoing minor mergers were done to a distance up to ~ 100 Mpc, corresponding to a redshift of $z \sim 0.02$ only (Schwarzkopf & Dettmar, 2000a). So we have no observational data on the merger rate for minor merger to redshifts up to $z = 1$ yet. For major merger a merger rate $R_{merger} \propto (1 + z)^m$ with $m \sim 3$ is observed (van Dokkum et al., 1999, Le Fevre et al., 2000) for $z \leq 1$. In fig.5.4 we plotted the merger rate in dependence of z and found a value for m of 1.419 which is

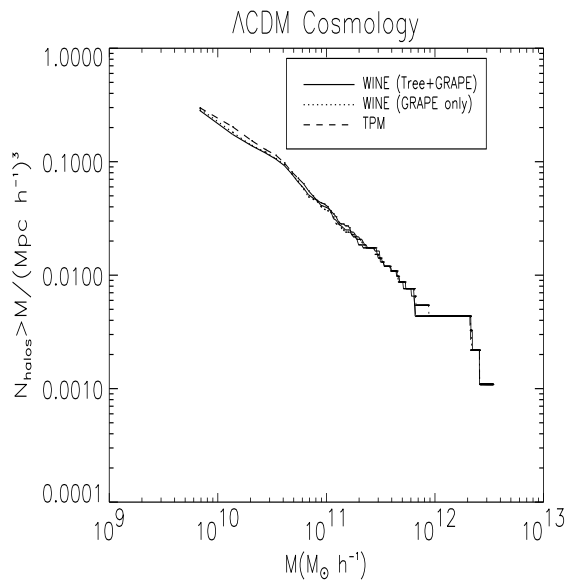


Figure 5.2: Comparison of the code WINE to Bode’s TPM code. WINE ran in two different modes: with activated tree and with GRAPE direct summation only. The results converge.

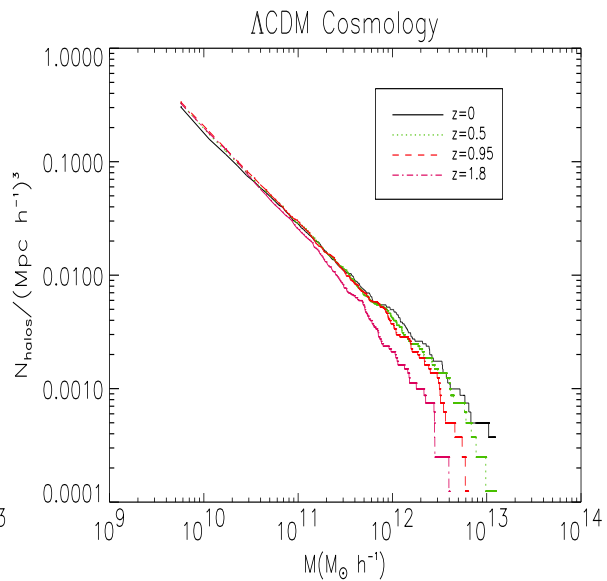


Figure 5.3: Cumulative mass function, summed up over all simulations. The different colors denote different redshifts.

quite different from the merger rates for major merger found in observations as well as in simulations (Khochfar, 2003). This means that the rate of minor mergers decreases more slowly with decreasing z than the major merger rate.

In fig.5.5 the frequency of minor mergers is shown, normalized to comoving Mpc and Gyr. The distribution rises during the first 3 Gyrs (from $t \sim 3$ Gyr to $t \sim 6$ Gyr), peaks at $t \sim 6$ Gyrs after the big bang and declines smoothly until present time. Qualitatively, this behaviour is clear:

- in the beginning the “universe” lacks bigger (i.e. Milky Way sized) halos - which are the objects we are interested in - therefore the number of minor merger is small
- on the other hand, the number of smaller halos decreases because they merge together to bigger halos while the material for new halos decreases. This leads to a decreasing number of smaller haloes and therefore to a decreasing number of minor merger (since it needs several small halos to build up a bigger halo the increasing number of bigger halos does not compensate). Note that we are well within the mass and cluster resolution of our simulations.
- both processes work against each other: the decreasing number of small halos against the (more slowly) increasing number of bigger halos. That indicates the existence of a maximum: the peak at $t \sim 6$ Gyrs after the big bang

We counted **862 Milky Way sized halos** which experienced overall **1041 minor merger**, their time dependent distribution is shown in fig.5.5 and in fig.5.4. We can summarize the results:

5.3 The orbital parameter of Minor Merger

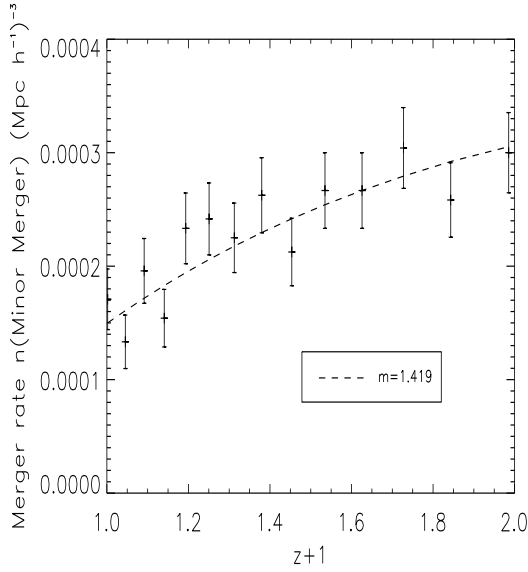


Figure 5.4: The merger rate of minor merger with redshift $z \leq 1$. It can be fitted via $R_{merger} \propto (1+z)^m$ with $m=1.419$. Error bars denote the Poissonian error.

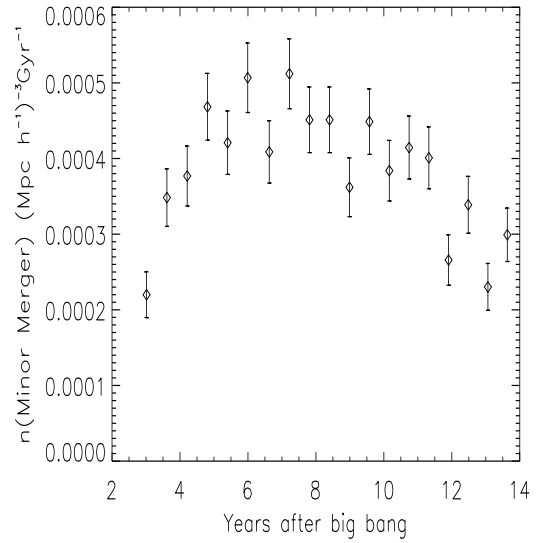


Figure 5.5: The frequency of Minor Merger in space and time. See text for further explanation. Error bars denote the Poissonian error.

1. The most likely time for a minor merger was 7 Gyrs in the past.
2. It is likely that our Milky Way experienced at least one minor merger, on average and in one out of five cases a second merger.
3. The merger rate for a minor merger declines more slowly than the major merger rate - which has to be shown by observations in the future.

5.3 The orbital parameter of Minor Merger

For self-consistent galaxy simulations it is necessary to derive the orbital parameters of a minor merger from cosmological simulations. We have identified halos that underwent a minor merger in simulations and calculated the essential orbital parameters out of the position and velocity information of the halos according to section 4.4. We found 61.7% of the minor merger having eccentricities in the range of 0.9 to 1.1 and therefore nearly parabolic and 7.5% having eccentricities greater than 1.

How can there be a merger if the orbit is not bound? During the merger angular momentum can be exchanged and transferred to particles that are leaving the system while the main parts of the halos merges. For the case of an initially unbound orbit it is possible, then, that the halos can merge. Fig.5.6 and fig.5.7 show the eccentricity distribution of the merger orbits where fig.5.7 divides the distribution up into two redshift regimes of equal-sized numbers of minor merger. In fig.5.10 the dependency of the pericenter distance on redshift is shown. Note the systematic increase of the pericenter distance towards lower redshift. It is interesting that for minor merger at smaller redshifts the orbits become less

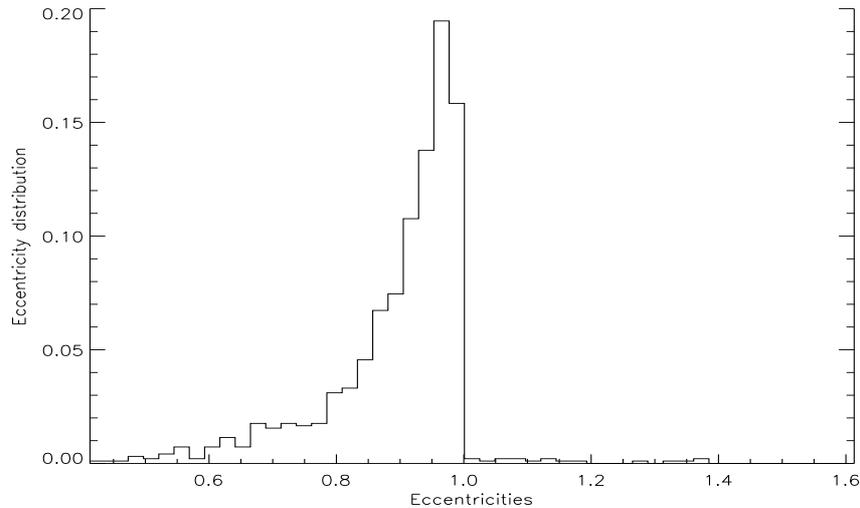


Figure 5.6: The eccentricity of all minor merger orbits. Note that most orbits have eccentricities close to 1.

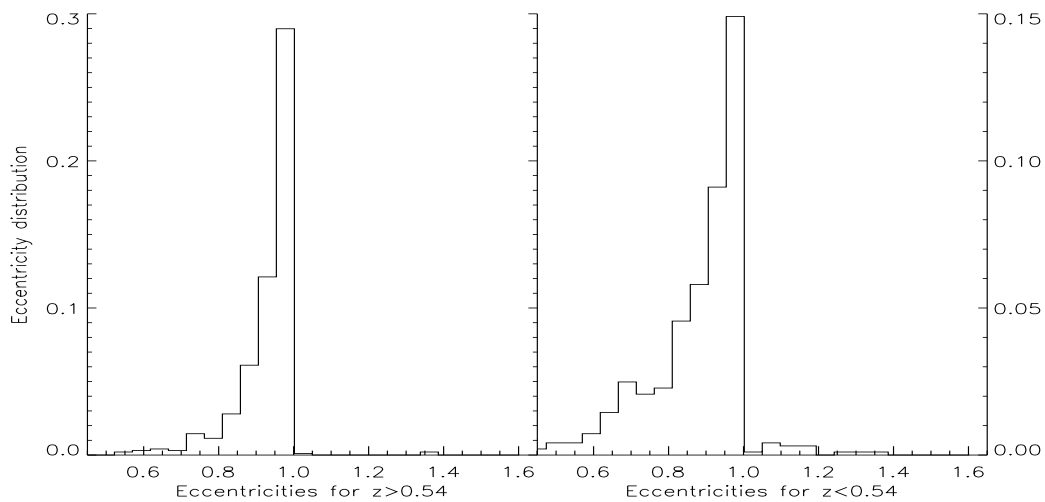


Figure 5.7: The eccentricity divided into two populations with $z > 0.54$ (left) and $z < 0.54$ (right). Note that at later times (right) the merger orbits become more circular: we find more orbits with eccentricities closer to 0 than in the left picture.

eccentric. This can be explained by the connection between the energy of the orbit and the angular momentum of the orbit, $E \propto 1/L^2$. The energy of the orbit increases when the angular momentum decreases. Halos at earlier times have not exchanged much angular momentum with other halos and therefore the energy of the orbit is higher and more eccentric. *It is not very likely to have an circular orbit in the beginning.* If this consideration is correct, orbits at higher redshift should also show lower peri-center distances since it is less likely to have a circular orbit at high redshift. In fact, this can be seen in fig.5.8 and fig.5.9: Here we have the log-distribution of the peri-center distance in kpc and in units of the virial radius of the bigger halo. Again, we divided the minor merger orbits into two

5.3 The orbital parameter of Minor Merger

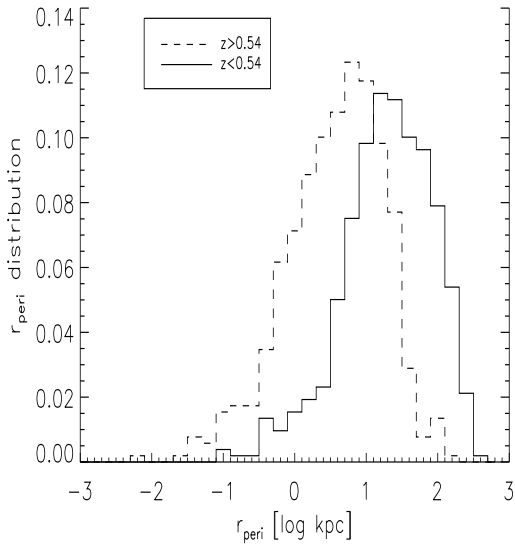


Figure 5.8: The peri-center distance of the minor merger orbits in kpc divided into two redshift populations. Note that for the higher redshift regime the peri-center distance is smaller.

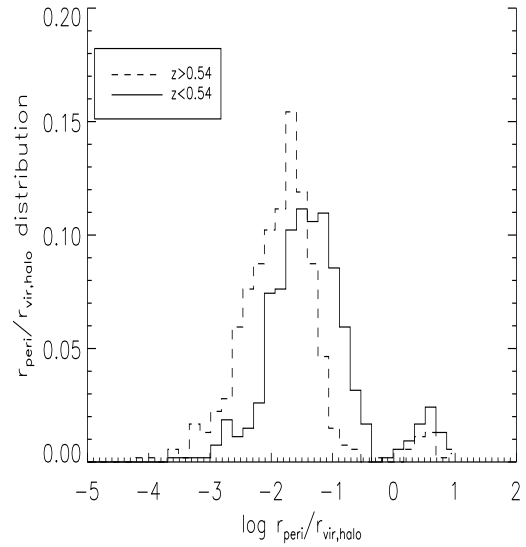


Figure 5.9: The peri-center distance of the minor merger orbits in units of the virial radius of the bigger halo. The small bump at the right is due to merger on hyperbolic orbits and therefore with higher pericenter distances.

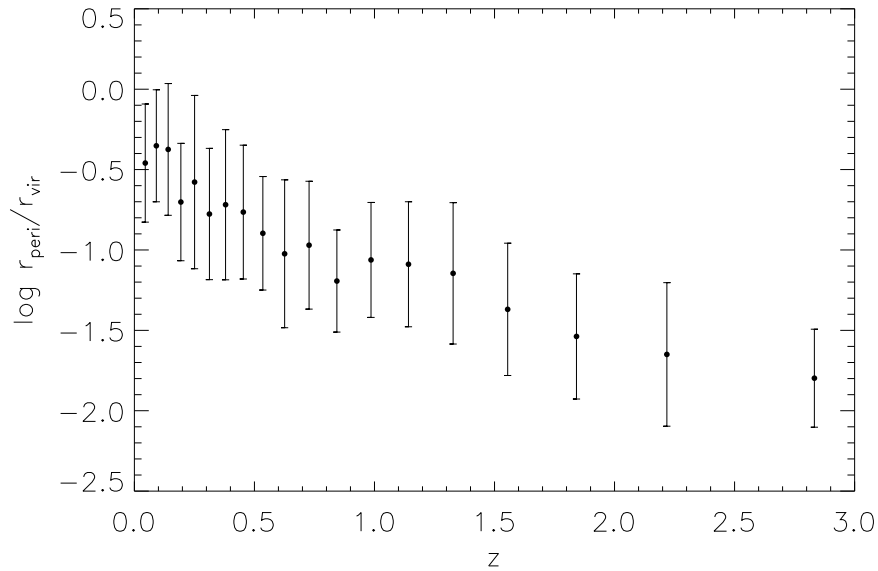


Figure 5.10: The peri-center distance in units of the virial radius of the bigger halo as a function of redshift z . Note that the pericenter distance is systematically increasing towards lower redshift. The error bars denote the 1σ error

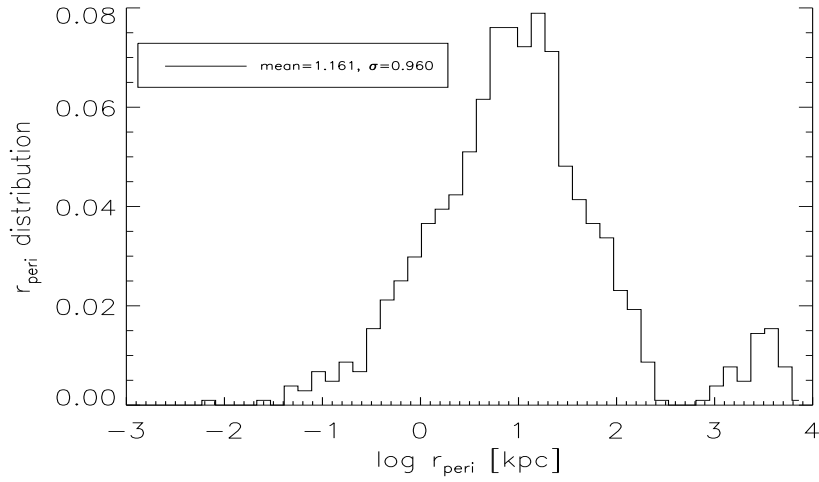


Figure 5.11: The peri-center distance in kpc. The mean value for the peri-center distance is $1.161 \hat{=} 14.45 \text{ kpc}$.

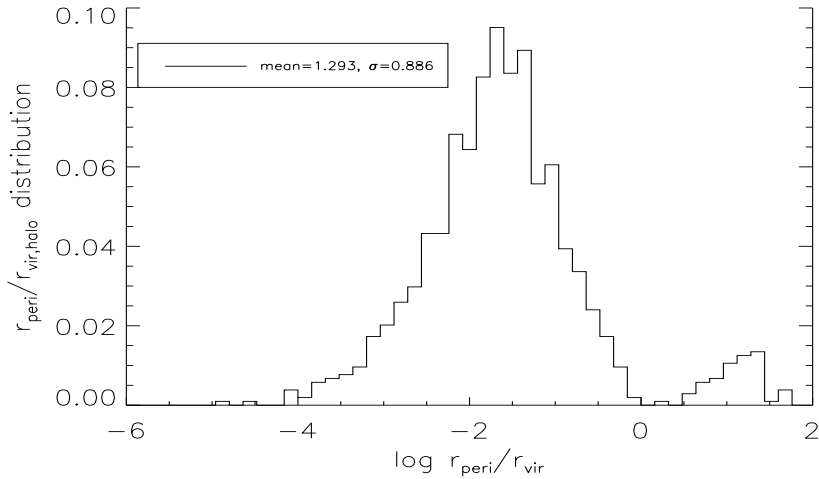


Figure 5.12: The peri-center distance in units of the virial radius of the bigger halo. The mean value for the peri-center distance is $-1.293 \hat{=} 0.051 r_{\text{vir}}$

redshift distributions to see if there is a dependency on redshift. As mentioned before, the peri-center distances are lower for higher redshifts meaning lower orbital angular momentum for the merging halos. The peri-center distance is proportional to angular momentum, $r_{\text{peri}} \propto L^2$, and therefore it is clear that earlier merger had lower angular momentum than merger that occurred more recently. We found that the two distributions differ in a factor of ~ 2.5 in the peri-center distance of the minor merger orbits: at higher redshift the peri-center distance was roughly 2.5 times smaller than in lower redshifts.

Fig.5.11 and fig.5.12 show the undivided distribution of the peri-center distances. In fig.5.11 the distribution peaks at 1.161, corresponding to a peri-center distance of 14.45kpc, in fig.5.12 we have a maximum at -1.293, corresponding to a peri-center distance of 0.051

5.3 The orbital parameter of Minor Merger

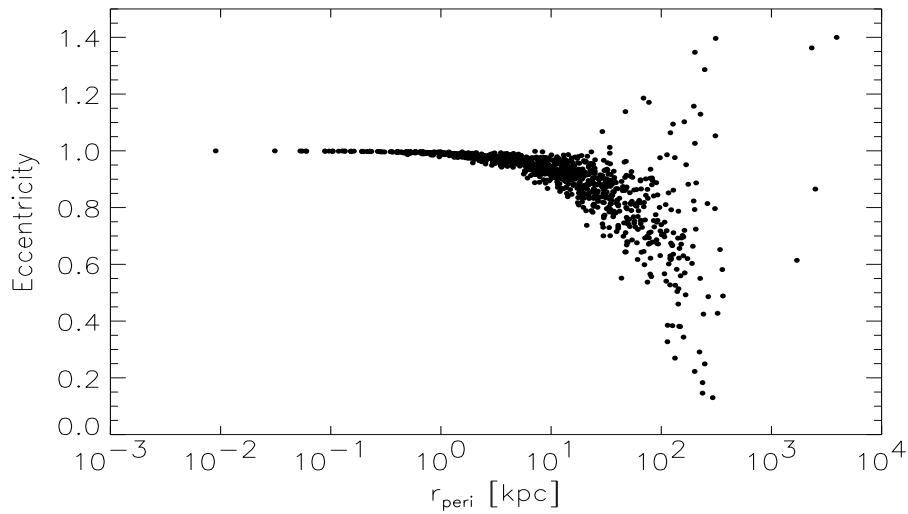


Figure 5.13: The eccentricity in dependence of the peri-center distance. Note that the orbits are mainly around eccentricity 1 and that for more circular orbits the peri-center distance increases.

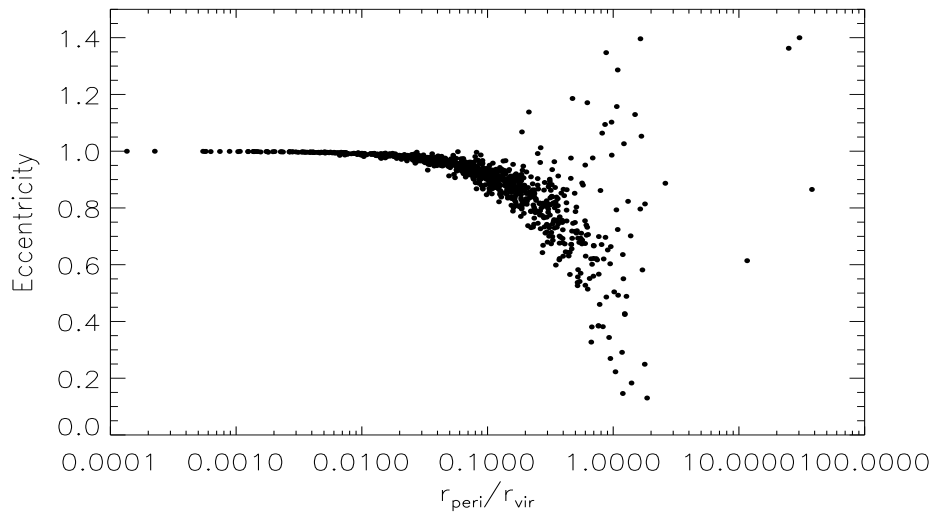


Figure 5.14: Same as fig.5.13, but in units of the virial radius of the bigger halo.

times the virial radius of the bigger halo. These results are similar to results for major merger (Khochfar, 2003) with the difference that major merger orbits have in general slightly higher peri-center distances. While in major merger 76% of the orbits are smaller than $0.3r_{\text{vir}}$, in minor merger we find that 87% of the orbits are smaller than $0.3r_{\text{vir}}$. This is not surprising if one remembers the hierarchical clustering pictures: big halos have merged from smaller ones and gained from this substantial angular momentum with respect to other big halos. When the big halos finally merge, they bring substantial

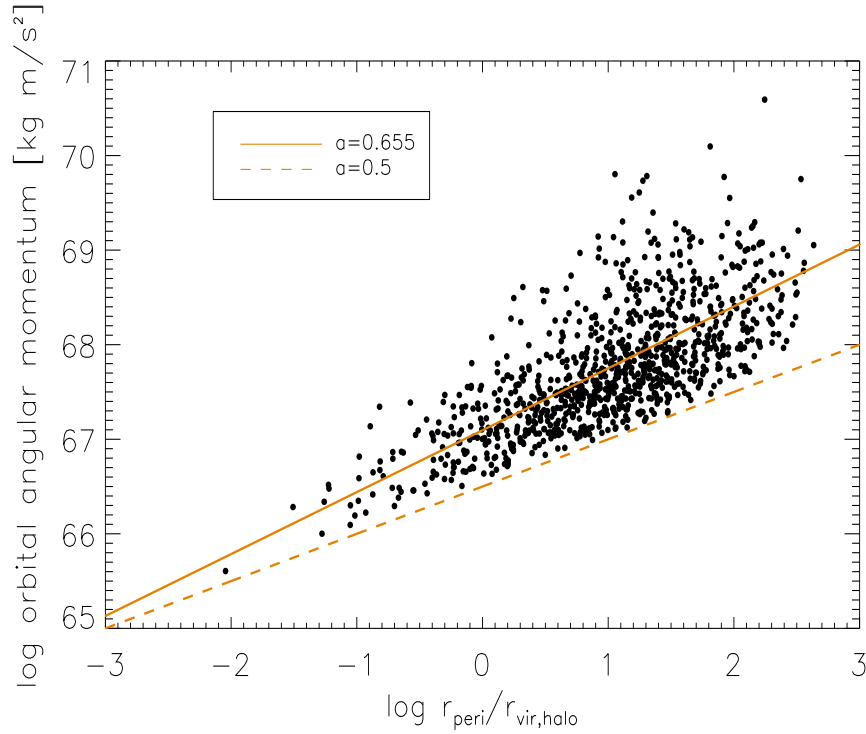


Figure 5.15: The angular momentum of the orbit versus the peri-center distance in units of the virial radius of the bigger halo in a log-log plot. The solid line denotes the fit, the dashed line shows the expectation which is able to form a boundary to the lower part of the distribution.

angular momentum into the merging process and therefore have orbits with higher peri-center distances.

We now focus on the connection between eccentricity and peri-center distance. We see in fig.5.13 and fig.5.14 the combined results of our former considerations: low peri-center distances force nearly parabolic orbits, while more circular orbits are only found with higher peri-center distances. The small bump at the right in fig.5.11 designates minor merger events with hyperbolic orbits and therefore within these considerations high values for peri-center distances.

We then performed a consistency check if the results so far are reasonable. We know from section 4.4 that the peri-center is connected to the angular momentum of the orbit via $r_{peri} \propto L^2$ with a scatter mainly due to the different mass ratios and slightly by different eccentricities (see 4.37). We expect the distribution to be limited at the lower end by a line with slope $a = 0.5$: these would be exact circular orbits with $\epsilon = 0$ with lowest mass ratio of the merging halos. This is checked in fig.5.15 and shows consistency with the expectation. The scatter plot could be fitted with a line with the slope of $a = 0.655$ with a boundary line with slope $a = 0.5$.

Another interesting parameter that is connected to the orbit of the minor mergers is

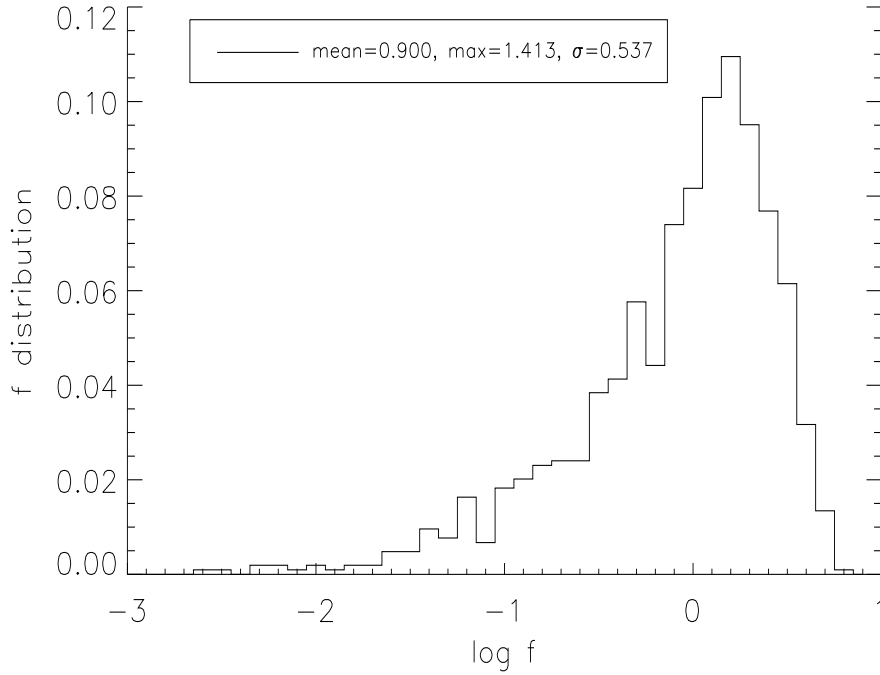


Figure 5.16: The merging parameter f . Shown here is the log-distribution which has its maximum at 1.413.

the merger parameter f which is defined as:

$$f = \frac{L}{v_{vir} R_{vir} \mu} \quad (5.1)$$

with v_{vir} and R_{vir} of the more massive halo (Maller et al., 2002). For major merger with $\mu \sim 0.3$ one would expect a value for $f \sim 0.4 - 0.7$ (Khochfar, 2003). For minor merger μ decreases to ~ 0.1 and therefore one would expect f for minor merger to be roughly three times bigger than for major merger. In fig.5.16 the log-distribution of f is shown with a maximum at 1.413. This would roughly fit into the expectations from major merger for minor merger. Another interesting point is the mass ratio of the minor merger and its dependency on redshift. We plotted the distribution of mass ratios for minor merger per comoving cosmological volume in fig.5.17 and fitted the distribution to a function $\propto x^{-a}$. This should be similar to the mass function of halos in fig.5.3 with $a = 0.819$. In fact we see a larger value for a , namely a slope of $a = 1.65$ which is quite exact twice as large as the value for the cumulative mass function in fig.5.3. This may be explained by two cooperating processes: we have small halos according to the mass function which merge with big halos that are less frequent according to the mass function.

If we again divide up the mass ratios of the minor merger into two redshift populations we see no clear difference between the two distributions in fig.5.18. We therefore would not expect different heating of galactic disks at different redshifts.

Finally, we address the question whether there is a dependency of the eccentricities on

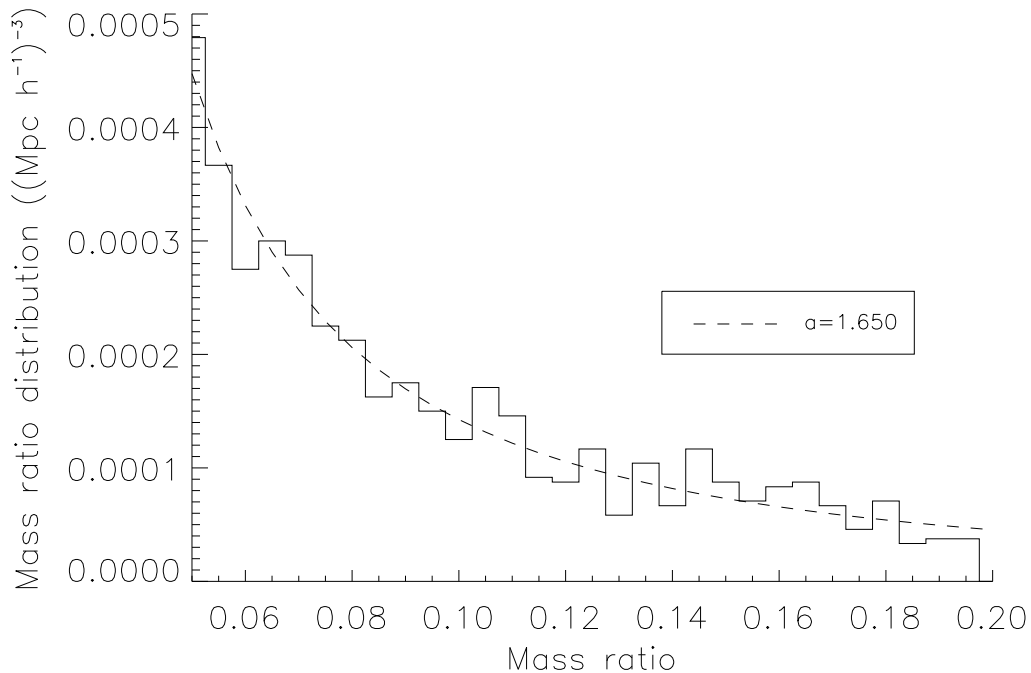


Figure 5.17: The mass ratio distribution for minor merger per comoving volume in units of Mpc/h . The dashed line shows the fit $\propto x^{-a}$ of this distribution with $a=1.65$.

the mass ratios in a minor merger event. We expect of course more minor merger events towards lower mass ratios because of the higher abundance of smaller halos. We plotted the dependency in fig.5.19 in a contour plot to visualize the result in a better way. The plot confirms the expectation of more minor merger at lower mass ratios, gathering together at eccentricity ~ 1 .

5.4 The angles in minor merging events

The next interesting point for the initial conditions of a minor merger is the impact angle of the satellite onto the galactic disk. Since we do not have any stars in the cosmological simulations, we assume that the spin of the bigger dark matter halo is correlated to the spin of a hypothetical stellar disk and therefore the angle with respect to the spin of the halo corresponds to the angle to the disk plane we simulated later on.

Since isotropy is fundamental in cosmology we do not expect any special angle for the impact of the satellites or for the spins of the objects. We checked 4 different angles in the minor merger events:

1. The angle between halo spin and satellite orbital plane. This is used for the simulations of a stellar disk experiencing a minor merger.
2. The angle between halo spin and satellite spin. This checks if there is any interaction

5.4 The angles in minor merging events

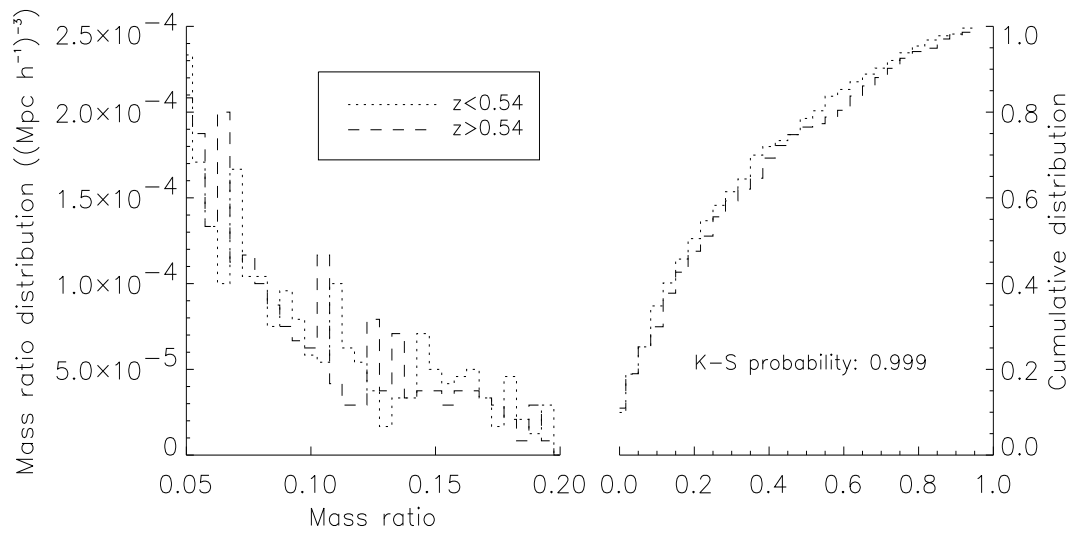


Figure 5.18: Left: the mass ratios distribution for two different redshift regimes. There is no clear difference visible. Right: the cumulative distribution including the result from a Kolmogorov-Smirnov test, showing that the distribution are closely correlated.

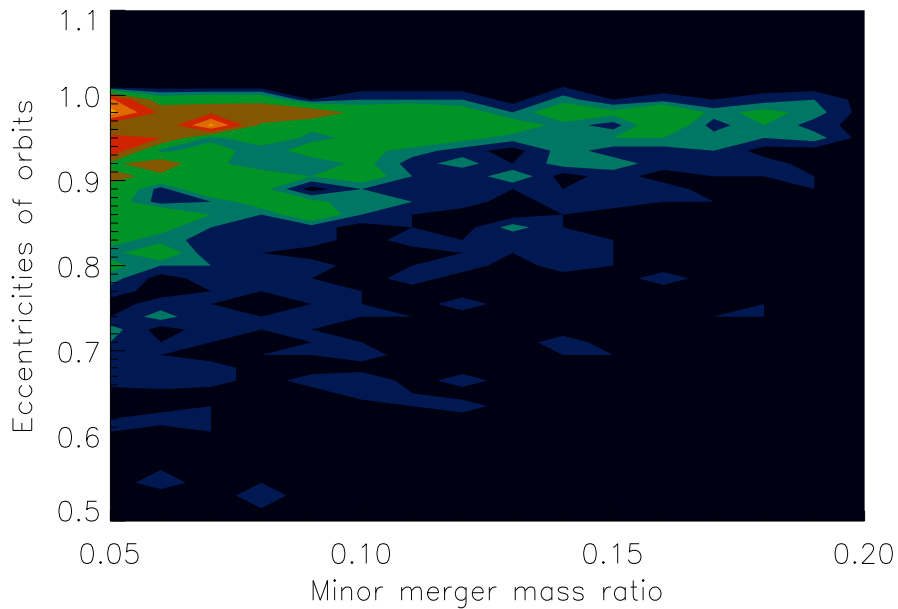


Figure 5.19: The correlation between the eccentricities of the orbits and the mass ratio of the minor merger. The number of minor merger found in the area increases from blue to yellow.

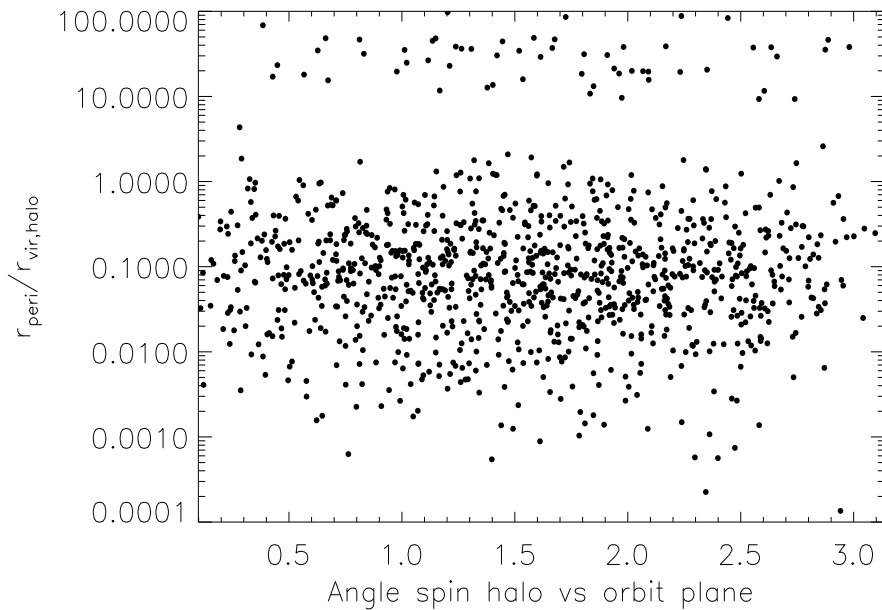


Figure 5.20: The peri-center distance versus the angle between orbital plane and halo spin. There is no visible correlation beyond the expected $|\sin(\alpha)|$.

between the halo spin and its satellite.

3. The angle between the satellite spin and its orbital plane. This checks if there is any coupling of the satellite spin and the orbit of the satellite.
4. The angle between the first and the second minor merger orbital plane. This checks if there is any preferred direction for two minor merger event in one halo.

We checked if the results are in concordance with the expectation that there is no preferred angle with a Kolmogorow-Smirnow test of the distribution versus the theoretically expected distribution of $\propto |\sin(\alpha)|$. The latter one is clear: The probability for a random vector pointing on a point of a sphere is proportional to the size of the surface of the sphere which is proportional to $\sin(\alpha)$. So if two vectors are not correlated the angle between them is sine-distributed. This is exactly what we found in our analysis: there is no correlation between the angles mentioned above. The results are shown in fig.5.21, fig.5.22, fig.5.23 and fig.5.24: we have K-S probability factors very close to 1, meaning that the distributions are fitted very well by the sine function. This means that the angles are randomly distributed. There is no correlation of any kind, no coupling of the spin of the satellite or of the halo with the orbit the satellite, no relation between the orbit of the first satellite with the orbit of the second satellite if the halo experienced two minor merger. This no-correlation may also play a role in estimating the impact of a minor merger on the spin parameter of dark matter halos - see chap.5.5.

We found another no-correlation in the plot of the angle between orbital plane and halo spin versus the peri-center distance, see fig.5.20.

5.4 The angles in minor merging events

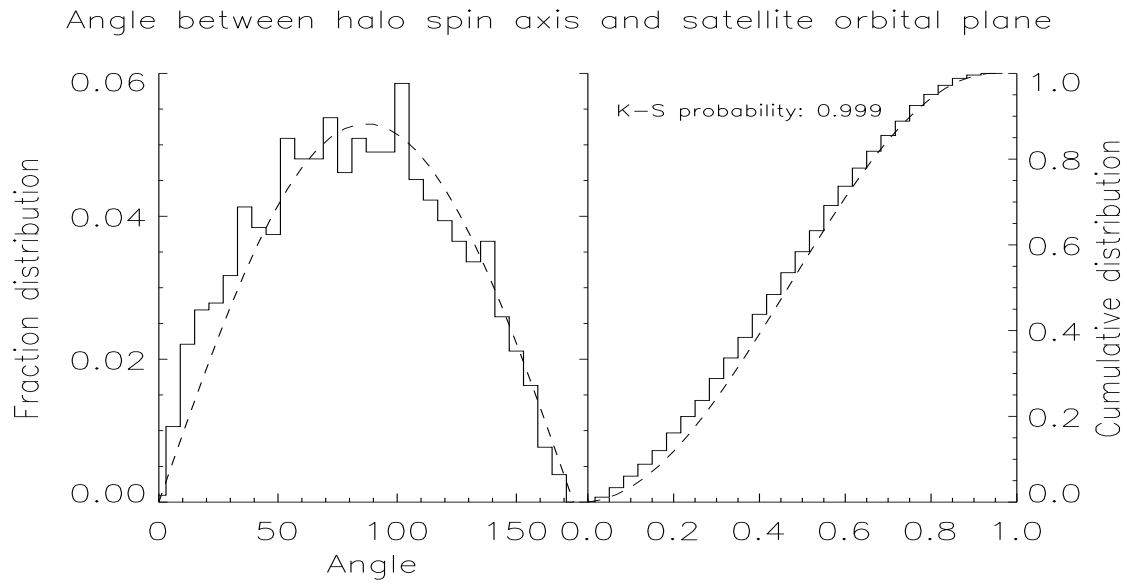


Figure 5.21: Left: Angle between the satellite orbit plane and the halo spin axis. Right: Cumulative distribution of angles and the fit to $|\sin(\alpha)|$ including the result of a Kolmogorov-Smirnov analysis

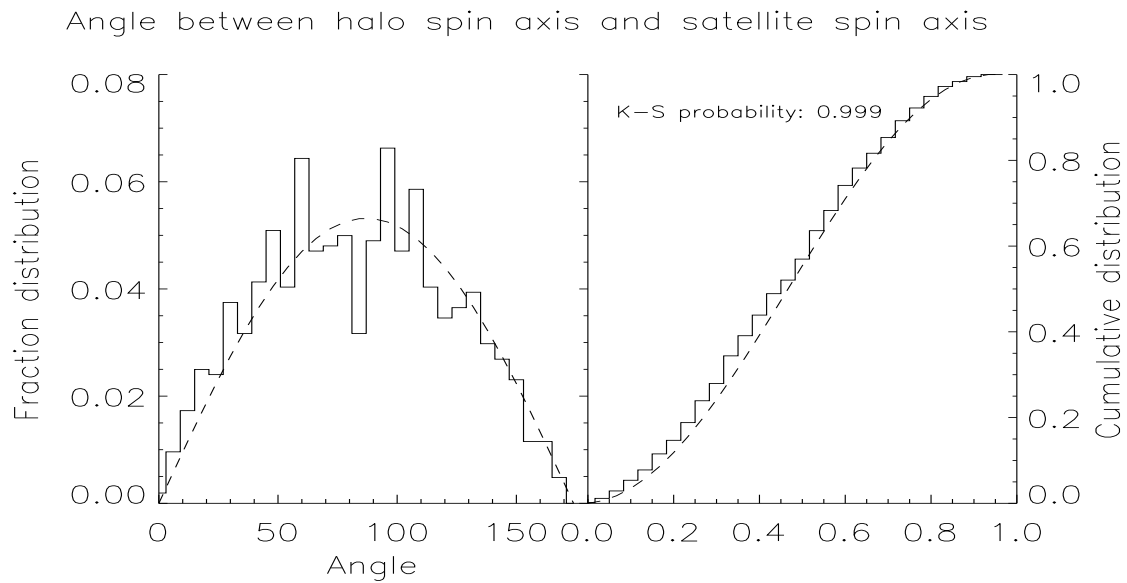


Figure 5.22: Left: Angle between the satellite spin axis and the halo spin axis. Right: Cumulative distribution of angles and the fit to $|\sin(\alpha)|$ including the result of a Kolmogorov-Smirnov analysis

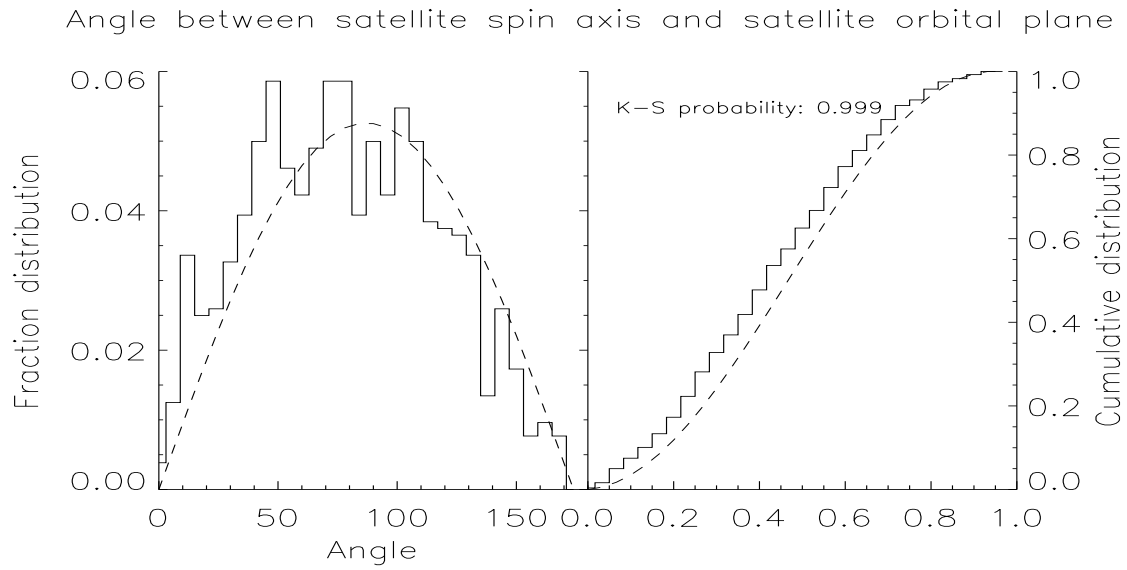


Figure 5.23: Left: Angle between the satellite spin axis and the satellite orbit plane. Right: Cumulative distribution of angles and the fit to $|\sin(\alpha)|$ including the result of a Kolmogorov-Smirnov analysis

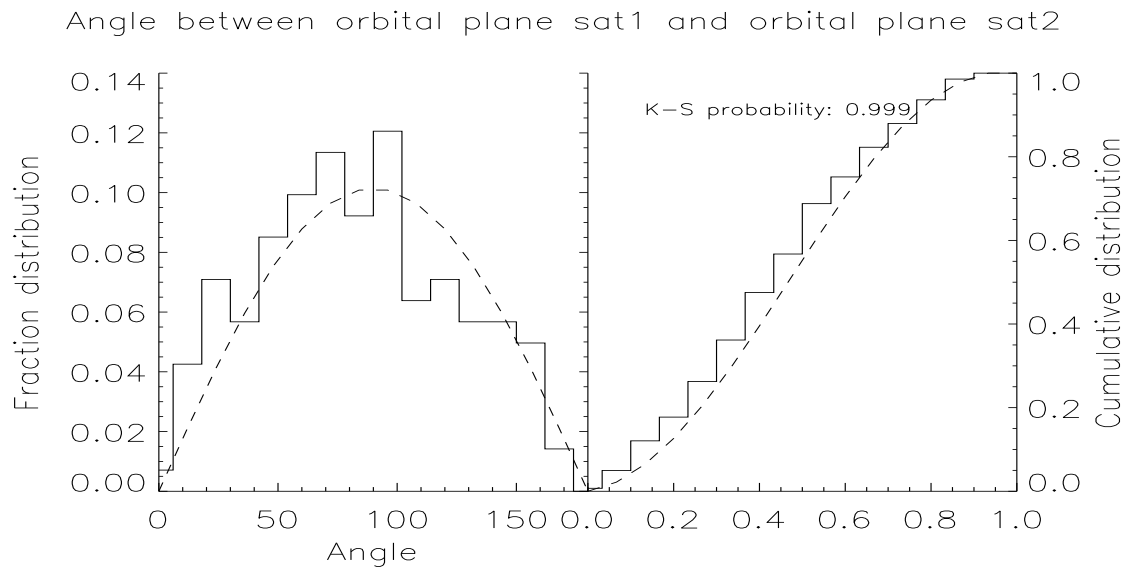


Figure 5.24: Left: Angle between the first satellite orbit plane and the second satellite orbit plane for a halo that experienced two minor mergers. Right: Cumulative distribution of angles and the fit to $|\sin(\alpha)|$ including the result of a Kolmogorov-Smirnov analysis

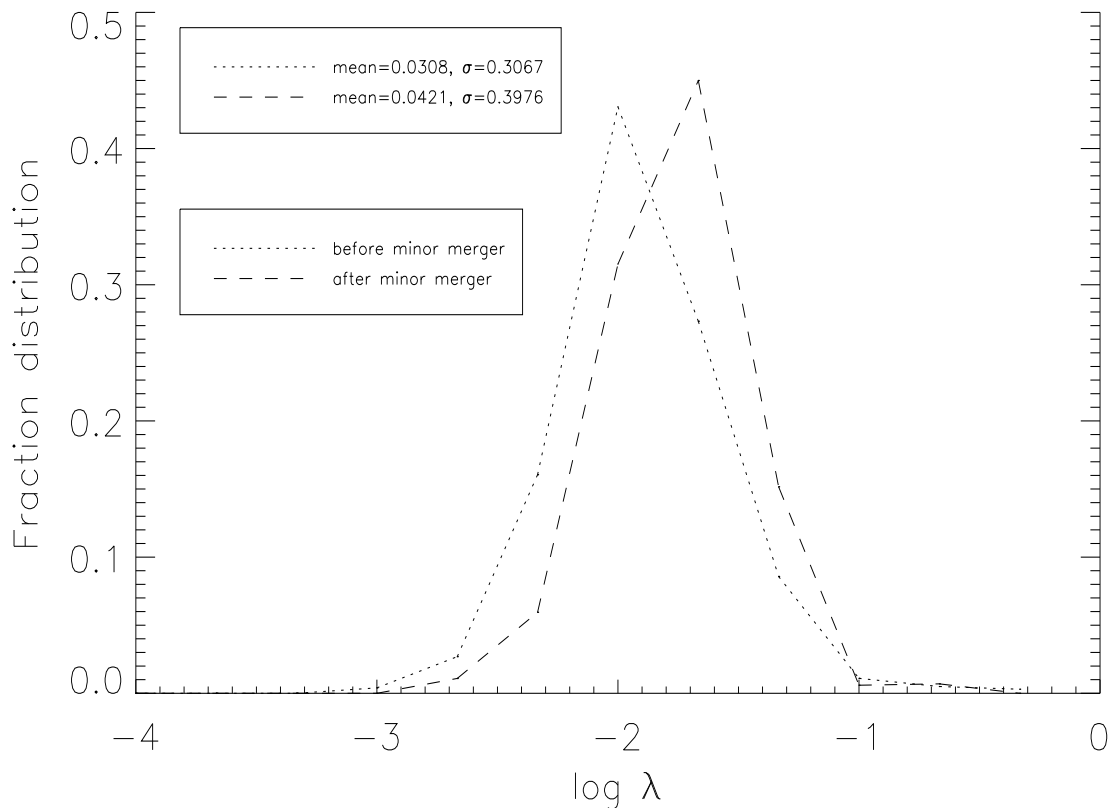


Figure 5.25: The log-normal distribution of the spin parameter λ' of the halos that experienced a minor merger

5.5 Minor merger and the spin parameter of the halo

Hierarchical clustering models predict that galactic disks form as a result of gas infall into cold dark matter halos. Disk properties like scale length and rotation curves are determined by the gravitational potential and by the specific angular momentum distribution which the gas acquired from tidal interactions with the dense regions. From analytical calculations (e.g. Fall & Efstathiou, 1980) we know that the observed scale lengths of galactic disks are reproduced if the disk material retained its initial specific angular momentum when settling into the dark matter halo as galactic plane. But cosmological N-body/SPH simulations showed that the angular momenta of simulated disks are a factor of 10 smaller than observed. That means that the gas appears to lose a large fraction of its initial angular momentum (e.g. Navarro & Steinmetz, 2000). This is stated as the *angular momentum problem of galaxy formation* while it is not clear if this discrepancy poses a problem for CDM or simply results from insufficient understanding of formation processes. Therefore it is interesting to know the evolution of angular momentum of halos in an evolving universe. We analyzed the problem from the minor merger point of

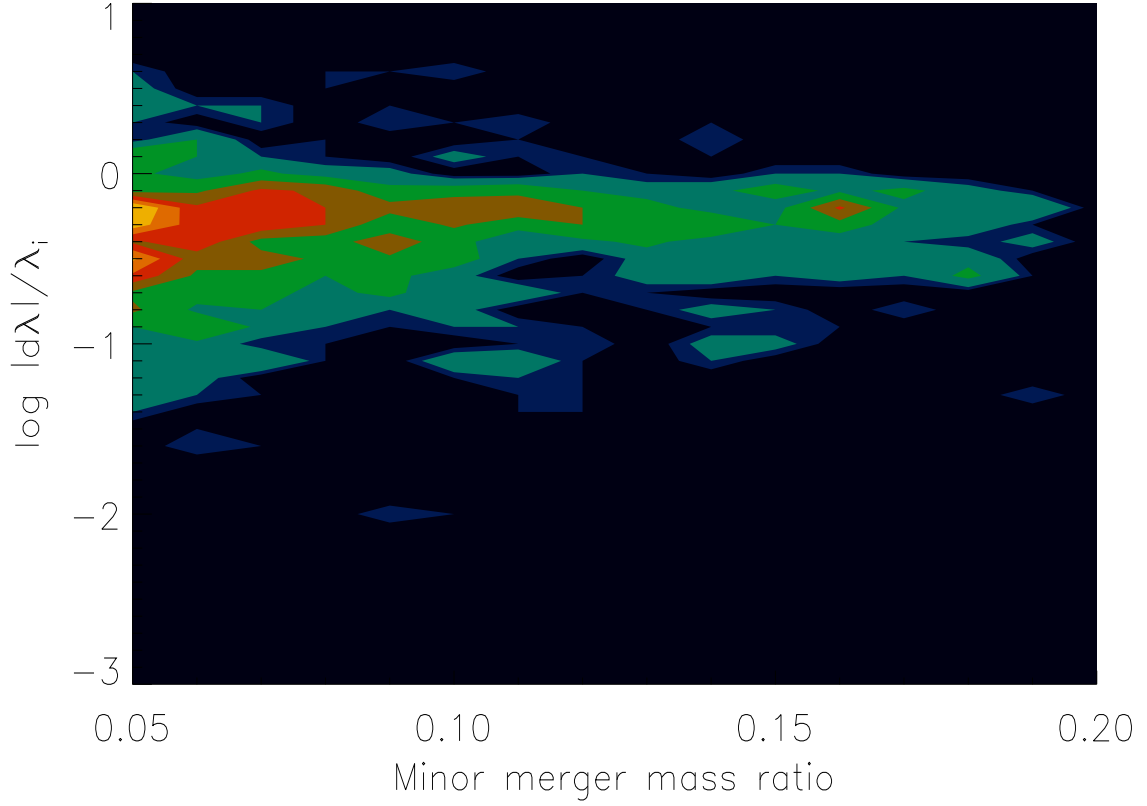


Figure 5.26: The change of the spin parameter $\log |d\lambda|/\lambda_i$ as a function of the mass ratio. From yellow to blue the abundance of minor merger decreases.

view.

The spin parameter λ can be derived (Hetznecker, 2001) by comparing the centripetal acceleration $a_z = v_\phi^2/r$ with the gravitational drag $g = \frac{GM}{r^2}$ to the center. We replace v_ϕ with $J \propto rMv_\phi$ and r with $E = GM^2/r^2$. From this we get:

$$\frac{a_z}{g} = \frac{v_\phi^2 r^2}{rGM} \propto J^2 E / (G^2 M^5) \equiv \lambda \quad (5.2)$$

λ is the dimensionless spin parameter of the system that characterizes the part of rotation for the stability of the system. For the case of $\lambda \sim 1$ the system is stable due to rotation. For the case of $\lambda \ll 1$ the system must be stabilized by pressure forces. For example, elliptical galaxies are supported by inner pressure (given by the velocity dispersion of the stars) because they have a $\lambda \sim 0.05$, while disk galaxies have $\lambda \sim 0.5$ and are mainly supported by rotation.

² E is the total energy of the system $E = E_{kin} + E_{pot}$ and therefore $E = GM^2/r$ is valid only in the virial case $E = E_{pot} - 2E_{pot} = -E_{pot}$

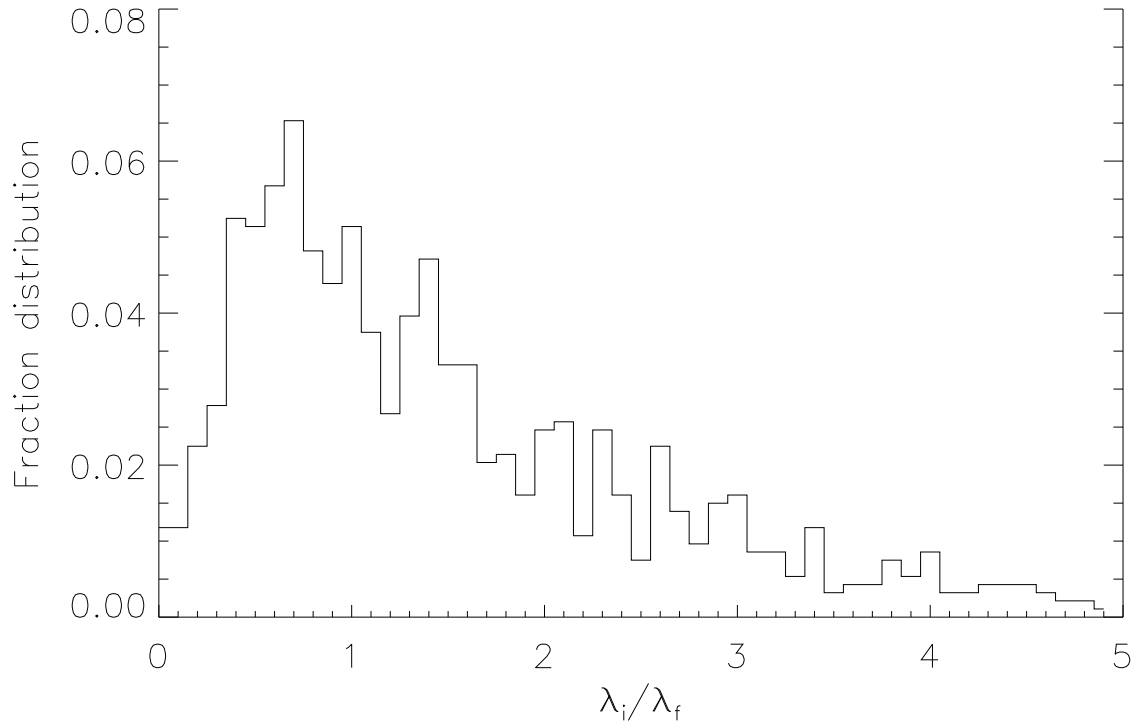


Figure 5.27: The distribution function of the value of λ'_i/λ'_f before (initial) and after (final) the merger.

(Bullock & Kravtsov, 2002) suggested another, more practical definition of the spin parameter:

$$\lambda' \equiv \frac{J}{\sqrt{2}M_{vir}v_{vir}R_{vir}} \quad (5.3)$$

We adopted this definition for our analyses of the spin parameter because it is easier to apply in simulations. The values for λ' found in simulations of Λ CDM cosmologies are typically ~ 0.04 (e.g. Bullock & Kravtsov, 2002) with a value for $\sigma = 0.5$. These values include major merger as well as minor merger and accretion events³. We know from section (5.4) that the satellites come in on random orbits and that it is possible for a minor merger to reduce the spin parameter if its orbit is counter-rotating to the halo. From this we would not expect a change of λ' in a minor merger. In fact, we see an increase of λ' in fig.5.25 from at average 0.0308 to 0.041 with $\sigma = 0.309$ and $\sigma = 0.398$. The final value for λ' is close the values for λ' found in other simulations, while the values for σ are well below the values found elsewhere. This may be due to a kind of “sorting effect”: we sorted out halos that experienced a major merger. Therefore we have a smaller deviation σ .

Another interesting point is the dependency of the spin parameter change on the mass

³The spin of the satellite does not play a significant role since the satellite has only $\sim 1/10$ of the halo mass

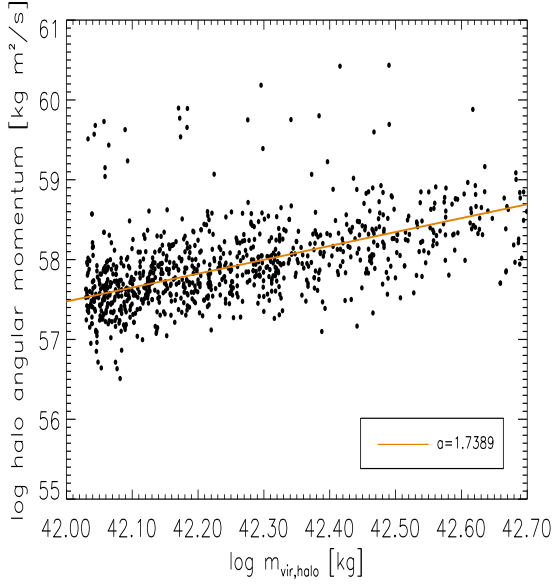


Figure 5.28: Angular momentum of the halos before the minor merger as a function of the virial mass of the halo. It is fairly consistent with expectations. Shown is a least-square fit with $a = 1.739$.

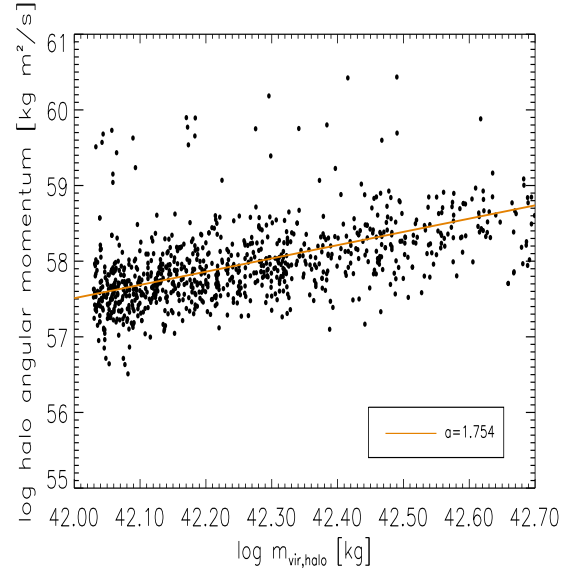


Figure 5.29: Angular momentum of the halos after the minor merger as a function of the virial mass of the halo. It is fairly consistent with expectations. Shown is a least-square fit with $a = 1.754$.

ratio. Intuitively, one expects the change increasing with the mass ratio. We found in fig.5.26 that there is no visible connection between the mass ratio and the change of λ' . Most minor merger have low mass ratio and gather around $d\lambda'/\lambda' \sim -0.2$. That means that most halos experienced a change of their spin parameter of $\sim 2/3$ of the initial value. There is a concentration at higher mass ratios with $d\lambda'/\lambda' \sim -0.2$. This may be connected to the following point: We found also that most halos gained angular momentum. In fig.5.27 the distribution function of the ratio λ'_i/λ'_f ⁴ is shown. We counted 366 minor merger leading to a smaller λ' and 675 minor merger causing a larger λ' . Since we have at average a higher λ' for the halos after the merger, this amount of halos leading to an increased λ' as well as the concentration mentioned above at higher mass ratios could be the reason, causing the overall-increase of the spin parameter.

Finally, we performed another consistency check. With $\lambda' \approx const.$ we can derive:

$$\lambda' \approx const. \Rightarrow J \propto \frac{M^{5/2}}{E^{1/2}} \propto \frac{M^{5/2}}{(M^2)^{1/2} = M^{3/2}} \quad (5.4)$$

We checked this correlation with a least-square fit in fig.5.28 and fig.5.29. We found $J \propto M^{1.739}$ for the halos before they suffered from a minor merger and $J \propto M^{1.754}$ which is fairly consistent with the expectation and shows a minor increase after the merger. The deviation is perhaps due to non-spherical halos found by FOF.

⁴ i denotes the initial value of λ' before the merger, f the value of λ' after the merger

5.6 Discussion and Conclusion

In this chapter we learned different things about the abundance and kinematics of minor mergers in cosmological simulations. First we checked if our new code WINE yielded reasonable results. Comparisons with other codes support the functionality of WINE. According to simulations we did with WINE minor merger occur at least once within a Hubble-time for a halo of the size of the Milky Way at the most likely time ~ 7 Gyrs ago. Early minor mergers have clearly smaller peri-center distances in their orbits and we found their eccentricities closer to 1 than for later minor mergers. We argued that this is consistent because of the gain of angular momentum of the orbits with time due to the interaction with other objects. The merger parameter f was found to fit the expectations regarding to major merger. The minor merger ratio does not depend on redshift. The angles we analyzed in the minor merger show no coupling or correlation of any kind, satellites collide with the bigger halo on randomly distributed orbits. Minor merger increase the spin parameter λ' of the orbit by depositing parts of their orbital angular momentum into the halo. But there was no dependence of the change of the spin parameter on the mass ratio as one would expect. We derived following parameters for follow-up simulations of a minor merger of a satellite with a stellar disk embedded in a alive halo:

- Because most of the eccentricities are close to parabolic orbits we chose a parabolic orbit for our satellite
- The peri-center distances peak at ~ 14.45 kpc or $\sim 0.05 r_{vir}$. Since we chose a medium sized galaxy we applied a peri-center distance for our minor mergers of 10 kpc
- There is no preferred angle at all. Therefore we chose 7 different angles within $[0^\circ, 180^\circ]$ and additional 2 angles of 45° and 90° between the Runge-Lenz vector \vec{A} and the disk plane.

Transferring the results from cosmological simulations to detailed simulations of a stellar disk in a dark matter halo helps to be consistent in our studies of the impact of minor merger on galaxies like our Milky Way.

Chapter 6

Results from galaxy simulations

If the Lord Almighty had consulted me before embarking on the Creation, I would have recommended something simpler.

Alfonso of Castile (ca. AD1250)

We show in this chapter the results from simulations of a minor merger where the parameters found in the cosmological simulations are used. We focus here on the velocity distributions of the particles of the galaxy and the merging satellite to make statements comparable to observations.

6.1 The Analysis

We found in chapter 5 that there is no preferred angle for the impact of the satellite. We therefore applied different angles to the simulation of an embedded galactic disk to cover a reasonable range of possibilities and let the simulation run for 4Gyrs. After this time the satellite is disrupted and has distributed its material in the vicinity of the disk. The particles of the satellite are now on certain orbits around the center of the galaxy where we can identify them and compare their velocity distributions with observations of similar stellar velocities available for the solar neighbourhood. Of course in observations we are limited to a small region around the sun for the determination of velocities of single stars. To mimic this effect we chose a small area of the system comparable to the solar neighbourhood and count the particles we found in this area. We favor this method to a “ring” over the whole disk to be sensitive to inclined orbits of satellite stars with respect to the disk plane. Fig.6.1 shows a face-on view of the galaxy where the boxes denote the area we picked out for the analyses. These areas correspond to the solar neighbourhood: the mean distance from the center is in simulation units $2.5R$, corresponding to 8.75kpc in reality. The box-length is $1R$, corresponding to 3.5kpc in reality, the box is centered at a distance of $2.5R$. This is a larger box than it is possible to survey in observations at the moment but our resolution in the simulations is much lower than in a real galaxy. For a number of particles sufficient for our statistics we have to extend the area of interest a bit. For better statistics of the LOSVD we extended the area even more towards galactic rotation: we chose the area to reach $3R$ towards galactic rotation and allowed the z -value of the box to be $2R$. This is justified since the observations also reached out quite far.

This should in principle not affect our results. In these areas we collected the velocity

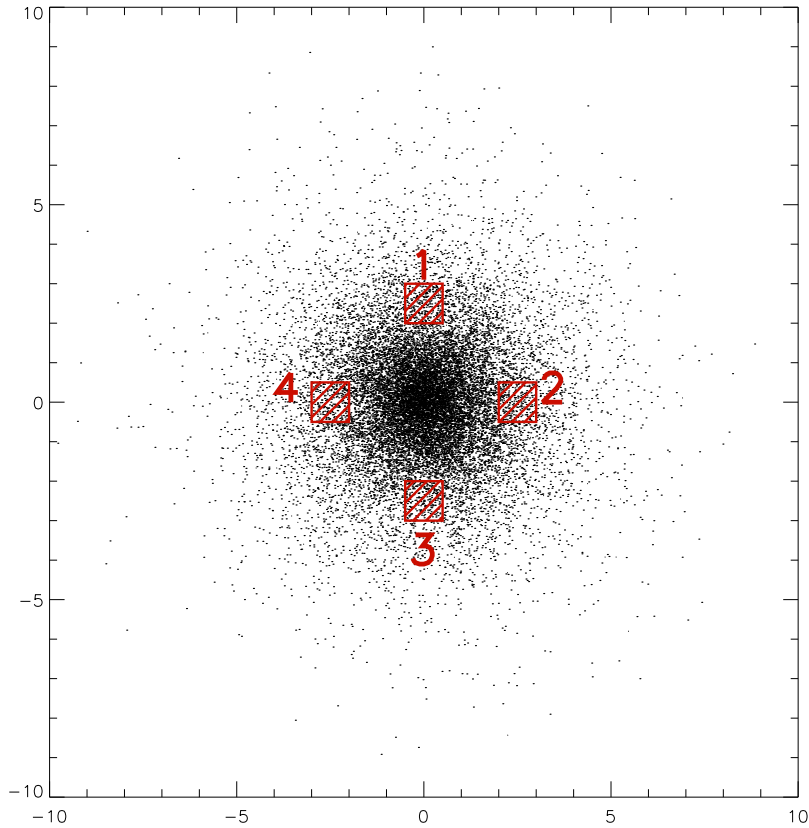


Figure 6.1: Face-on view of the galaxy disk model with the areas of interest marked where we applied our analyses. The box-length of each interest box is $1R \hat{=} 3.5\text{kpc}$ and its center is at a distance of $2.5R \hat{=} 8.75\text{kpc}$.

information of the particles and translated the velocity information in the case for the boxes 1-4 to the U,V,W system of galactic velocities. This system relates to the local standard of rest frame. This is the velocity of an object on a circular orbit around the galactic center in the disk plane. The U velocity is the velocity radial to the galactic center, it is positive if the star is moving away from the galactic center, and vice versa. The V velocity is the velocity in direction of galactic rotation, it is zero if the velocity matches the circular velocity around the center, positive if the stars revolves faster and negative if the star is slower. The W velocity is the star's velocity perpendicular to the galactic plane. If a star is moving towards the north galactic pole the value of W is positive. The sun, for example, has velocities (U=-9, V=+12, W=+7) in this system. Our analysis would then result in a similar picture seen in fig.2.12. We combined the different velocity-coordinates resulting into three different plots: an UV-plot, a VW-plot, an UW-plot. For the LOSVD we adopt the type of plot seen in fig.2.9.

We actually chose four “areas of interest” (see fig.6.1) to collect the information of the different geometries of the simulated minor merger. In fig.6.2 a plot of the initial conditions is shown where the satellite orbital plane enclosed an angle of 30° with the disk

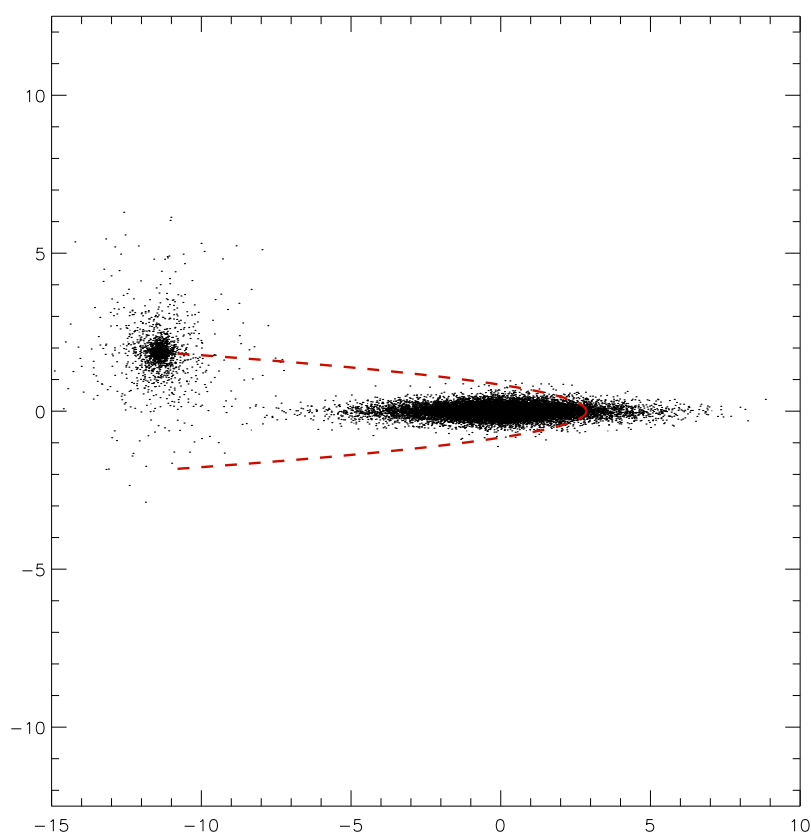


Figure 6.2: Edge-on view of the galaxy disk model with the initial position of the satellite. Plotted here is the parabolic orbit of the satellite. In this case the orbital plane encloses an angle of 30° with the disk plane.

plane. Plotted is also the parabolic orbit of the satellite. The pictures of the results of our analyses are numbered: first the angle between orbital plane and disk plane is mentioned (eg. “030”), then the number of the area (see fig.6.1), separated by an underscore (“030_1”). For the two cases where we varied the angle between the Runge-Lenz vector \vec{A}^1 (which has in any other case an angle of 90° between orbital plane and disk plane) and the disk plane we added the angle, separated by another underscore (“090_1_045”). See section 4.5 for more information on the simulation parameters. We plotted within the UVW-plots the disk particles (black points), the halo particles (red crosses) and the satellite particles (filled green circles) for a galactic system that suffered from a minor merger. We take halo particles into account to see if the satellite stars are distinguishable from halo stars. The LOSVD plot takes into account the thin disk particles (solid line) taken from initial conditions of the galactic disk, the particles of a “thick disk” (dashed line), i.e. a disk which suffered from a minor merger, and particles from the satellite (dash-dotted line). This assures the possibility to compare the results to observations of Torres et al.,

¹The Runge-Lenz vector always points from the center of the orbit to the peri-helium, see section 4.4

2001 and Gilmore et al., 2002 seen in fig.2.12 and fig.2.9.

In general, we expect to see the disk to be heated and puffed up, which means in the LOSVD distribution a broader distribution of the “thick disk” velocities. The maximum number of this distribution should be reduced because less particles of the heated and puffed up disks are in our areas of interest. Note that in the UVW plots the halo - which is not rotating with respect to disk - should have a mean V-velocity of $\sim -200\text{km/s}$. The satellite particles should be distributed randomly since the satellite is destroyed and disrupted in the merging event, their velocities should then be similar to the velocities of halo particles. With exception of the orbits close to the disk plane (i.e. angles of 0° , 30° , 150° , 180°) we would not expect satellite particles on orbits near to the disk plane. For angles of 150° and 180° we would expect a counter-rotating population in our LOSVD. The halo particles should not be visibly affected by the merger event when looking at the UVW plots (because they have quite high velocity dispersion and are therefore not heated easily), the disk particles should show changes in the UVW velocities by the input of kinetic energy by the satellite.

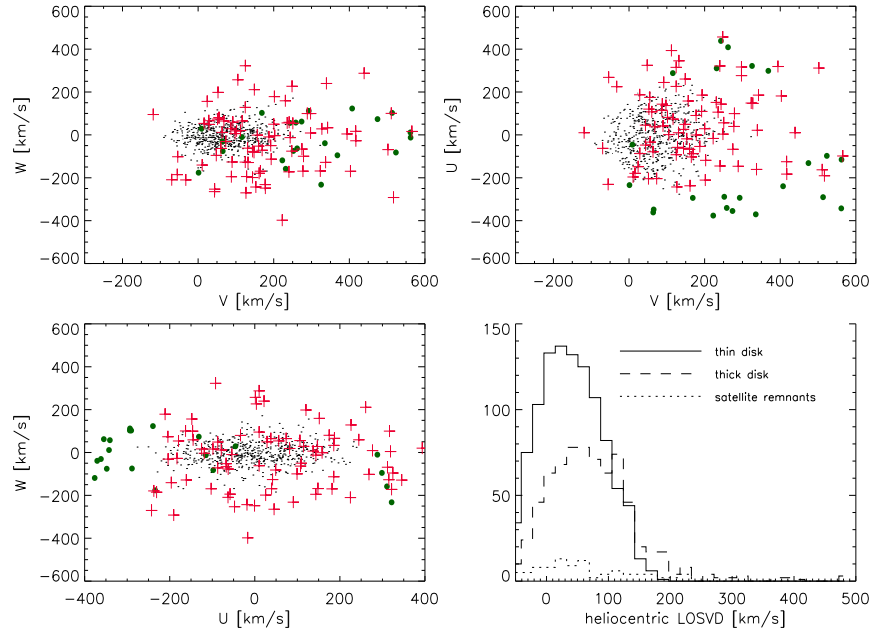


Figure 6.3: Simulation no. 000_1. In the UVW plots red crosses denote halo particles, black dots denote disk particles, green circles denote satellite particles.

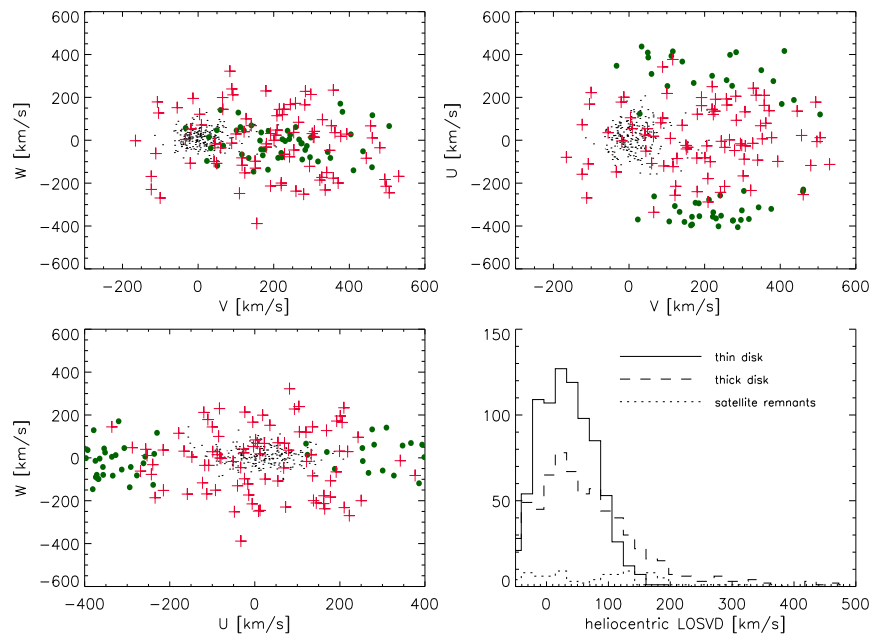


Figure 6.4: Simulation no. 000_2

6.1 The Analysis

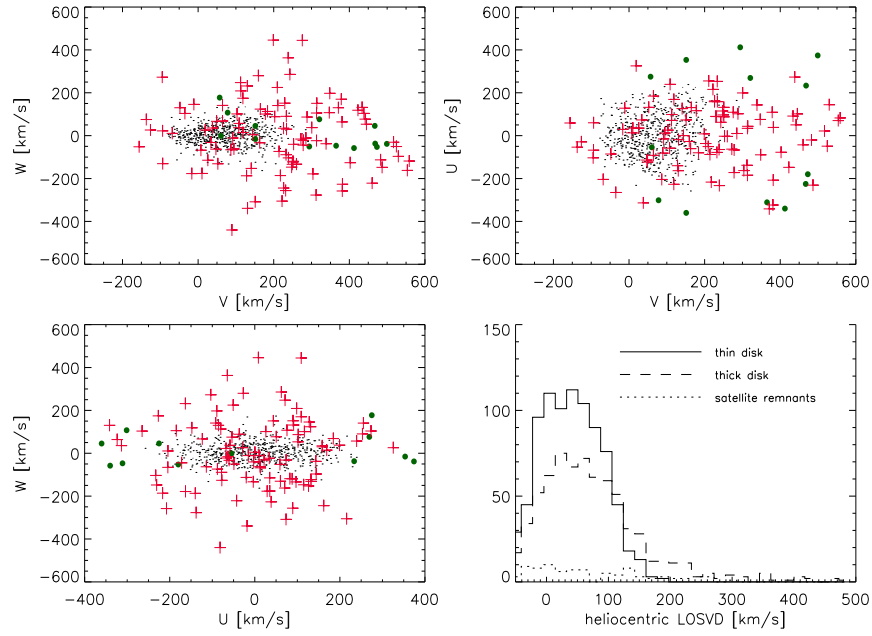


Figure 6.5: Simulation no. 000_3

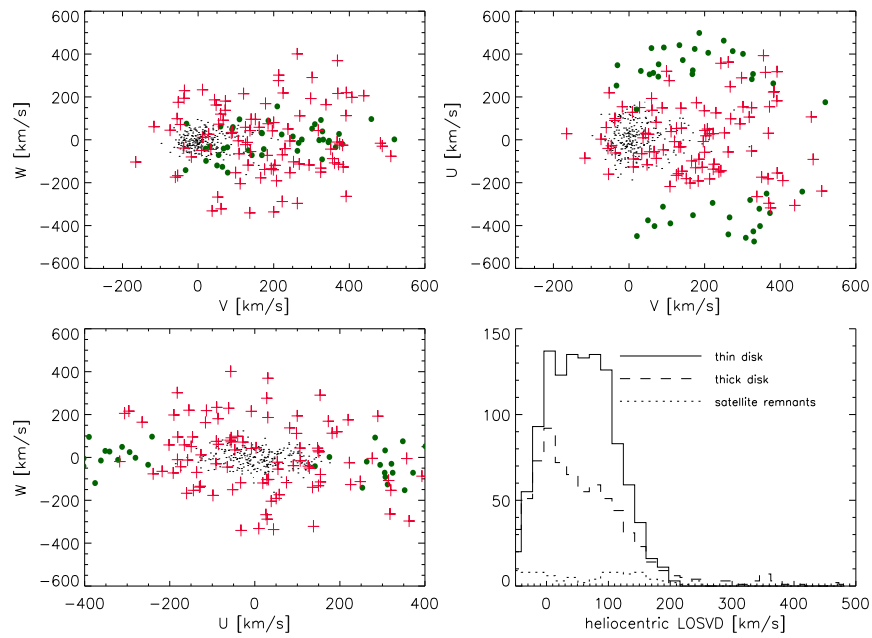


Figure 6.6: Simulation no. 000_4

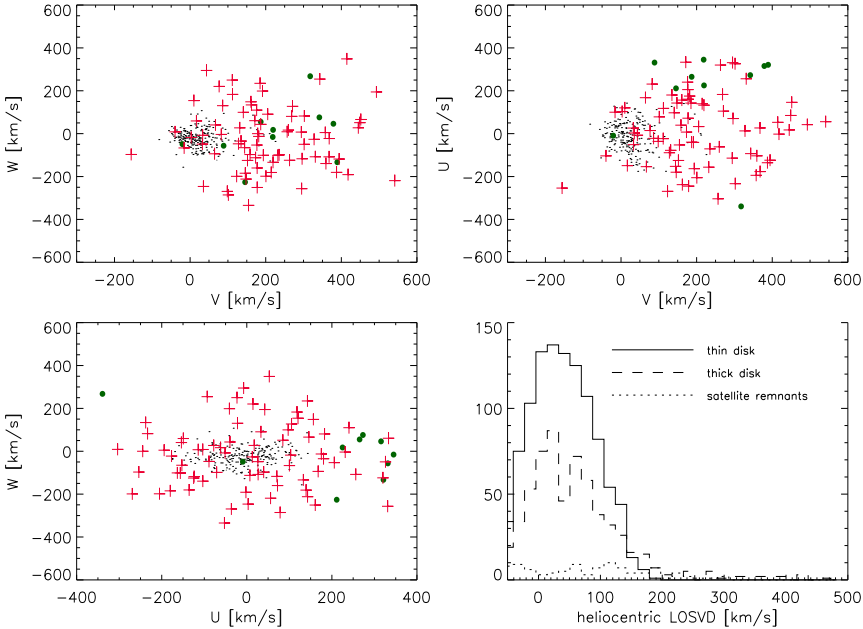


Figure 6.7: Simulation no. 030_1

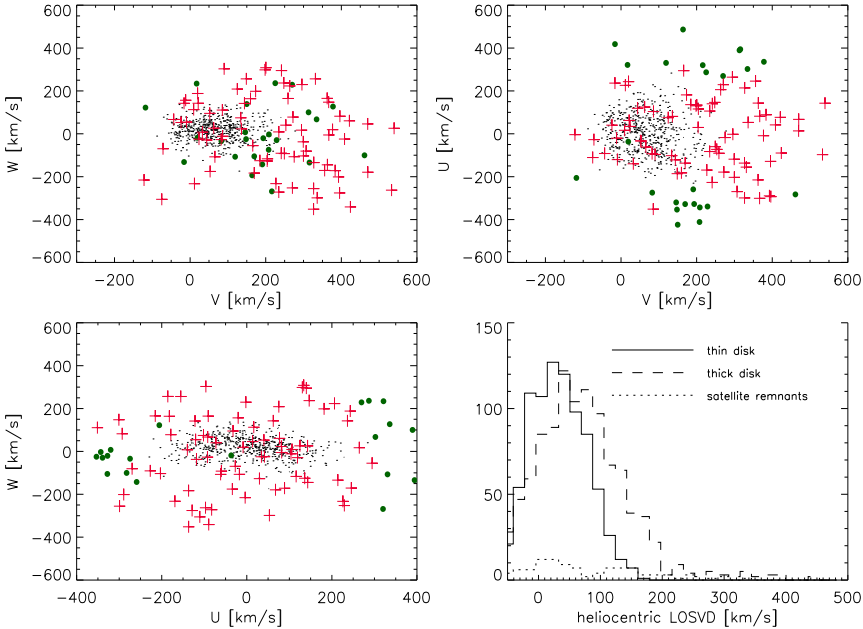


Figure 6.8: Simulation no. 030_2

6.1 The Analysis

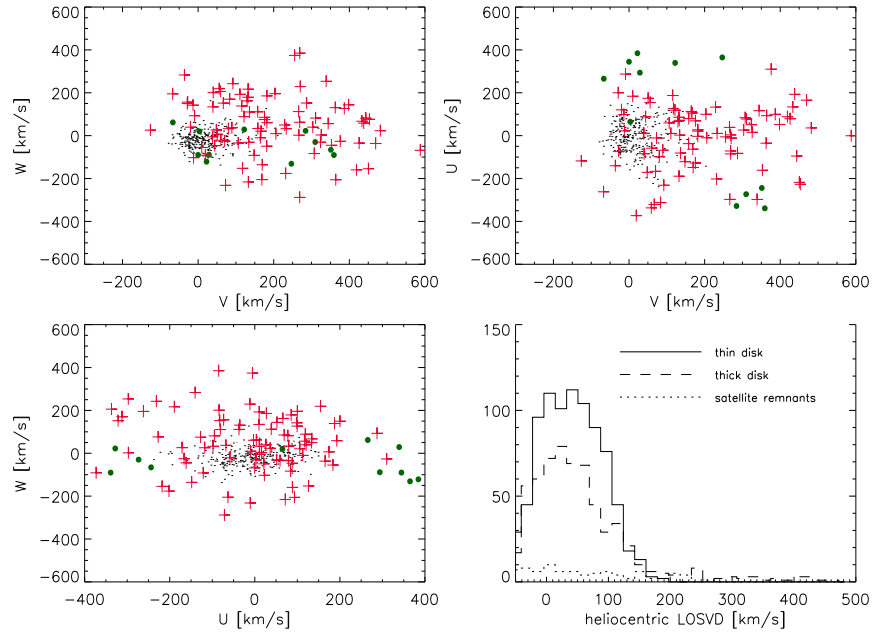


Figure 6.9: Simulation no. 030_3

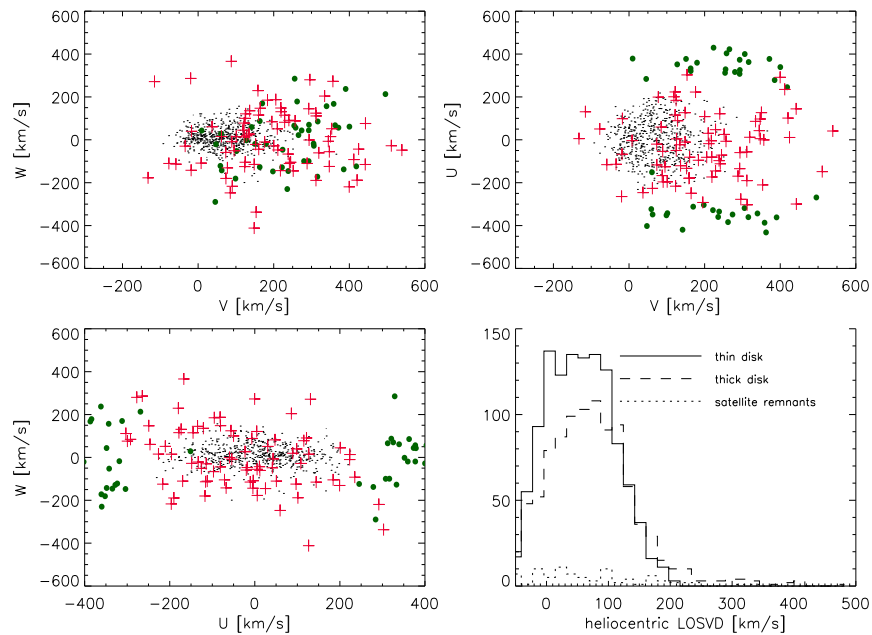


Figure 6.10: Simulation no. 030_4

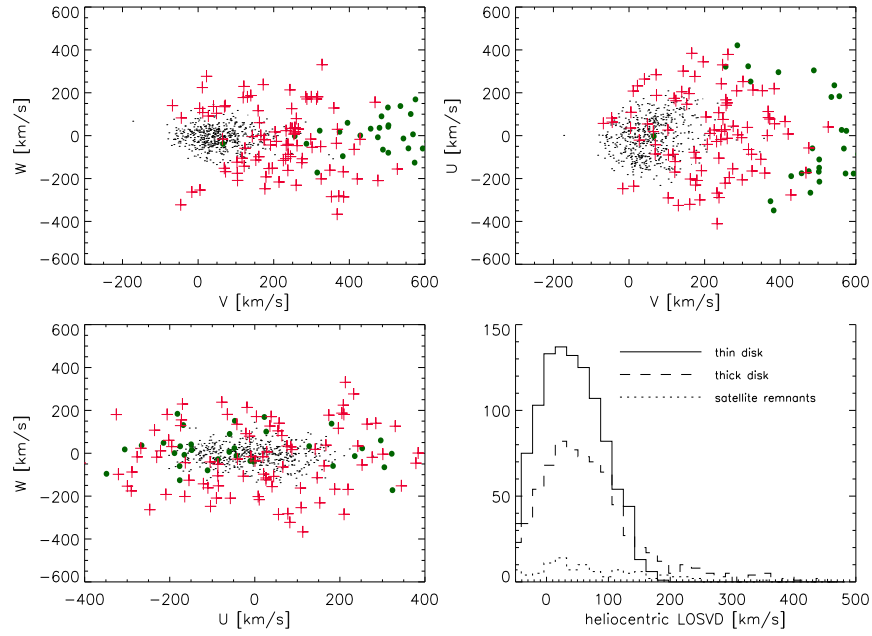


Figure 6.11: Simulation no. 060_1

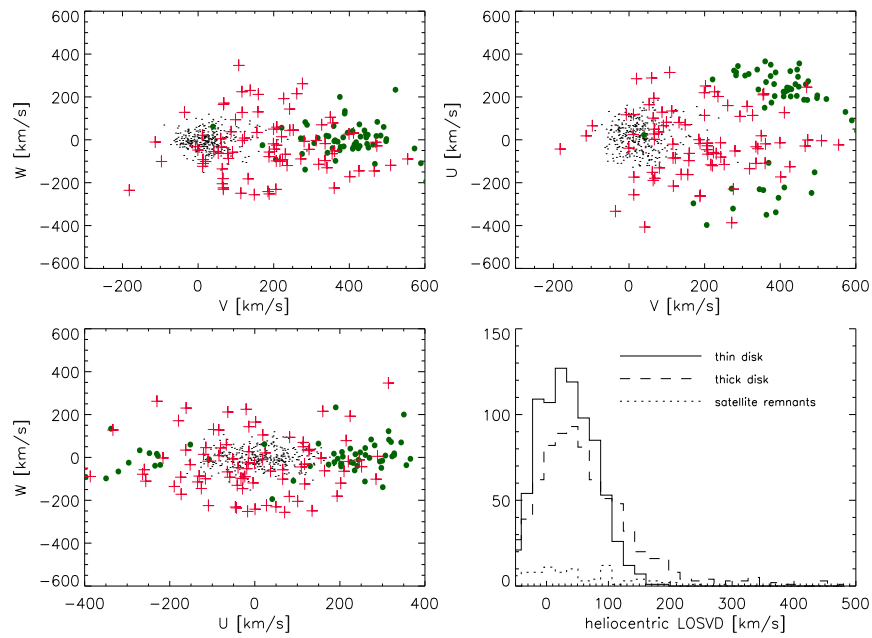


Figure 6.12: Simulation no. 060_2

6.1 The Analysis

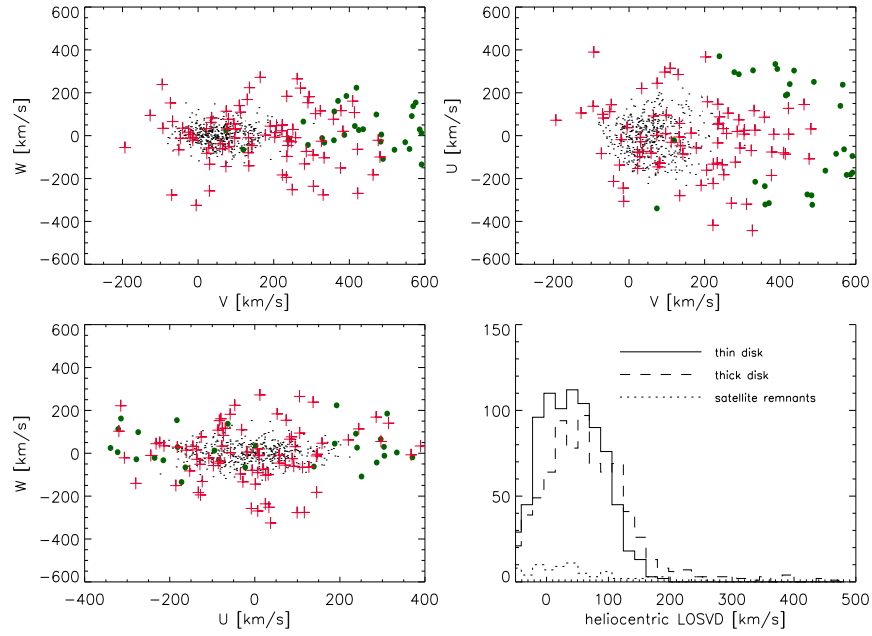


Figure 6.13: Simulation no. 060_3

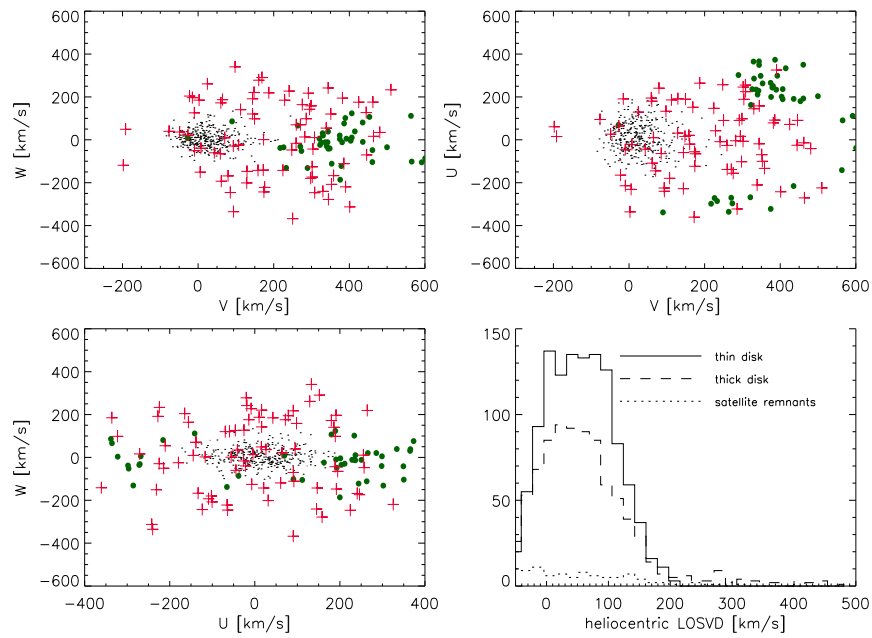


Figure 6.14: Simulation no. 060_4

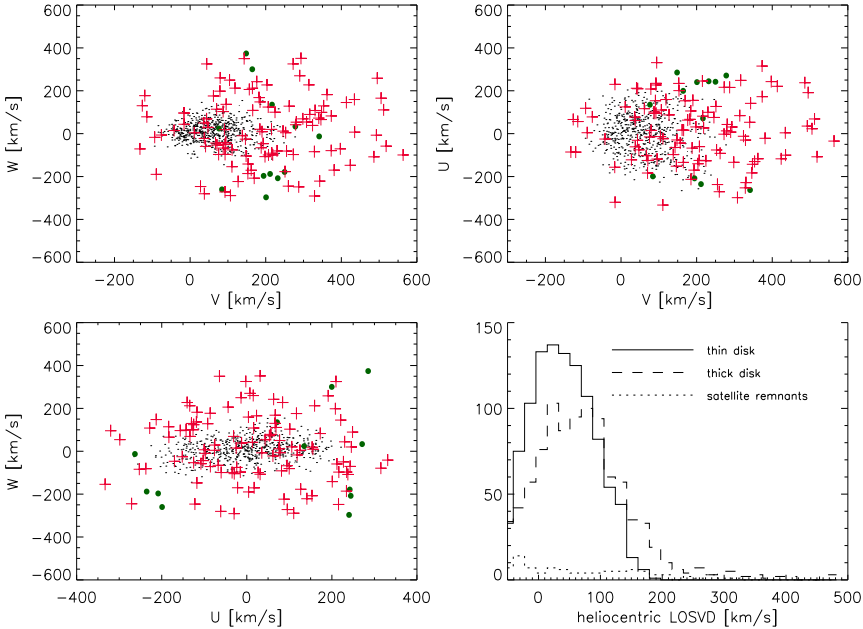


Figure 6.15: Simulation no. 090_1

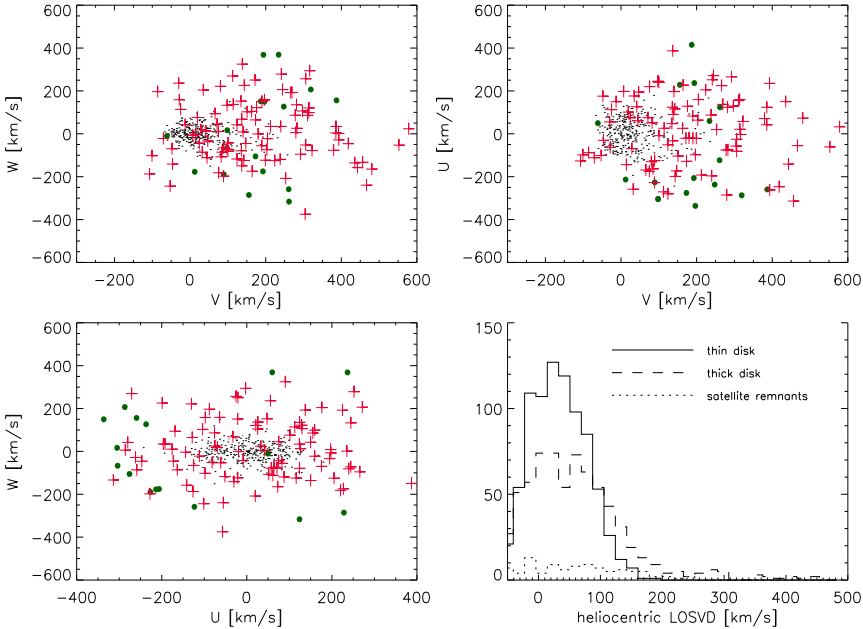


Figure 6.16: Simulation no. 090_2

6.1 The Analysis

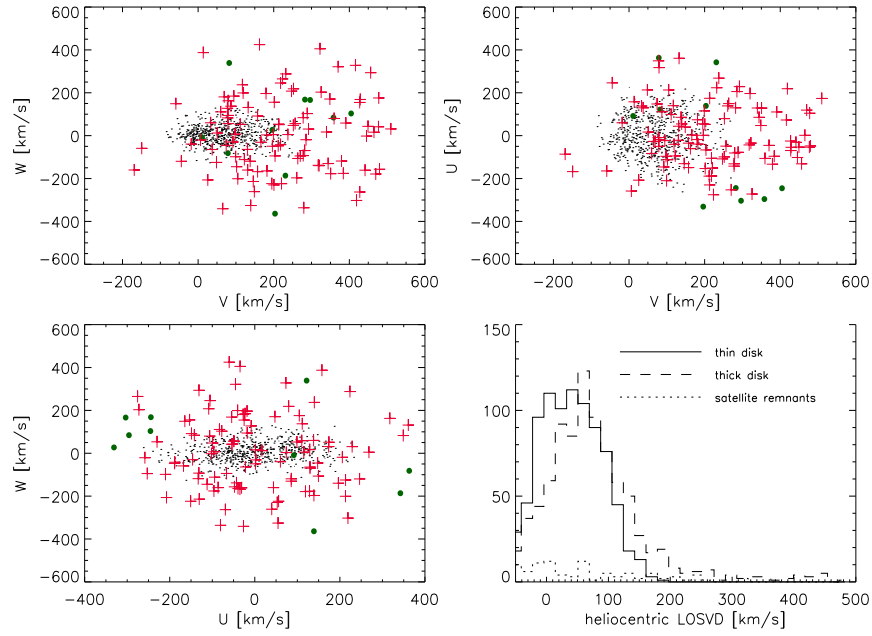


Figure 6.17: Simulation no. 090_3

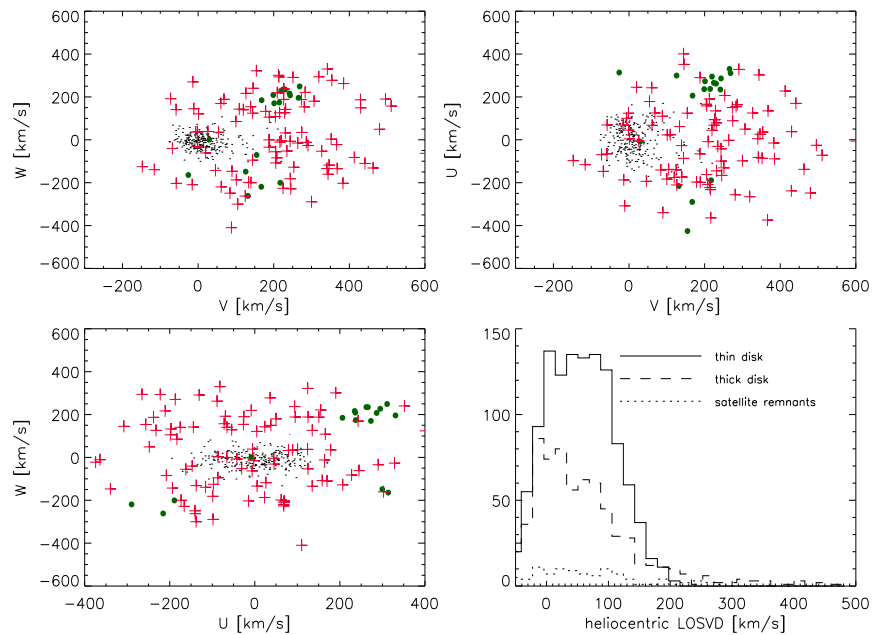


Figure 6.18: Simulation no. 090_4

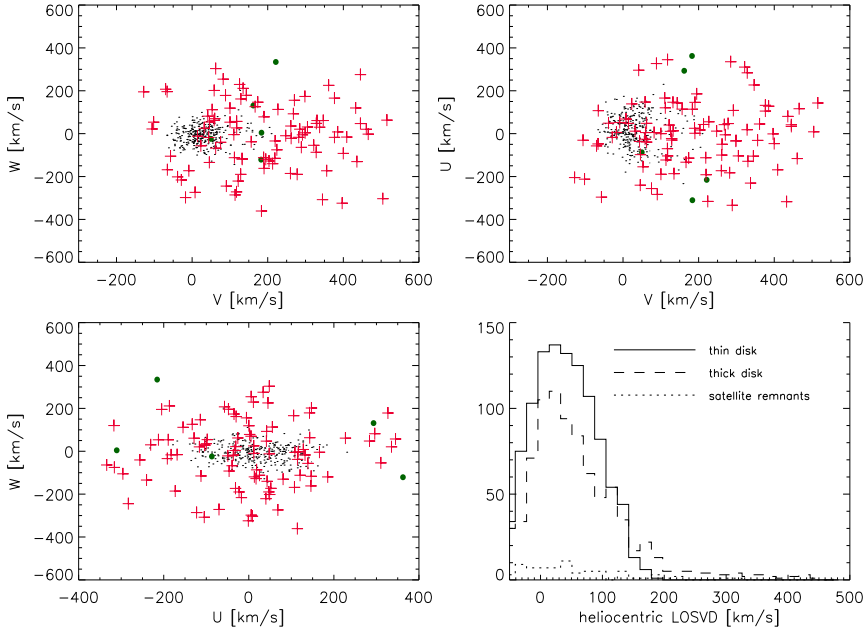


Figure 6.19: Simulation no. 120_1

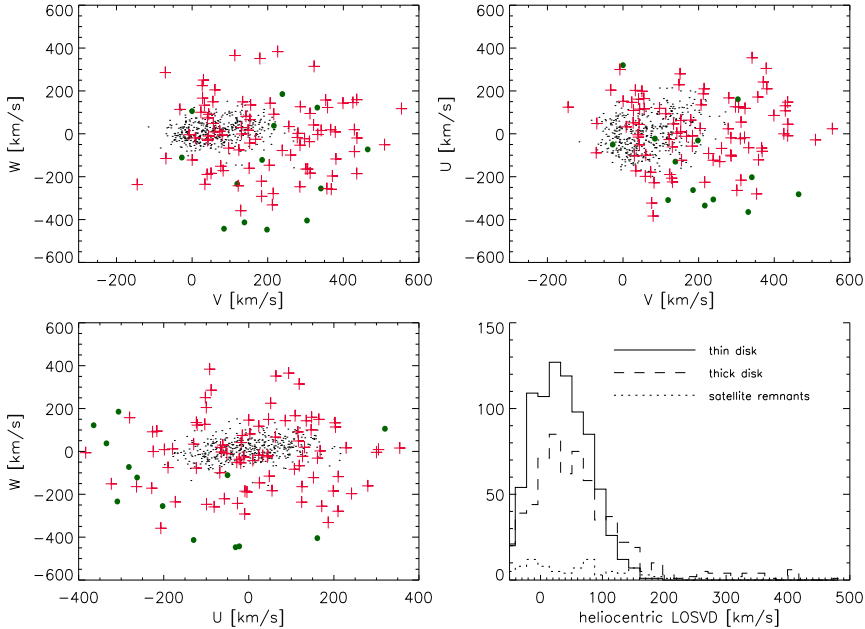


Figure 6.20: Simulation no. 120_2

6.1 The Analysis

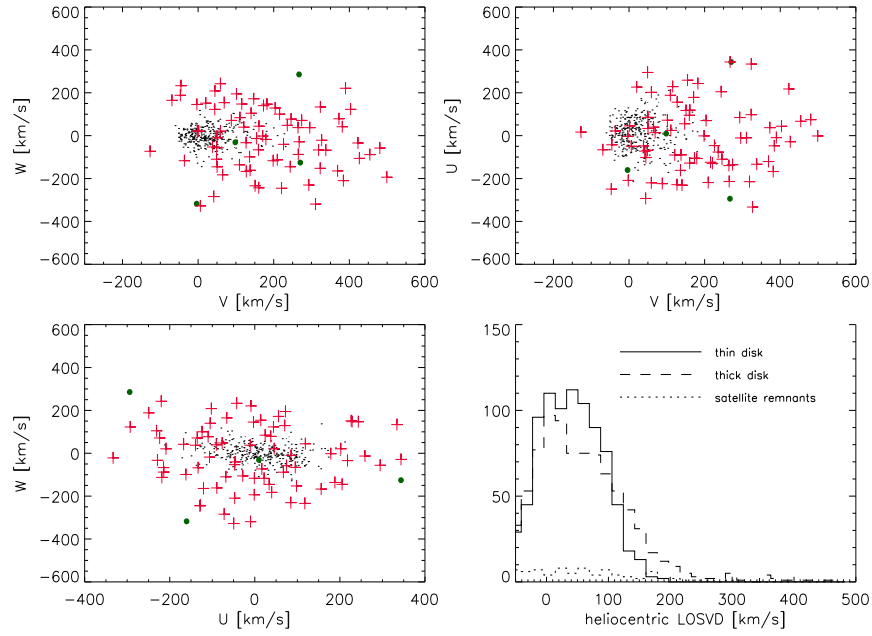


Figure 6.21: Simulation no. 120_3

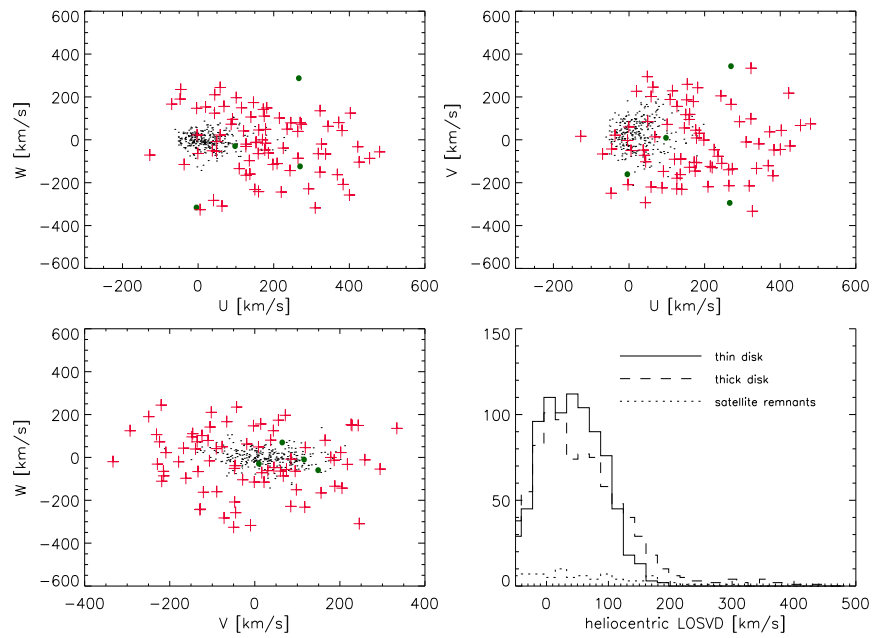


Figure 6.22: Simulation no. 120_4

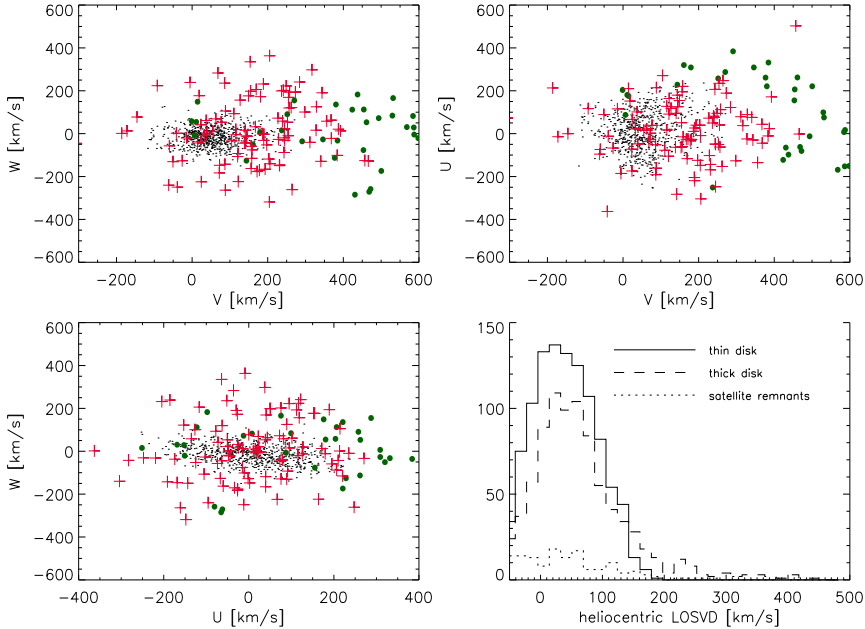


Figure 6.23: Simulation no. 150_1

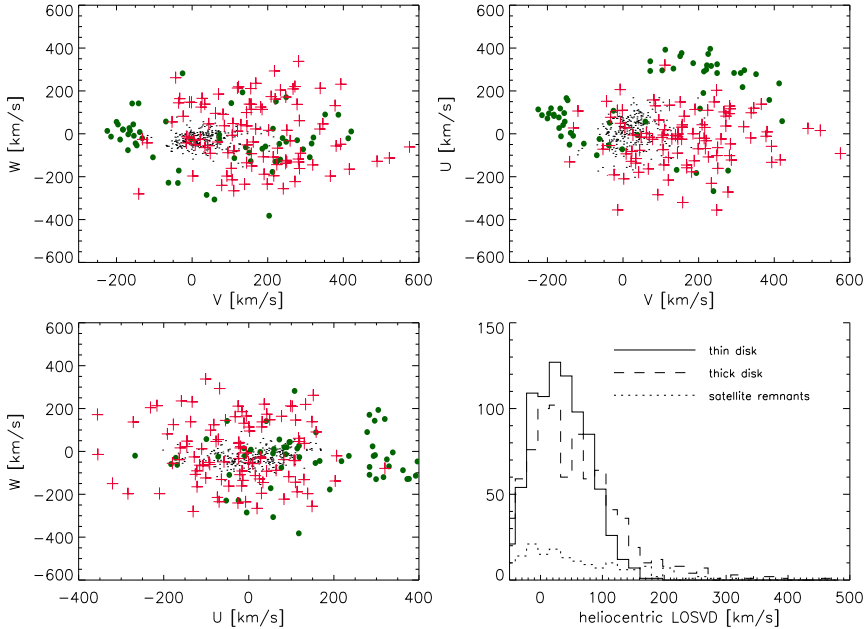


Figure 6.24: Simulation no. 150_2

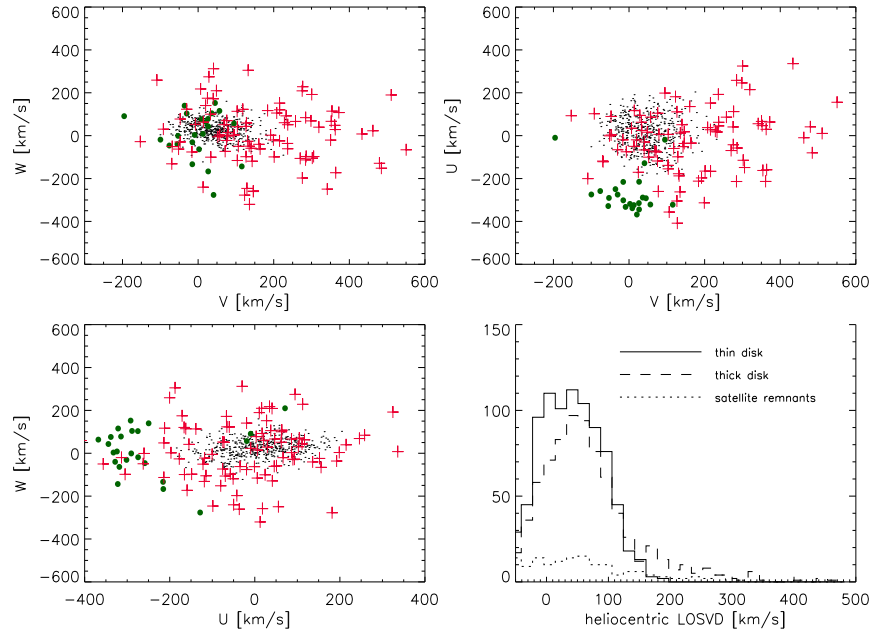


Figure 6.25: Simulation no. 150_3

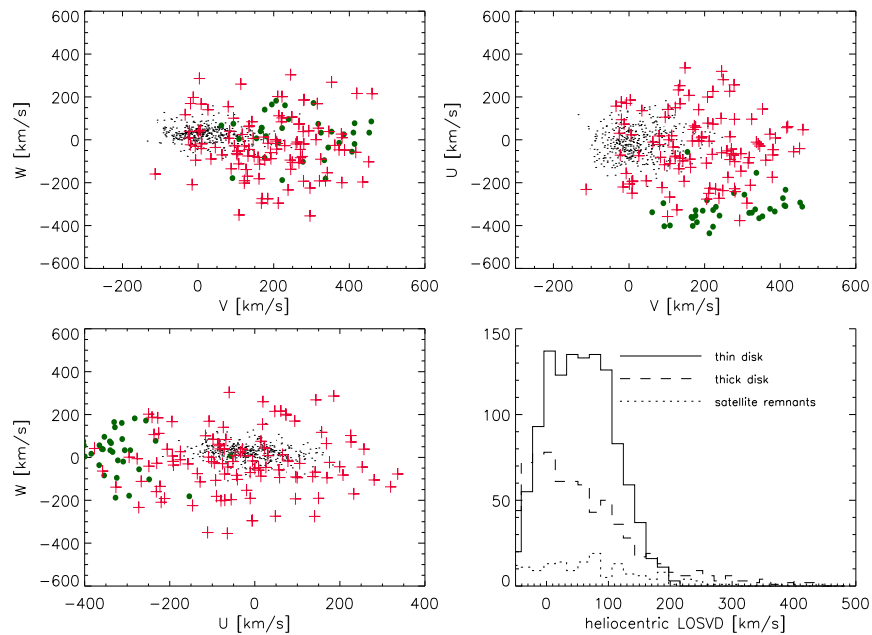


Figure 6.26: Simulation no. 150_4

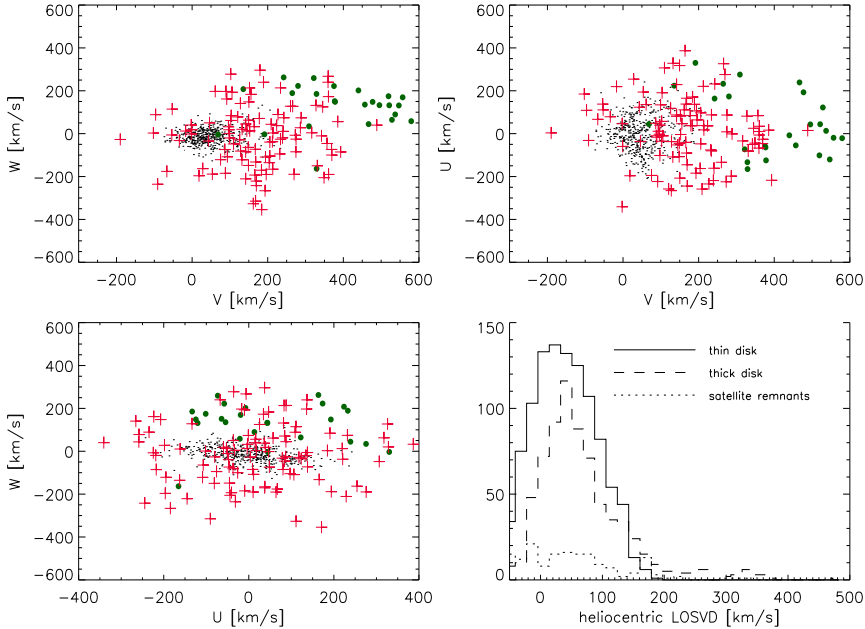


Figure 6.27: Simulation no. 180_1

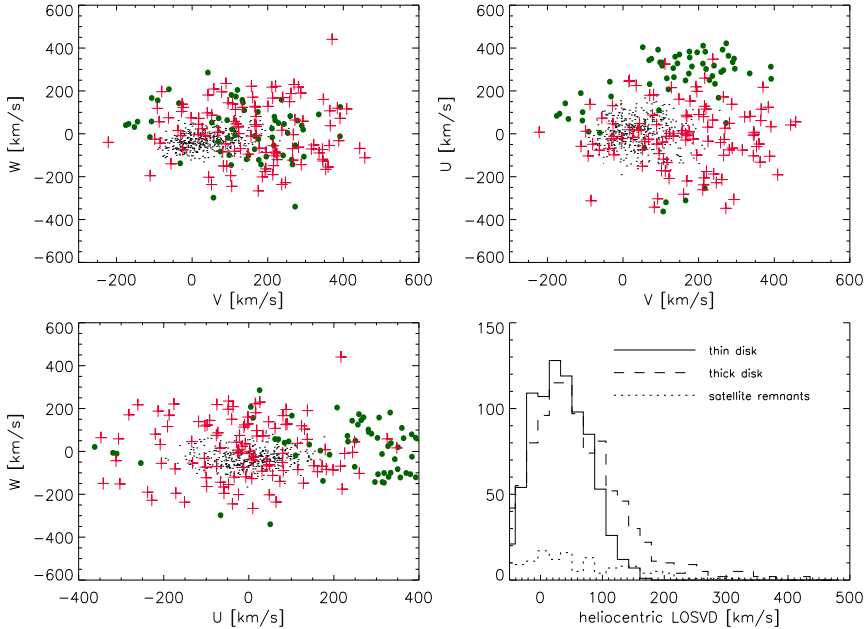


Figure 6.28: Simulation no. 180_2

6.1 The Analysis

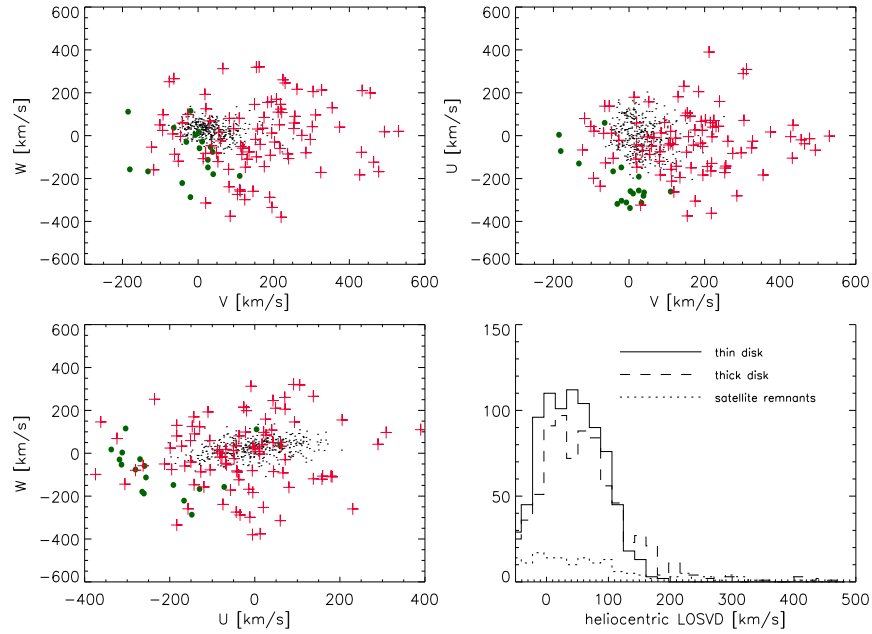


Figure 6.29: Simulation no. 180_3

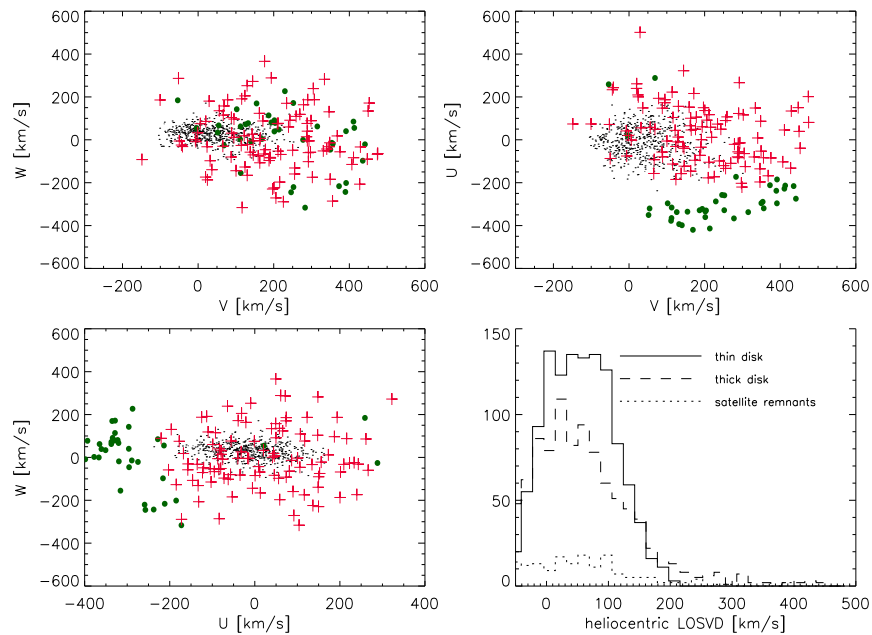


Figure 6.30: Simulation no. 180_4

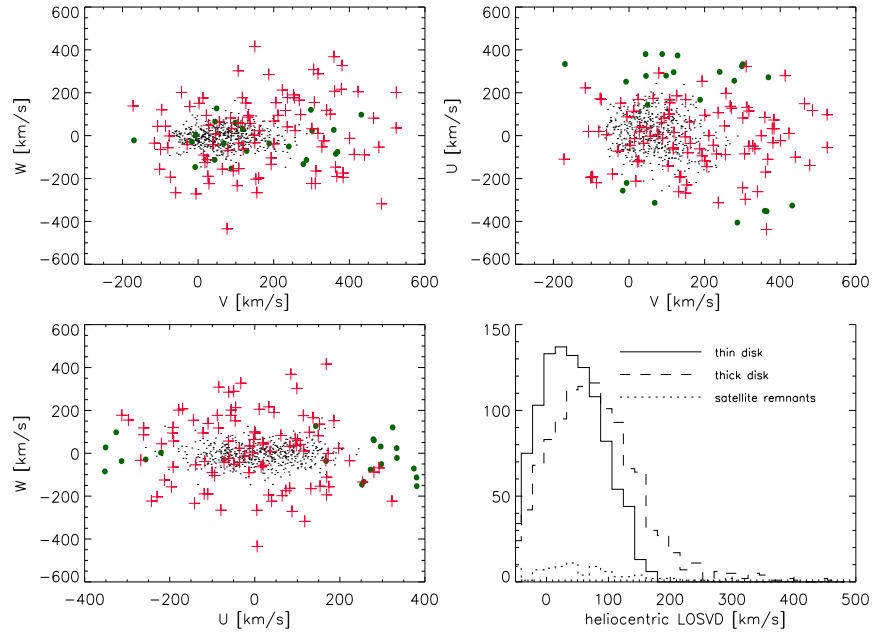


Figure 6.31: Simulation no. 090_1_045

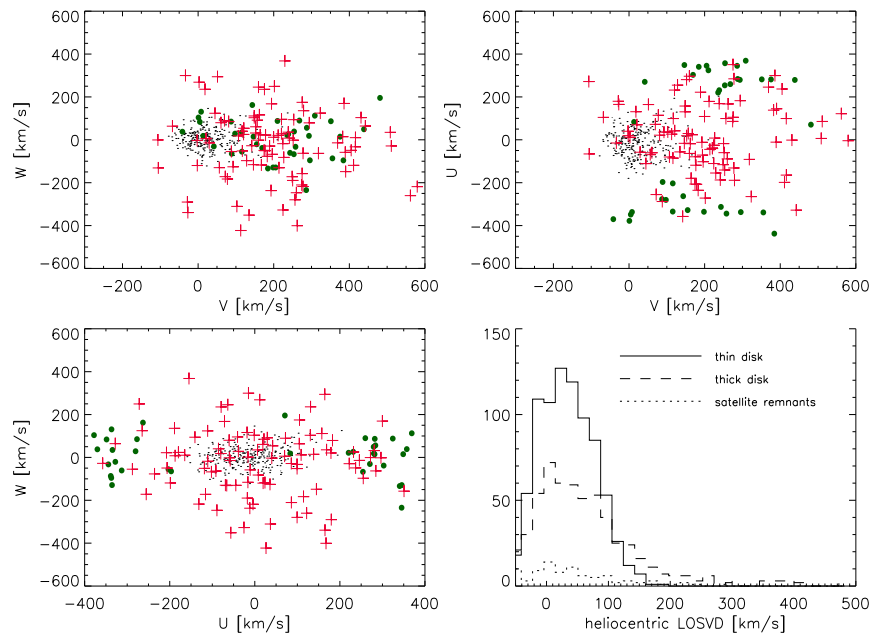


Figure 6.32: Simulation no. 090_2_045

6.1 The Analysis

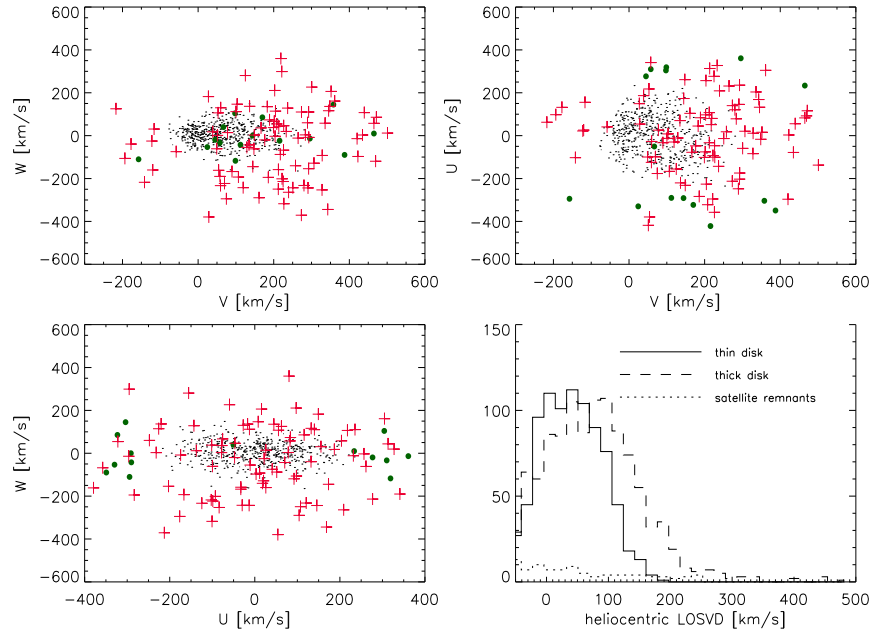


Figure 6.33: Simulation no. 090_3_045

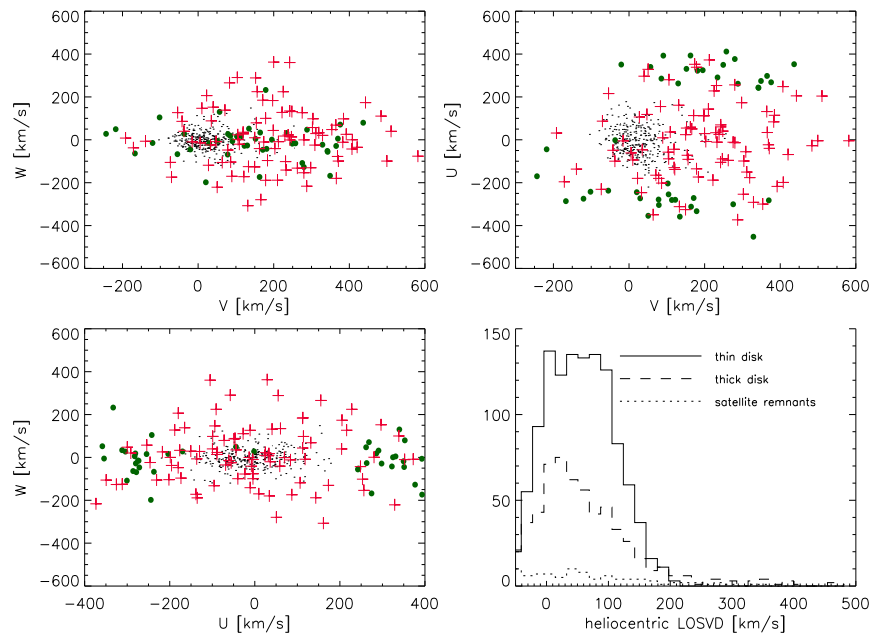


Figure 6.34: Simulation no. 090_4_045

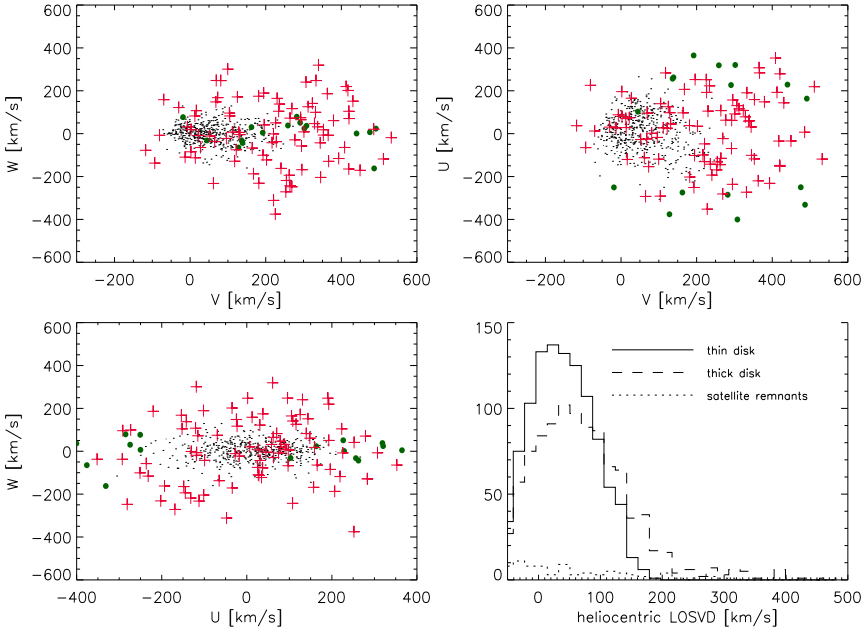


Figure 6.35: Simulation no. 090_1_090

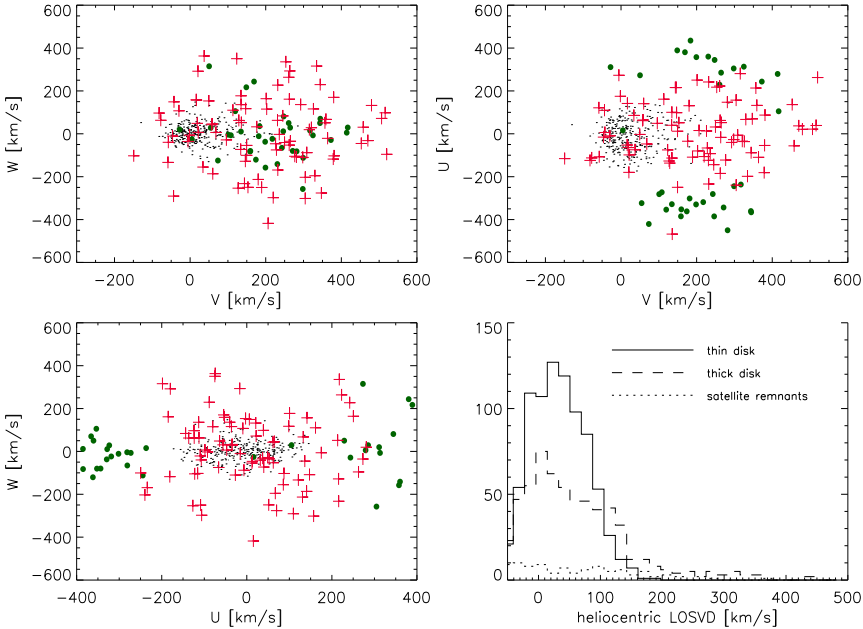


Figure 6.36: Simulation no. 090_2_090

6.1 The Analysis

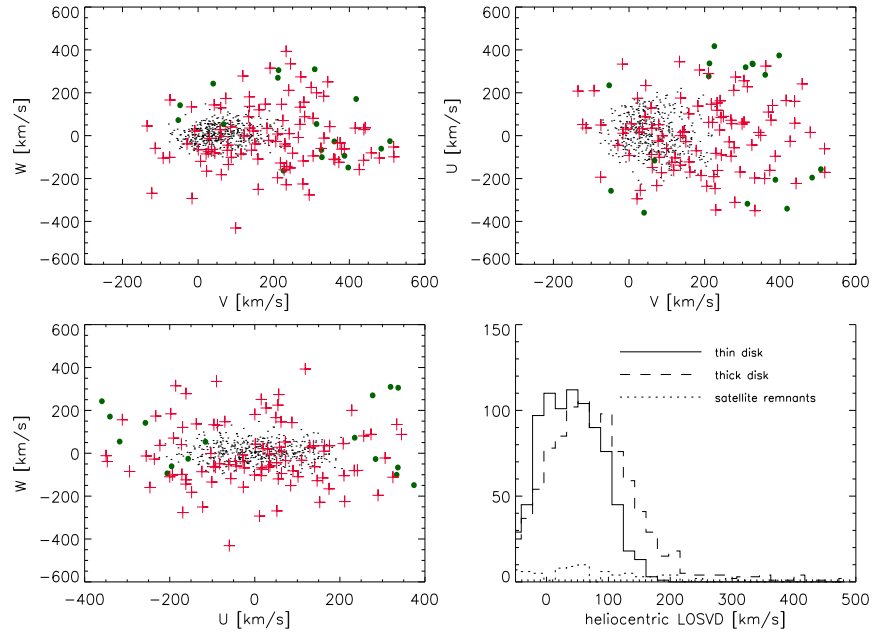


Figure 6.37: Simulation no. 090_3_090

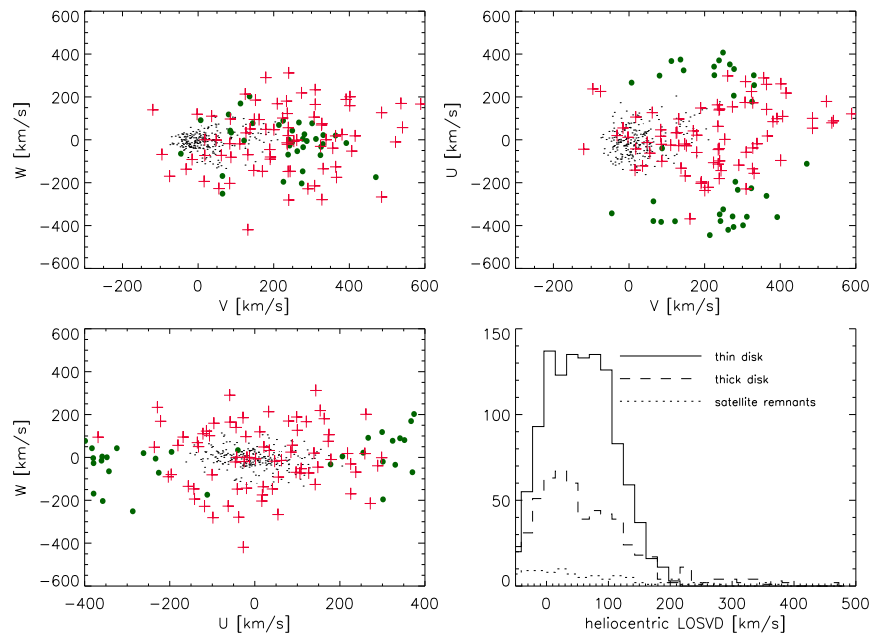


Figure 6.38: Simulation no. 090_4_090

6.2 Results

First, we can fix some general results: in the LOSVD the covers the expectation that the thick disk LOSVD is broadened and has a smaller peak value than the thin disk stars; see simulation no.090_01 for a nice example, where the peak is reduced and the distribution extends more to higher velocities. We also find that the results in the UVW velocities for one angle does not differ too much with the next angle for the first seven simulations: there is a “smooth” evolution visible. Another general result is that we did not have many satellite particles (relative to the disk particles it differs by factor of ~ 15 instead of the factor of 5 of N_{disk}/N_{sat}) in our areas of interest which points to the assumption that the satellite particles are widely distributed (as seen in simulation no.120_x where we only have a handful of satellite particles). The general velocity structure is of such that the satellite particles can be easily mixed up with halo particles if there is no special concentration of satellite particles like, for example, in simulation no.180_02. The W velocities of the satellite particles commonly scatter narrowly around zero even for the cases where the satellite came in with a large angle between the disk plane and the velocity vector (simulations no.090_x_45 and no.090_x_90). This may be due to the effect that satellite particles with significant W velocities are able to leave the system on a short timescale (e.g. seen in fig.2.8).

Another general result is that the UVW velocities and LOSVD does not depend on the choice of the area of interest. Usually the behaviour in one area is similar to the behaviour in the other areas.

An interesting feature arises in some simulations where we found a bimodal distributions of the U velocities for the satellite particles meaning that there are particles which are moving quite fast into the direction of the galactic center and into the opposite direction, out of the galaxy. Here the satellite seems to be disrupted in a way that in a ringlike structure (i.e. all four areas) the particles are “collapsing” or “exploding”.

We now pick out some simulations which show deviations from the general results:

- Simulation no.060_x shows high positive V velocity for the satellite particles while having the common bimodal distribution in U. This means that the particles are moving fast into the direction of galactic rotation and having a population moving towards to and away from the galactic center. This may be due to the disruption of the satellite in two part that are now moving on different trajectories around the center.
- Simulation no.150_x shows a change of the position of the satellite particles in the UV plane, the concentration of particles runs counterclockwise from positive UV to positive V and negative U. This may correspond to an elliptical orbit of the satellite particles with focal points roughly at $x = 3R$, $y = 3R$ and $x = 0$, $y = -3R$ (where of course this orbit not has to be a really closed one.)
- Simulation no.180_x shows a similar behaviour as simulation no.150_x - which is not surprising since the merger had similar initial conditions and angles.
- We see in the LOSVD only weak traces for a counter-rotating population of satellite particles in simulation no.150_x and simulation no.180_x although the satellites were on orbits counter-rotating to the disk.

6.3 Discussion

In (Bertschik, 2001) it was already shown that it is possible to create a jump in velocity dispersions similar to the jump seen in observations: within 1Gyr after the minor merger the velocity dispersion were increased by $\sim 50\%$ at solar radius around the galactic center. We list in tab.6.1 and tab.6.2 the change of velocity dispersion in U, V and W velocities (named $\Delta\sigma_U$, $\Delta\sigma_V$ and $\Delta\sigma_W$) compared to a quite galactic disk that did not suffer from a minor merger ($\sigma_U = 35.9\text{km/s}$, $\sigma_V = 26.4\text{km/s}$ and $\sigma_W = 25.5\text{km/s}$). The results do not show a clear dependence on the merging parameter. The V component was heated most, the U component least. Since σ_U was highest in the initial cold disk, this is an expected result. The increase of the U, V and W velocity dispersions is comparable to what is found by (Quillen & Garnett, 2000) but lacks clear traces of the different orbits of the satellite.

simulation no.	$\Delta\sigma_U$ (km/s)	$\Delta\sigma_V$ (km/s)	$\Delta\sigma_W$ (km/s)
000_x	14.9	17.3	10.3
030_x	10.8	13.6	7.9
060_x	13.2	15.6	8.5
090_x	10.3	13.9	10.2
120_x	10.0	15.8	8.9
150_x	14.3	14.6	8.3
180_x	15.3	15.5	8.4
045_x	12.2	15.5	9.4
090_x	11.5	15.7	9.2

Table 6.1: The absolute changes in UVW velocities after the merger event for different simulation runs.

simulation no.	$\Delta\sigma_U$ (%)	$\Delta\sigma_V$ (%)	$\Delta\sigma_W$ (%)
000_x	41.5	65.5	40.4
030_x	30.0	51.5	30.1
060_x	36.7	59.1	33.3
090_x	28.7	52.7	40.0
120_x	27.9	59.8	34.9
150_x	39.8	55.3	32.5
180_x	42.6	58.7	32.9
045_x	34.0	58.7	36.9
090_x	32.0	59.4	36.1

Table 6.2: The relative changes in UVW velocities after the merger event for different simulation runs. Note the increase in the components with low velocity dispersion (V, W) and the heating of the disk: increased velocity dispersion of the W component.

6.3 Discussion

The simulations did not give a definite hint on the consequences of a minor merger with different parameters. It is not possible to derive the exact orbit of the minor merger with

fair accuracy from the velocity structure of its particles, and it is already hard to distinguish the satellite remnants of different orbit families of the initial orbit of the satellite. This is not that surprising, though, since with more and more time the system shows more and more non-linear or even chaotic behaviour. Besides, our statistics are not very good even with several 100,000 particles in the system. The LOSVDs show the expected behaviour of being flattened and stretched out but lacks a clear signal for a counter-rotating satellite population when having a minor merger with a counter-rotating orbit. Nevertheless, it was possible to detect some features coming from a certain choice of the orbit. This may help to identify the result of merger in a certain orbit.

One way out may be to perform more detailed simulations with much higher resolution in the disk and in the satellite, perhaps including gas to see the effects of an dissipational component. Since our simulations were done making a compromise of saving time and disk space we see here some improvement to make in the future. Additionally, one could apply an analysis of the orbits of the involved particles to derive other features from this.

Chapter 7

Discussion and Conclusions

One of the things that makes the history of science so endlessly fascinating is to follow the slow education of our species in the sort of beauty to expect in nature.

Steven Weinberg

CDM predicts large amounts of substructure that merges together and forms bigger clumps. The interest of the community is quite focused on spectacular major mergers, the collision of two massive halos with embedded stellar disks. Or it deals with accretion events of satellites, small lumps of dark matter accreted by a giant halo without any substantial effect on its structure. We paid more attention to the medium regime of minor merger which may have substantial effects on stellar disks without destroying them.

We performed quite a lot of simulations to address following questions: Did the Milky Way suffered from a minor merger event with a satellite in the past which is supported by several hints (Torres et al., 2001, Quillen & Garnett, 2000, Gilmore et al., 2002)? What is the likelihood of such an event, and what are the parameters of a minor merger if it is happening? Is there anything left over we could see even if the minor merger happened Gyrs before?

We addressed the first questions with the analysis of cosmological simulations of structure formation of dark matter done by our new code WINE. After we checked the functionality of WINE by comparison to other codes we derived the abundance of minor mergers of mass ratios from 1:20 to 1:5 in space and time and found that it peaks 6Gyrs after the big bang. The mass ratio of minor mergers does not depend on redshift, the merging parameter f fairly fits expectations from simulations and observations of major merger while the merger rate R_{merger} differs from observations and simulations of major merger. The orbits of minor mergers depend slightly on redshift, early minor merger have more parabolic orbits with less peri-center distances than later ones (they differ by a factor of ~ 2.5). Comparing this to orbits of major merger we found that minor merger have in general smaller peri-center distances than major merger. We found this connected to the gain of angular momentum of the orbits with time due to the interaction with other objects where the big halos involved in major merger are interacting more than the halos involved in minor merger.

The angles between the orbits and the spins of the merging halo are found to be as random as one would expect from isotropy in cosmology. We found that the spin parameter of the halos which suffered from a minor merger are influenced slightly, the spin parameter λ' was increased by the minor merger from 0.0308 to 0.0421.

All our considerations regarding minor merger suffer from the lack of sufficient observations of minor merger events to which one could compare our results. Since relatively small objects are involved, minor merger are hard to detect to far or even medium range. One of the few observations that was done is that of Schwarzkopf & Dettmar, 2000b, and they reached only a small redshift, not comparable to our statistics. But since our results seemed to be reasonable (which we found by several consistency checks) we transferred them to additional simulations of a galactic disk, applying the parameters found in cosmological simulations in a consistent way.

We performed a bunch of simulations with having the parameters from cosmological simulations applied and chose certain regions where we analyzed the velocity structure of the particles in UVW diagrams and in heliocentric LOSVD distributions. Doing this we tried to distinguish if a certain geometry of the merger induces different effects in the velocity structure when seen from different viewpoints. Several features were found that matches expectations: the LOSVD distribution of the thick disk flattens and broadens due to the merger, satellite particles were not caught in the areas of interest because they were distributed elsewhere, satellite particles have low W velocity while they could have high U and V velocities. We found in general that in UVW velocities the satellite particles are hard to distinguish from halo particles with exception of certain geometries (simulations no.150_x and no.180_x). The latter ones show significant concentrations of UV velocities relative to the halo particles. The signal of satellite remnants in the LOSVD is very weak which is probably mainly due to limited resolution of the satellite. The increase of the U, V and W velocities is comparable to the difference between the observed values of the thin and the thick disk of our Milky Way, supporting the idea that the thick disk is due to a minor merger.

Chapter 8

Outlook

The history of cosmology shows us that in every age devout people believe that they have at last discovered the true nature of the universe.

Edward R. Harrison

Minor mergers happen. They are quite frequent for a galaxy like our Milky Way although there was obviously no substantial merging event in the last 6Gyrs. More sensitive instruments, more detailed observations will reveal more of these small collisions between galactic objects in other galaxies and may even reach out to higher redshifts to confirm or reject the results from cosmological simulations. Same for the local galaxy: Further observations of the thin and the thick disk of our Milky Way (Gilmore et al., 2002), e.g. a more extended evaluation of the white dwarf population (Torres et al., 2001) and other old stars which can trace a minor merger that happened in the past via their velocities with respect to the thin disk. Besides, looking at velocity distributions that could give a hint to streams and therefore point to remnants of merging companions event would be important, too.

Of course, from the theorists side on can expect some progress. One could do an analysis of the orbits of satellite particles after the minor merger which requires high resolution in the satellite. Besides, one could to perform simulations with higher resolutions, especially for the galaxy simulations, and include gas dynamics and feedback to see whether a dissipational component and additional energy input could change the results. With further increase of computer power and with improved evolution models one could be able to perform fully self-consistent simulations where realistic disks are evolving within the cosmological context (where at the moment the simulations (?) fail and produce the angular momentum problem). With star formation included and feedback taken into account (what is planned for our code WINE in the near future) we would be able to trace the full merger history and interaction of a galaxy like our Milky Way in our simulations and would be able to see all the effects we mentioned in this work directly without relying on additional simulations with limited parameter space.

And once again we will be astonished by the fact that we are able to understand another part of an infinite universe, standing on a lonely planet around an ordinary star in the outer skirts of a standard galaxy.

Appendix A

Figures

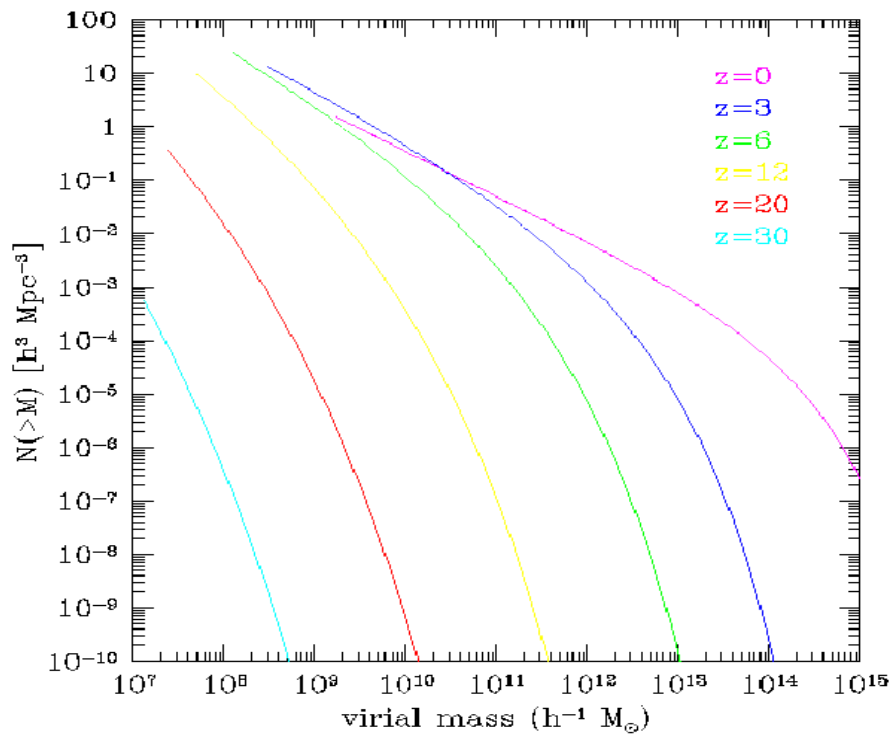


Figure A.1: Results from semi-analytical calculations. The picture shows the cumulative number of halos given by the Press-Schechter formalism. Note that for $z = 0$ the number of smaller halos is smaller than at higher redshifts. (Graphic kindly provided by Sadegh Khochfar)

Bibliography

- Bahcall, J. N. & Soneira, R. M. (1980). The universe at faint magnitudes. I - Models for the Galaxy and the predicted star counts. *Astrophysical Journal Supplement Series*, 44, 73-110.
- Balsara, D. (1990). *The SPH formalism*. Ph.D. thesis, University of Illinois.
- Barnes, J. (1990). A modified tree code: don't laugh, it runs. *Journal of Computational Physics*, 87, 161.
- Bennett, C., Halpern, M., Hinshaw, G., & et al. (2003). First year WMAP observations: Preliminary maps and basic results. *Astrophysical Journal Supplement Series*, 148, 1.
- Bertschik, M. (2001). *Entstehung und Entwicklung der Andromedagalaxie*. Diplomarbeit.
- Bertschik, M. & Burkert, A. (2003). Minor merger of galaxies: Theory vs. observations. *Galaxy Evolution: Theory & Observations, Revista Mexicana de Astronomia y Astrofisica (Serie de Conferencias)*, 17, 144.
- Bertschinger, E. (2001). Multiscale gaussian random field and their application to cosmological simulations. *Astrophysical Journal Supplement Series*, 137, 1.
- Binney, J. & Tremaine, S. (1987). *Galactic Dynamics*. Princeton University Press.
- Bode, P. & Ostriker, J. (2003). Tree Particle-Mesh: An adaptive, efficient, and parallel code for collisionless cosmological simulations. *Astrophysical Journal Supplement Series*, 145, 1.
- Bullock, J. & Kravtsov, A. (2002). Angular momentum profiles of warm dark matter halos. *Astrophysical Journal*, 564, 1.
- Burkert, A. (1993). Do elliptical galaxies have $R^{(1/4)}$ brightness profiles? *Astronomy and Astrophysics*, 278, 23-28.
- Burkert, A. (1995). The structure of dark matter halos in dwarf galaxies. *Astrophysical Journal Letters*, 447, 25.
- Connors, T., Kawata, D., Maddison, S., & Gibson, B. (2004). High-resolution N-body simulations of galactic cannibalism: The Magellanic Stream. *astro-ph/0402187*, 0, 1.
- Davis, M., Efstathiou, G., Frenk, C., & White, S. (1985). The evolution of large-scale structure in the universe dominated by cold dark matter. *Astrophysical Journal*, 401, 371.

BIBLIOGRAPHY

- Dehnen, W., Odenkirchen, M., Grebel, E., & Rix, H. (2004). Modeling the disruption of the globular cluster pal5 by galactic tides. *astro-ph/0401422*, 0, 1.
- Doran, M., Schwindt, J., & Wetterich, C. (2001). Structure formation and the time dependence of quintessence. *Physical Review D*, 64, 520.
- Dubinski, J. (1996). A parallel tree code. *New Astronomy*, 1, 2.
- Einstein, A. (1916). Die Grundlagen der allgemeinen Relativitaetstheorie. *Annalen der Physik*, 49, 769.
- Fall, S. & Efstathiou, G. (1980). Formation and rotation of disk galaxies with halos. *Monthly Notices of the Royal Astronomical Society*, 193, 189.
- Gardiner, L., Sawa, T., & Fujimoto, M. (1994). Numerical simulations of the Magellanic system - part one - orbits of the Magellanic Clouds and the global gas distribution. *Monthly Notices of the Royal Astronomical Society*, 266, 567.
- Ghigna, S., Moore, B., Governato, F., & et al. (2000). Density profiles and substructure of dark matter halos: Converging results at ultra-high numerical resolution. *Astrophysical Journal*, 544, 616.
- Gilmore, G., Wyse, R., & Norris, J. (2002). Deciphering the last major invasion of the Milky Way. *Astrophysical Journal Letters*, 574, 39.
- Goetz, M., Huchra, J., & Brandenberger, R. (1998). Group Identification in N-body simulations: SKID and DENMAX vs. FOF. *astro-ph/9811393*, 0.
- Guth, A. (1981). Inflationary universe: A possible solution to the horizon and flatness problems. *Physical Review D*, 23, 1110.
- Hawkins, E., Maddox, S., Cole, S., & et al. (2003). The 2dF Galaxy Redshift Survey: correlation functions, peculiar velocities and the matter density of the Universe. *Monthly Notices of the Royal Astronomical Society*, 346, 78.
- Hernquist, L. (1990). An analytical model for spherical galaxies and bulges. *Astrophysical Journal*, 356, 359–364.
- Hernquist, L. (1993a). N-body realizations of compound galaxies. *Astrophysical Journal Supplement Series*, 86, 389–400.
- Hernquist, L. (1993b). Structure of merger remnants. II: Progenitors with rotating bulges. *Astrophysical Journal*, 409, 548–562.
- Hernquist, L. & Katz, N. (1989). Treesph - A unification of SPH with the hierarchical tree method. *Astrophysical Journal Supplement Series*, 70, 419–446.
- Hernquist, L., Spergel, D. N., & Heyl, J. S. (1993). Structure of merger remnants. III: Phase-space constraints. *Astrophysical Journal*, 416, 415–424.
- Hetznecker, H. (2001). *Die Entstehungsgeschichte der dichten Kerne in CDM-Halos*. Doktorarbeit.

- Heyl, J. S., Hernquist, L., & Spergel, D. N. (1996). Structure of merger remnants. V: Kinematics. *Astrophysical Journal*, 463, 69–79.
- Hut, P. & White, S. (1984). Can a neutrino-dominated universe be rejected? *Nature*, 310, 637.
- Ibata, R., Gilmore, E., & Irwin, M. (1994). A dwarf satellite galaxy in Sagittarius. *Nature*, 370, 194.
- Jenkins, A., Frenk, C., White, S., Colberg, J., Cole, S., Evrard, A., Couchman, H., & Yoshida, N. (2001). The mass function of dark matter haloes. *Monthly Notices of the Royal Astronomical Society*, 321, 372.
- Kawai, A., Fukushige, T., Makino, J., & Taji, M. (2000). GRAPE-5: A special purpose computer for N-body simulations. *Journal of Computational Physics*, 52, 659.
- Khochfar, S. (2003). *Origin and Properties of Elliptical Galaxies in a Hierarchical Universe*. Ph.D. thesis.
- Klapdor-Kleingrothaus, H. & Zuber, K. (1997). *Teilchenastrophysik*. B.G. Teubner Stuttgart.
- Klypin, A., Kravtsov, A., Valenzuela, O., & Prada, F. (1999). Where are the missing galactic satellites? *Astrophysical Journal*, 522, 82.
- Kolb, E. & Turner, M. (1990). *The Early Universe, Frontiers in Physics, Vol.69*. Addison Wesley.
- Le Fevre, O., Abraham, R., Lilly, S., Ellis, R., & Brinchmann, J. (2000). HST imaging of the CFRS and LDSS redshift surveys -IV. Influence of mergers in the evolution of faint field galaxies from $z \approx 1$. *Monthly Notices of the Royal Astronomical Society*, 311, 565.
- Lin, D., Jones, B., & Klemola, A. (1995). The motion of the Magellanic Clouds, origin of the Magellanic Stream, and the mass of the Milky Way. *Astrophysical Journal*, 439, 652.
- Luminet, J., Weeks, J., Riazuelo, A., Lehoucq, R., & Uzan, J. (2003). Dodecahedral space topology as an explanation for weak wide-angle temperature in the cosmic microwave background. *Nature*, 425, 593.
- Ma, C. & Bertschinger, E. (1994). Do galactic systems form too late in cold + hot dark matter models? *Astrophysical Journal Letters*, 434, 5.
- Maddison, S., Kawata, D., & Gibson, B. (2002). Galactic cannibalism: The origin of the Magellanic Stream. *Astrophysics and Space Science*, 281, 421.
- Maller, A., Dekel, A., & Somerville, R. (2002). Modelling angular-momentum history in dark matter halos. *Monthly Notices of the Royal Astronomical Society*, 329, 423.
- Martin, N., Ibata, R., Bellazzini, M., Irwin, M., Lewis, G., & Dehnen, W. (2004). A dwarf galaxy remnant in Canis Major: the fossil of an in-plane accretion on to the Milky Way. *Monthly Notices of the Royal Astronomical Society*, 348, 12.
- Mathewson, D. (1985). The clouds of magellan. *Scientific American*, 252, 106.

BIBLIOGRAPHY

- Meszaros, P. (1974). The behaviour of point masses in an expanding cosmological substratum. *Astronomy and Astrophysics*, 37, 225.
- Mihos, J. (2004). The evolution of tidal debris. *Recycling intergalactic and interstellar matter, IAU Symposium Series*, 217, 1.
- Milgrom, M. (1983). A modification of the Newtonian Dynamics as a possible alternative to the hidden mass hypothesis. *Astrophysical Journal*, 270, 365.
- Moore, B., Ghigna, S., Governato, F., & et al. (1999). Dark matter substructure within galactic halos. *Astrophysical Journal Letters*, 524, 19.
- Morris, J. & Monaghan, J. (1997). A switch to reduce SPH viscosity. *Journal of Computational Physics*, 136, 41.
- Murai, T. & Fujimoto, M. (1980). The Magellanic Stream and the galaxy with a massive halo. *Publications of the Astronomical Society of Japan*, 32, 581.
- N-body shop (2001). Fof group finder. <http://www-hpcc.astro.washington.edu/tools/fof.html>.
- Naab, T. (1998). *Structure and Dynamics of Interacting Galaxies*. Ph.D. thesis.
- Navarro, J., Frenk, C., & White, S. (1997). A universal density profile from hierarchical clustering. *Astrophysical Journal*, 490, 493.
- Navarro, J. & Steinmetz, M. (2000). Dark halo and disk galaxy scaling laws in hierarchical universes. *Astrophysical Journal*, 538, 477.
- Peebles, P. (1980). *The Large-Scale Structure of the Universe*. Princeton University Press.
- Perlmutter, S., Gabi, S., Goldhaber, G., & et al. (1997). Measurements of the cosmological parameters Omega and Lambda from the first seven supernovae at $z \geq 0.35$. *Astrophysical Journal*, 483, 565.
- Press, W. (1986). Techniques and tricks for N-body simulations. *The use of supercomputers in stellar dynamics*, eds. P. Hut, S. McMillan, Springer, New York, 1, 184.
- Press, W. & Schechter, P. (1974). Formation of galaxies and clusters of galaxies by self-similar gravitational condensation. *Astronomy and Astrophysics Supplemental Series*, 95, 129.
- Quillen, A. & Garnett, D. (2000). The saturation of disk heating in the solar neighborhood. *astro-ph/0004210*, 0, 0.
- Quinn, P. J. & Goodman, J. (1986). Sinking satellites of spiral systems. *Astrophysical Journal*, 309, 472-495.
- Quinn, P. J., Hernquist, L., & Fullagar, D. P. (1993). Heating of galactic disks by mergers. *Astrophysical Journal*, 403, 74-93.
- Riess, A., Filippenko, A., Challis, P., & et al. (1998). Observational evidence from supernovae for an accelerating universe and a cosmological constant. *Astronomical Journal*, 116, 1009.

- Schwarzkopf, U. & Dettmar, R. (2000a). The influence of interactions and minor mergers on the structure of galactic disks i. *Astronomy and Astrophysics Supplemental*, 144, 85-129.
- Schwarzkopf, U. & Dettmar, R. (2000b). The influence of interactions and minor mergers on the structure of galactic disks ii. *Astronomy and Astrophysics*, 361, 451-464.
- Smoot, G., Bennett, C., Kogut, A., & et al. (1992). Structure in the COBE differential microwave radiometer first-year map. *Astrophysical Journal*, 396, 1.
- Smoot, G., Bennett, C., Weber, R., & et al. (1990). COBE differential microwave radiometer - instrument design and implementation. *Astrophysical Journal*, 360, 685.
- Springel, V., Yoshida, N., & White, S. (2001). Gadget: A code for collisionless and gasdynamical cosmological simulations. *New Astronomy*, 6, 79.
- Stoehr, F., White, S., Tormen, G., & Springel, V. (2002). The Milky Way's satellite population in a LCDM universe. *Monthly Notices of the Royal Astronomical Society*, 335, 84.
- Torres, S., Garcia-Berro, E., Burkert, A., & Bertschik, M. (2002). White dwarfs as a tracer of minor merger events. *Joint projects in 2002 and 2003 via DAAD*, 0, 0.
- Torres, S., Garcia-Berro, E., Burkert, A., & Isern, J. (2001). The impact of a merger episode in the galactic disk white dwarf population. *Monthly Notices of the Royal Astronomical Society*, 328, 492.
- Toth, G. & Ostriker, J. (1992). Galactic disks, infall, and the global value of Omega. *Astrophysical Journal*, 389, 5.
- van der Kruit, P. C. & Searle, L. (1981). Surface photometry of edge-on spiral galaxies. I - A model for the three-dimensional distribution of light in galactic disks. II - The distribution of light and colour in the disk and spheroid of NGC 891. *Astronomy and Astrophysics*, 95, 105-126.
- van der Marel, R., Alves, D., Hardy, E., & Suntzeff, N. (2002). New understanding of Large Magellanic cloud structure, dynamics, and orbits from carbon star kinematics. *Astronomical Journal*, 124, 2639.
- van Dokkum, P., Franx, M., Fabricant, D., Kelson, D., & Illingworth, G. (1999). A high merger fraction in the rich cluster MS1054-03 at $z=0.83$: direct evidence for hierarchical formation of massive galaxies. *Astrophysical Journal Letters*, 520, 95.
- van der Kruit, P. C. & Searle, L. (1982). Surface photometry of edge-on spiral galaxies. III - Properties of the three-dimensional distribution of light and mass in disks of spiral galaxies. *Astronomy and Astrophysics*, 110, 61-78.
- Velazquez, H. & White, D. (1999). Sinking satellites and the heating of galaxy disks. *Monthly Notices of the Royal Astronomical Society*, 304, 254-270.
- Walker, I. R., Mihos, J. C., & Hernquist, L. (1996). Quantifying the fragility of galactic disks in minor mergers. *Astrophysical Journal*, 460, 121-135.

BIBLIOGRAPHY

- Wang, L. & Steinhardt, P. (1998). Cluster abundance constraints for cosmological models with time-varying, spatially inhomogeneous energy component with negative pressure. *Astrophysical Journal*, 508, 483.
- Warren, M. & Salmon, J. (1995). A portable parallel particle program. *Computer Physics Communications*, 87, 266.
- Weinberg, M. (1995). Production of Milky Way Structure by the Magellanic Clouds. *Astrophysical Journal Letters*, 455, 31.
- Wetterich, C. (1995). An asymptotically vanishing time-dependent cosmological "constant". *Astronomy and Astrophysics*, 301, 321.
- Wetterich, C. (2002). Cosmon dark matter? *Physical Review D*, 65, 512.
- Yanny, B., Newberg, H., Grebel, E., & Kent, S. (2003). A low-latitude halo stream around the Milky Way. *Astrophysical Journal*, 588, 824.
- Zel'dovich, Y. (1993). *Selected works of Yakov Borisovich Zel'dovich*. Princeton University Press.

Danksagung

Ich danke...

...ganz besonders Prof. Dr. Andreas Burkert für die Idee zu meiner Doktorarbeit und seine geduldige Betreuung. Der Austausch mit ihm war sowohl in fachlicher wie auch in persönlicher Hinsicht eine echte Bereicherung und Inspiration.

...Prof. Dr. Hans-Walter Rix für die Begutachtung dieser Arbeit.

...Prof. Dr. Hans-Walter Rix und Prof. Dr. Thomas Henning für die Möglichkeit, meine Arbeit unter hervorragenden Bedingungen am Max-Planck-Institut fertigzustellen.

...Markus Wetzstein für die unermüdliche und geduldige Zusammenarbeit am Code WINE und für die kurzweiligen gemeinsamen Zimmerbesetzungen und Unternehmungen auf Konferenzen.

...Helmut Hetznecker, Sadegh Khochfar und Thorsten Naab für ihre Unterstützung und Hilfsbereitschaft in punkto Kosmologie und Galaxiendynamik.

...Thorsten, Steffi P., Helmut, Markus, Markus, Bernd, Sadegh, Roland, Robert, Sami, Boris, Angela und dem Rest Mittagessen- und Kaffee-Gang für die Gespräche, die mal nichts mit der Arbeit zu tun hatten.

...Thorsten, Markus, Helmut und Steffi E. für den Spass und für das Geld von den vielen Pokerabenden.

...Sven, Tillmann, Ralf, Johannes, Ansgar für die Kumpelschaft während der Doktorarbeit. Ich hoffe, wir werden die Treffen der "Heidelberg-Gang" beibehalten...

...Tillmann, Ralf, Sven, Roland und Sami für den gemeinsamen computergestützten Kampf gegen das Böse in der Welt.

...der Systemgruppe für die Computerhilfe.

...Roland, Angela, Andrea und Carsten für die entspannte Arbeitsatmosphäre im Büro.

Mein allergrösster Dank gilt meinen Eltern für ihre Geduld, ihr Verständnis und ihre Unterstützung bei meiner Arbeit - und Sabine, die immer für mich da ist.